学位論文

Studies on the synthesis of structurally regulated oligosiloxanes and their application to organic–inorganic hybrids

（構造制御されたオリゴシロキサンの合成と

その有機－無機ハイブリッドへの応用に関する研究）

2024 年 3 月

佐藤　陽平

Index

Chapter 1. General introduction

Chapter 1

General introduction

1.1 Polysiloxanes

Polysiloxanes consisting of alternating atoms of O and Si, which are abundantly present on earth [1], are used in various applications in our daily lives because of their excellent physical and chemical properties. Polysiloxanes also exist as silica or silicates in rocks and minerals. Actually, flint knives and stone axes were the first tools of humanity in the Paleolithic age.

Specifically, the compounds comprising Si atoms bonded to organic groups were termed silicones by Kipping based on their similarities with ketones [2]. Development of Si chemistry includes several principal steps [3,4]. Si was discovered by Berzelius in 1824 via the reduction of potassium fluorosilicate with K. Additionally, in the same year of the discovery of Si, Berzelius synthesized tetrachlorosilane as a volatile compound by reacting Si with Cl_2. In 1846, Ebelman, which was one of the pioneers of the sol–gel synthesis of silica, synthesized tetraethoxysilane (TEOS) via alkoxylation of tetrachlorosilane. In 1863, Friedel and Craft synthesized tetraethylsilane as the first silicon organic compound. In 1871, Ladenburg observed that an oil with high thermal stability was produced by the hydrolysis of diethyldiethoxysilane. Kipping laid the foundation of organosilicon chemistry by preparing various silanes via Grignard reactions and hydrolyzing chlorosilanes to yield large molecules. Polymeric natures of silicones were confirmed by the study of Stock. In the 1940s, silicones were commercialized after Hyde of Dow Corning Corporation demonstrated the thermal stabilities and high electrical resistances of silicone resins and Rochow of General Electric discovered

a direct method for the synthesis of alkylchlorosilanes from Si and MeCl, as described later.

Si–C bonds are stable against hydrolysis (the stability follows the order Si–C sp^3 > Si–C sp^2 > Si–C sp) [5]. Hydrolytic stabilities of other bonds are in the following order: Si–C > Si–OR > Si–Cl. Methyl and phenyl groups are adequately used as the functional groups on the silicon atom because of their high thermal stabilities (Table 1) [6]. Hydride and vinyl groups on the silicon atom can be applied in hydrosilylation for crosslinking the reactants to fabricate resins and foams. Silicones used in these reactions exhibit not only high thermal and chemical stabilities and weatherabilities, but also functional abilities originating from their structures and organic (and/or inorganic) substituents. Therefore, silicones have been employed as fluids, emulsions, compounds, resins, rubbers, and elastomers in numerous applications and diverse fields [7]. For example, silicones are commonly used in the aerospace industry mainly due to their outstanding low- and high-temperature performances. In the electronics field, silicones are utilized as electrical insulators and potting compounds and in other applications specific to semiconductor manufacturing. Long-term durabilities of silicones have facilitated the use of silicone sealants, adhesives, and waterproof coatings in the construction industry. These excellent properties arise from the high bonding energy of the siloxane bond (C–C: 356 kJ/mol vs. Si–O: 444 kJ/mol) [8]. Generally, trialkylsiloxy ($R_3SiO_{1/2}$), dialkylsiloxane (R_2SiO), alkyl silsesquioxane ($RSiO_{3/2}$), and silicate ($SiO_{4/2}$) units may be referred to as M, D, T, and Q units, respectively (Fig. 1) [6].

Table 1. Half-lives of Organic Groups at 250 °C

Organic group bonded to Si	Approximate half-life at 250 °C in air/ h
Phenyl	>100000
Methyl	>10000
Ethyl	6
Propyl	2
Butyl	<2
Pentyl	4
Nonyl	8
Decyl	12
Dodecyl	8
Octadecyl	26
Cyclohexyl	40
Vinyl	101

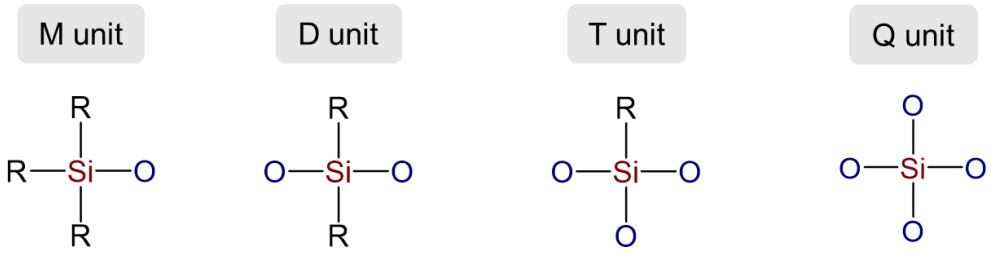

Figure 1. Structures of siloxane units.

1.2. Siloxane bond formation

Siloxane bond formations are depicted in Scheme 1 [9, 10]. Self-condensations followed by hydrolysis of silanes with functional groups (Scheme 1a) are a versatile approach to form siloxane oligomers and

polymers, particularly with chloro and alkoxy groups. This reaction corresponds to the sol–gel process. Heterofunctional condensations involving silanol groups or alkali metal silanolate groups (Scheme 1b) are a potential route to control reactions and/or construct siloxanes with well-defined structures because of the minimized cleavage of the siloxane bond by nucleophiles such as water, alcohols, and acids/bases. Another type of heterofunctional condensation is shown in Scheme 1c. Similarly, condensations of silanes containing alkoxy and halogen groups may occur in the presence of suitable catalysts including Lewis acids [11]. Recently, condensation between alkoxysilane and hydrosilane catalyzed by $B(C_6F_5)_3$, which is a strong soft Lewis acid, has been reported. This reaction leads to the detachment of alkane. The Si–Si bond can be oxidized with peroxides, nitrosamines, ozone, and hydrogen peroxide to produce siloxanes (Scheme 1d). However, almost no studies have been reported on the reaction that causes the detachment of alkene (Scheme 1e) [12, 13].

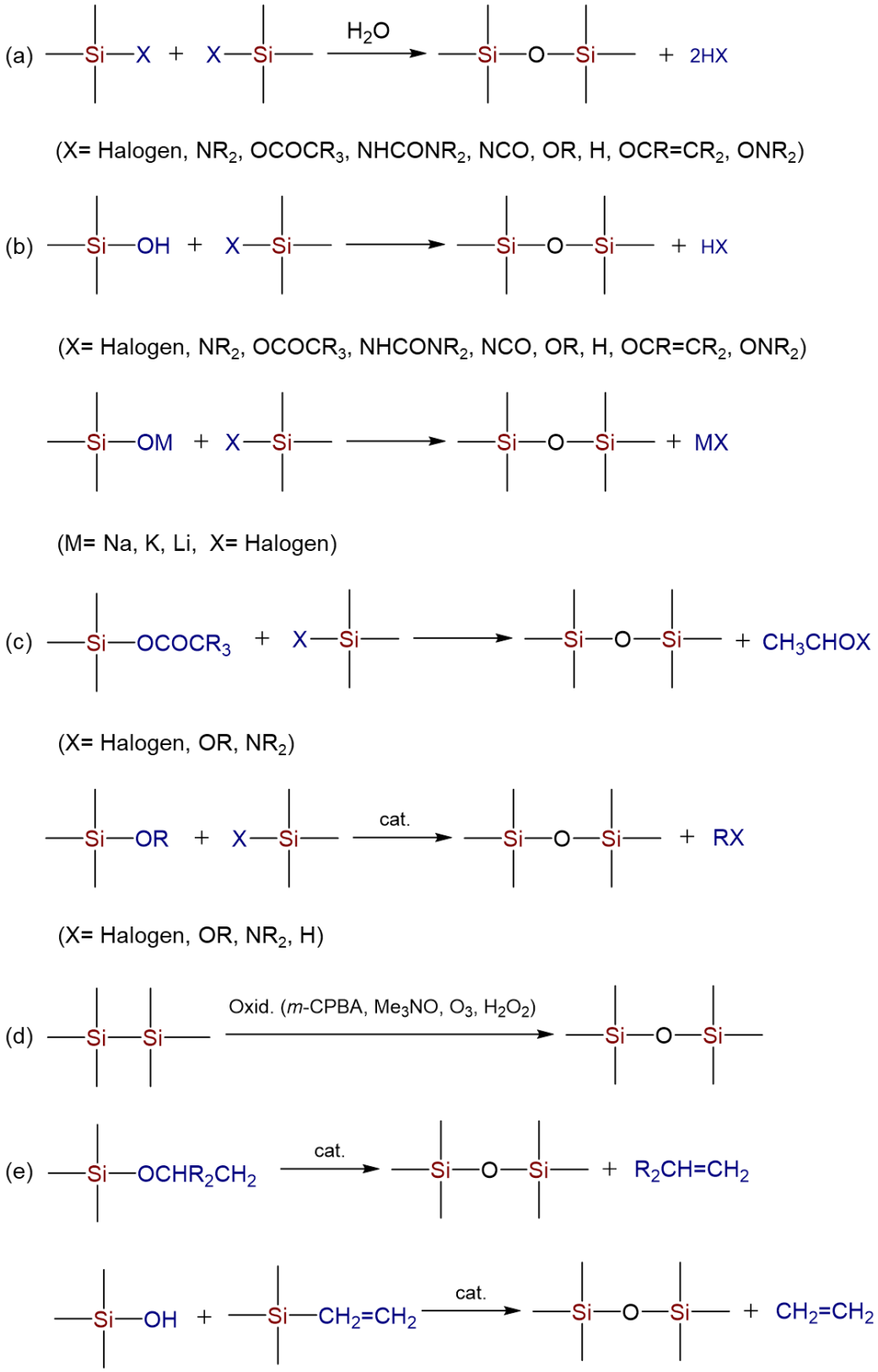

Scheme 1. Schematics of siloxane bond formations [9,10].

1.3 Sila-functional silanes

Silanes, for instance, $R_{4-n-m}Si(OR)_nX_m$ and $(RO)_{4-n}SiX_n$ (m = 1, 2; n = 1–3; R = alkyl, alkenyl, aryl; and X = halogen, OR′, OH, NR_2, OCOR, NCO), with functional groups are termed sila-functional silanes. Sila-functional groups, which are essential for the formation of siloxane bonds and/or synthesis of siloxane compounds, facilitate various types of siloxane formations.

Reactivities of different sila-functional groups in substitution reactions, such as hydrolysis and alcoholysis, follow the order H, OR, OH < NCO, $OCOCH_3$, < $NHCONR_2$, NR_2, Cl [14, 15]. In the selective formation of siloxane bonds, the selection of sila-functional groups is a key factor.

1.3.1 Chlorosilanes

Chlorosilanes are probably one of the most widely used starting materials for siloxane synthesis because of their ready availabilities and high reactivities. During substitution, hydrogen chloride is generated from chlorosilanes.

Several sila-functional silanes have been prepared from chlorosilanes (Scheme 2). Chlorosilanes are generally synthesized by the following process: gaseous alkyl chloride is passed through a crushed Cu−Si mixture prepared by the carbothermal reduction of silica stone in a tube furnace at 300 °C, and then, a mixture of alkyl chlorosilanes is obtained [16, 17]. This process is called the Müller–Rochow process. Nevertheless, as this process is a typically high-energy-consuming

process, an alternative process has been proposed [18, 19].

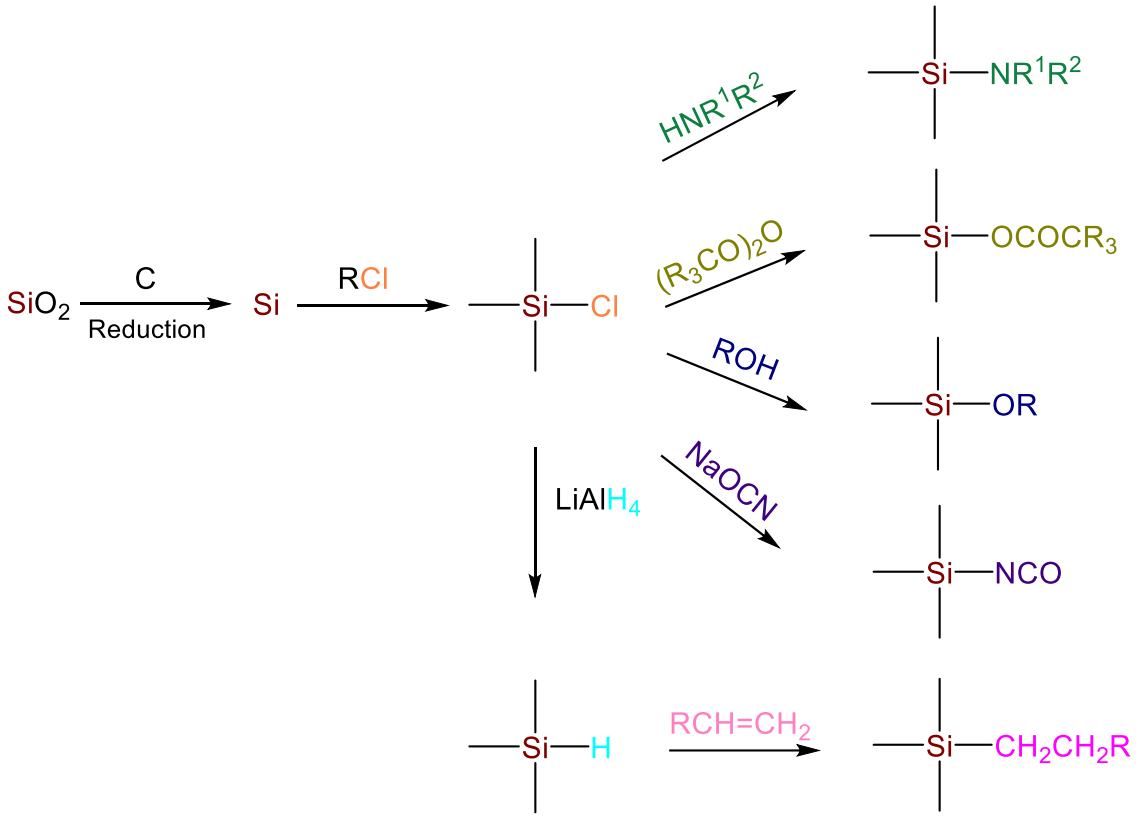

Scheme 2. Schematic of the synthesis of sila-functional silanes.

1.3.2 Alkoxysilanes

Alkoxysilanes are also one of the most extensively employed starting materials for siloxane production because of their easy accessibilities and facile handling. Alkoxysilanes are prepared by the alcoholysis of chlorosilanes.

Representative reactions of alkoxysilanes as are follows: (i) Silanols are generated by the

hydrolysis of alkoxysilanes. Then, condensation of silanols immediately occurs, leading to siloxanes. (ii) Under acidic or basic conditions, transalkoxylation takes place between alkoxysilanes and alcohols [20]. Generally, the rates of these reactions depend on the steric hindrance of the alkoxy group, which is in the following order: MeOH > EtOH > iPrOH > tBuOH. During transalkoxylation, removal of the eliminated alcohol by distillation is necessary because transalkoxylation is an equilibrium reaction. Reactions of alkoxysilanes are shown in Scheme 3.

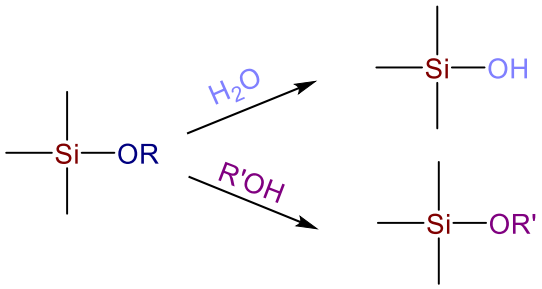

Scheme 3. Reactions of alkoxysilanes.

1.3.3 Isocyanatosilanes

Isocyanatosilanes are heterocumulene-type pseudo-halides and expected to be alternatives of chlorosilanes as they produce cyanic acid instead of hydrogen chloride upon substitution with nucleophiles. Applications of isocyanatosilanes are based on their substitution or addition with hydroxyl and amino groups: (i) Nucleophilic substitutions with alcohols and amines provide alkoxysilanes or aminosilanes [21, 22]. (ii) Addition with amines forms silylureas [23, 24]. However, addition competitively occurs with substitution depending on the structures and basicities of the

amines and reaction conditions. Reactions of isocyanatosilanes are depicted in Scheme 4.

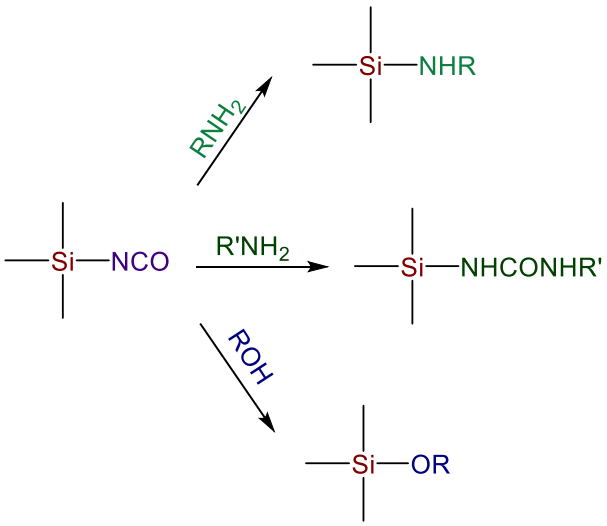

Scheme 4. Reactions of isocyanatosilanes.

1.4 Sol–gel method

Hydrolysis–condensation of metal alkoxides and other functional metal species (M–Cl, M–NR^1R^2, M–OCOR, and M–NCO, where M: metal, for example, Si, Ti, and Al)) is referred to as sol–gel reaction. Typically, metal alkoxides along with a catalyst are used in the sol–gel method. The reaction proceeds in two steps as follows: transformation of metal alkoxide (M–OR) to metal hydroxide (M–OH) by hydrolysis and formation of metalloxane (M–O–M) bonds via dehydration of metal hydroxides with each other or dealcoholization of metal hydroxides with metal alkoxides.

Although the history of the sol–gel reaction is ancient, its first report and namer are unclear. Description of the “sol–gel method” was verified by the studies on the preparation of nuclear fuels in

the 1960s [25]. Nevertheless, in 1846, Ebelmen had already reported the fabrication of transparent silica gel by slow hydrolysis of TEOS with air moisture [26]. In 1930, Geffcen and Berger from Shott Company established the industrial method of coating glass using silica precursor prepared by the sol–gel process [27]. In 1956, Roy employed metal alkoxide mixtures to construct phase equilibrium diagrams [28]. In the 1960s, various metal alkoxides and their derivatives, including amides, *β*-diketonates, and metalloxanes, were also examined by Bradley [29–31], Mehrotra [32], and Kijima and Abe [33]. From around 1960, attention was paid to the gels prepared from several alkoxide mixtures. Around 1969 and later, the sol–gel activity became high. In 1969, coating materials, such as SiO_2 and TiO_2–SiO_2 thin films, were synthesized by Schott Glass Company in West Germany [34]. Mazdiyasni *et al.* prepared high-purity barium titanate powders from barium and titanium alkoxides and indicated that multicomponent oxides could be synthesized by the sol–gel method [35]. In 1971, Dislich reported a study on a new route to multicomponent oxide glasses consisting of Na, B, Al, and Si, which are known as Pyrex glasses [36]. Many glass scientists, for example, Sakka, which is one of the pioneers in this field, were highly interested in Dislich's study and started research on the sol–gel method.

To date, numerous researchers have investigated and used the sol–gel method because of its various advantages such as (1) production of highly pure and homogeneous compounds and materials, (2) easy introduction of trace amount of elements, (3) facile control over the structure and

molecular weight of the product via reaction condition modification, (4) generation of oxide materials at low-temperatures (from tens to hundreds of °C), (5) applicability to the formations of fibers, films, powders, and bulks, and (6) synthesis of new crystallites and new glasses with superior properties determined by the specific properties of gels [37]. However, the sol–gel method also exhibits some disadvantages [38]: (a) high costs of precursors, (b) need for trial and error to determine appropriate reaction conditions (*e.g.*, reaction temperature, reaction time, and scale in operation), (c) difficulty in fabricating materials with large sizes, (d) complexity of producing the same products with excellent reproducibility due to significant variation in the reaction conditions during the sol–gel method, and (e) necessity of removing solvents and by-products including alcohols and organic compounds. Despite its initial development by glass researchers, the sol–gel method is almost only used for coating films because of the abovementioned disadvantages.

1.4.1 Sol–gel reactions with alkoxysilanes

The most famous sol–gel reaction utilizes alkoxysilanes ($Si(OR)_xR'_{4-x}$) and catalysts (such as acid, base, and metal compounds) and produces silica or silicone materials with different textures, molecular weights, and properties depending on the preparation conditions. Specifically, the mechanism of hydrolysis–condensation varies with respect to the kind of catalysts (acid or base) (Figure 2) [39]. Variation of reaction rate with respect to pH is also depicted in Figure 3 [39]. When an acid catalyst is

employed, the proton of the catalyst attacks the O atom of the alkoxy group, thereby protonating the alkoxyl group. Electron densities of Si atoms decreases, rendering them prone to attack by water, thereby forming an intermediate of penta-coordinated silicon species. Silicon compounds comprising silanol (Si–OH) groups are produced by the desorption of alcohol and proton from penta-coordinated silicon species (hydrolysis). The obtained silicon compounds with silanol groups attack other silicon compounds, leading to siloxane bonding (Si–O–Si) via the elimination of water (condensation) (Figure 3a). Under acidic conditions, hydrolysis and condensation are the fast and rate-determining reactions, respectively. Therefore, linear oligosiloxanes have been estimated as intermediates by gas chromatography/mass spectrometry [40–42]. Similarly, the generation of linear polysiloxanes is expected. In contrast, under basic conditions, the hydroxyl groups of the catalyst attack Si atoms, forming a pentavalent silicon species as an intermediate. Via desorption of the alkoxide ion (RO^-), a silanol group is produced (hydrolysis); moreover, the number of silanol groups increases at high rates with a decrease in steric hindrance around the Si atom. Finally, the anionic species, generated by the deprotonations of silanol groups by base, attack other silicon compounds, and siloxane bonds are formed. Under basic conditions, hydrolysis and condensation are the rate-determining and fast reactions, respectively. Thus, the obtained precursor demonstrates a three-dimensional network (Figure 3b). As mentioned earlier, generally, acid catalysts are used in the sol–gel reactions of alkoxysilanes to regulate and achieve reproducibility for the reaction.

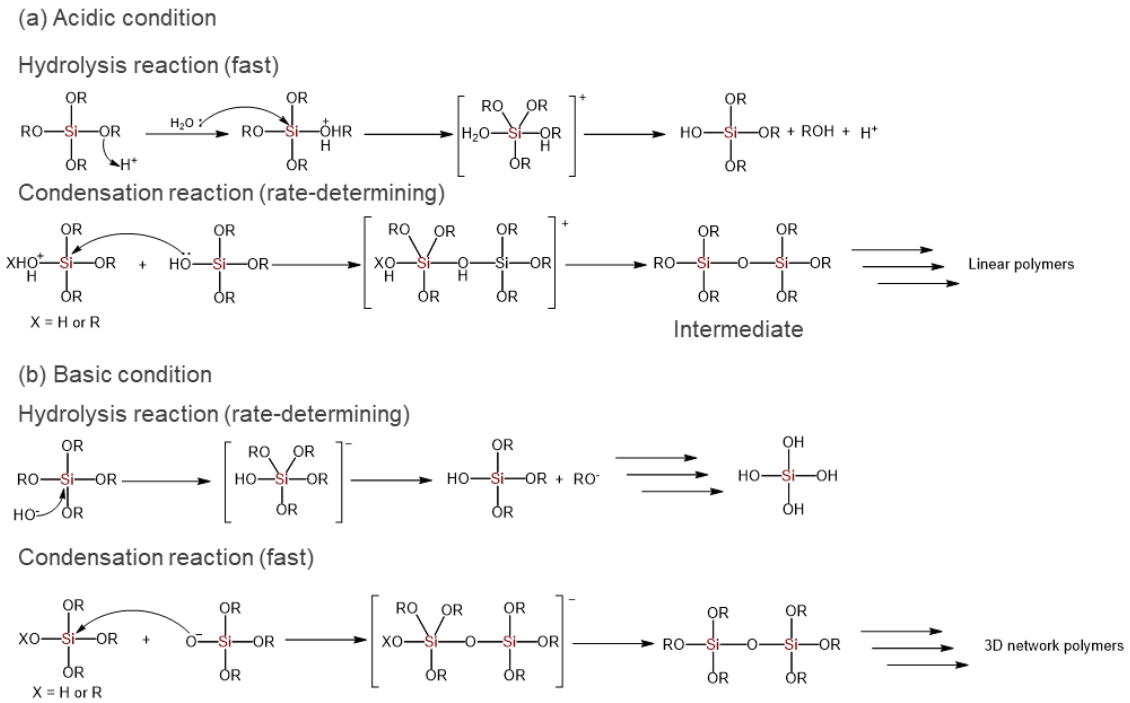

Figure 2. Mechanisms of hydrolysis and condensation over (a) acid and (b) base catalysts.

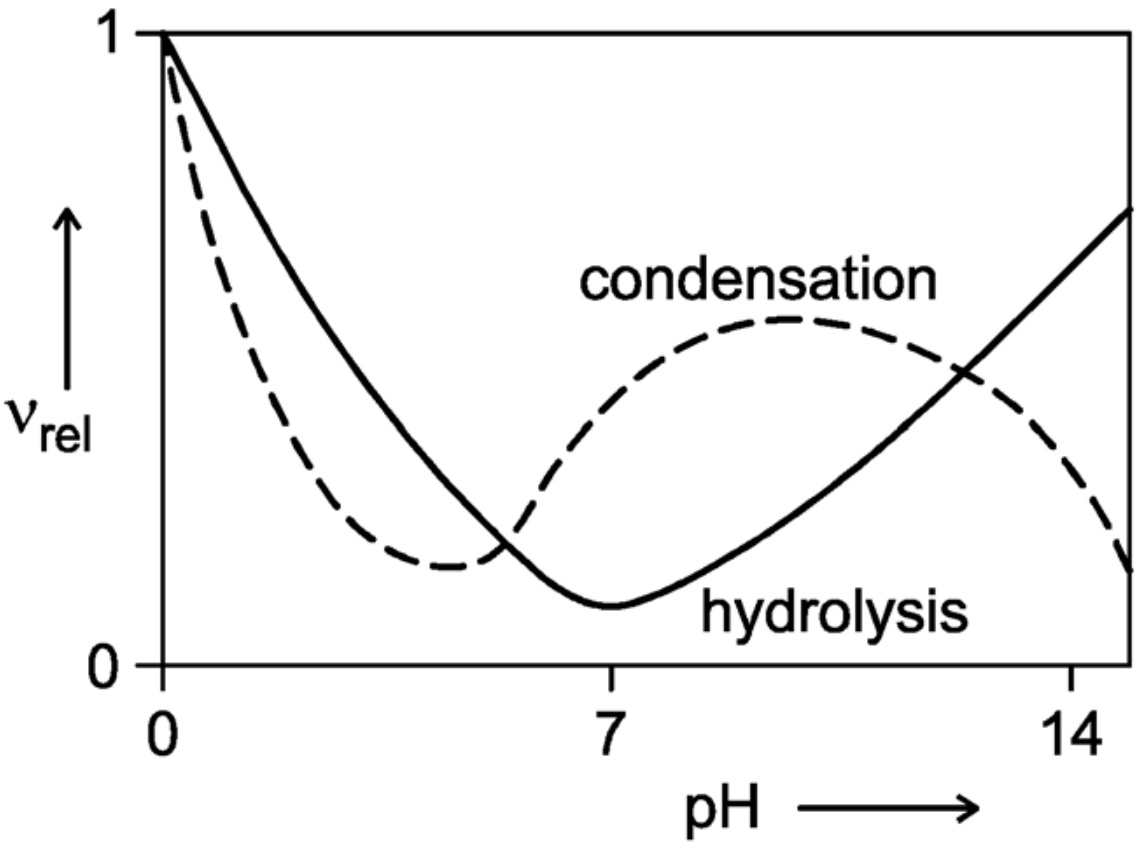

Figure 3. Variation of reaction rate with respect to pH [39].

Behavior and morphology of silicic acid with respect to pH are shown in Figure 4 [43]. The individual steps are as follows: (a) $Si(OH)_4$ is soluble and remains stable in water at 25 °C for long periods at concentrations less than approximately 100 ppm in terms of SiO_2. When a $Si(OH)_4$ solution with concentrations higher than approximately 100–200 ppm in terms of SiO_2 is formed, the monomer condenses, producing dimer and higher-molecular-weight species of silicic acid. Silicic acid is also extracted from an aqueous solution of sodium metasilicate using organic solvents. Tetrahydrofuran (THF) is a convenient solvent for the extraction of silicic acid because the degree of extraction of silicic acid using THF is the highest among those in the cases of other organic solvents [44]. Condensation rate of silicic acid in organic solvents also depends on the concentration of silicic acid [45]. (b) At pH > 2, the condensation rate is proportional to OH^- concentration, whereas at pH < 2, the condensation rate is proportional to H^+ concentration. (c) In the earliest stage of polymerization, condensation quickly leads to ring structures, for example, cyclic tetramer, followed by the addition of monomers to these ring structures and linking of the resulting compounds to larger 3-dimensional molecules. (d) The resulting spherical units are the nuclei that develop into larger particles. (e) At pH > 7, where the rates of dissolution and deposition of silica are high, particle growth continues at ordinary temperatures until the particles are 5–10 nm in diameter, after which the growth is slow. Nevertheless, at low pH, where the polymerization and depolymerization are slower, particle growth

becomes negligible after a particle size of 2–4 nm is reached. At higher temperatures, particles continue to grow to larger sizes, specifically at pH > 7. (I) At pH > 6–10.5, silica begins to dissolve as silicate. Silica particles are negatively charged and repel each other. Under certain conditions, precipitation or gelling is prevented by increasing the temperature. (g) At low pH, because the silica particles bear very little ionic charges, they can collide and aggregate into chains followed by the production of gel networks.

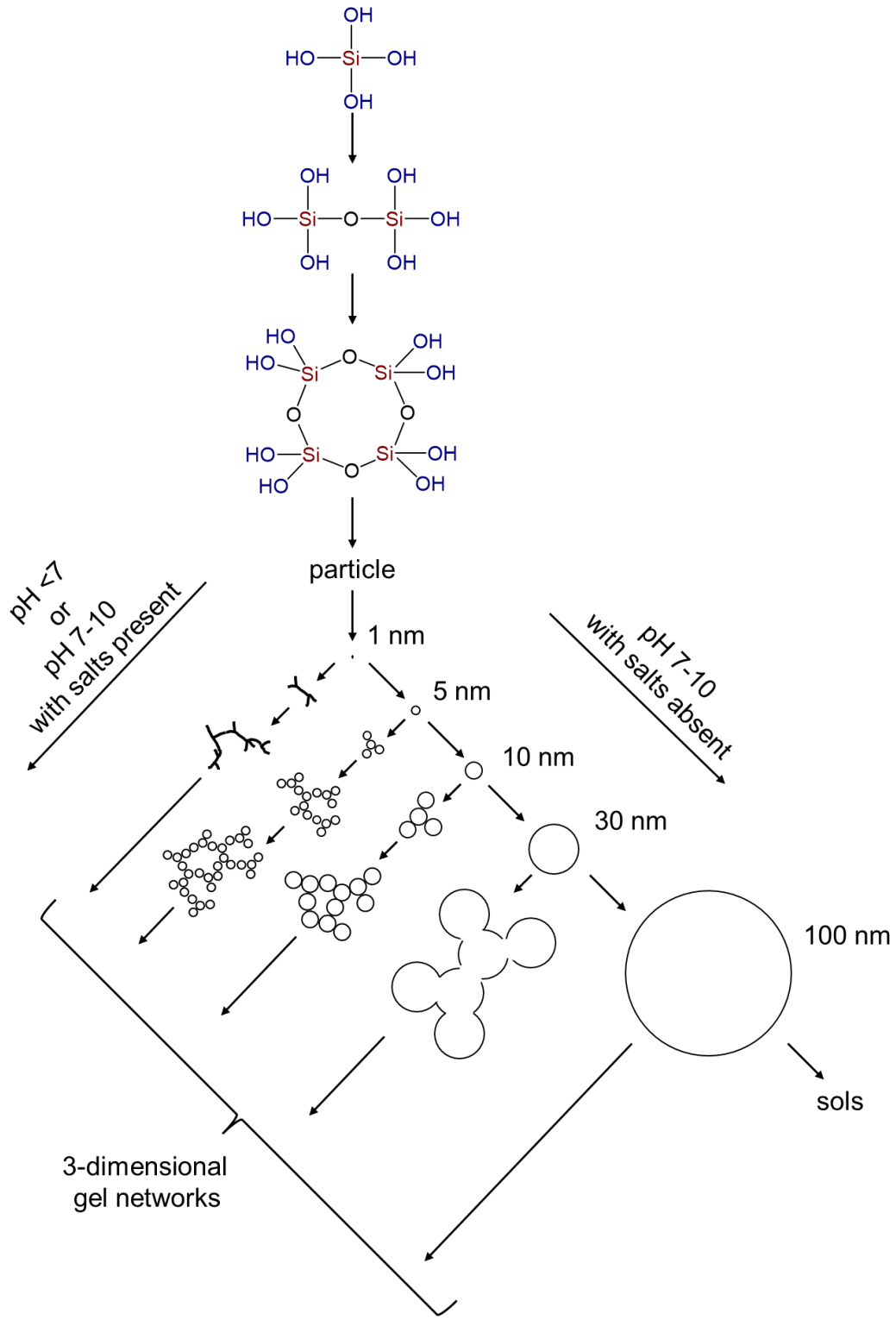

Figure 4. Schematic of the growth and texture of silicic acid at different pH values [43].

1.4.2 Influencing factors of sol–gel reactions

Several studies have been conducted on sol–gel reactions regarding kinetic rate constants and hydrolysis behaviors under various pH, temperature, and catalytic conditions [46–50]. With respect to the kinetic rate constant of hydrolysis–condensation of tetramethoxysilane under acidic conditions, Kay and Assink reported the following observations: (1) hydrolysis is faster than condensation; (2) water-producing condensation is faster than methanol-producing condensation (hydrolysis: 0.2 mol^{-1} min^{-1}, water-producing condensation: 0.006 mol^{-1} min^{-1}, and methanol-producing condensation: 0.001 mol^{-1} min^{-1}) [51]. These kinetic rate constants are widely accepted. In contrast, we have recently stated that ethanol-producing condensation is faster than water-producing condensation during condensation between triethoxysilane and triethoxysilanol (ethanol-producing condensation: 0.12 $Lmol^{-1}$ min^{-1} and water-producing condensation: 0.08 $Lmol^{-1}$ min^{-1}) [52,53]. These results indicate that steric hindrance dominates the hydrolysis–condensation of alkoxysilanes.

1.4.3 Sol–gel reactions using polyfunctional alkoxysilanes

Bifunctional silanes are used as starting materials for the preparation of linear and cyclic oligosiloxanes and polysiloxanes. Polysiloxanes, generated from bifunctional silanes, are employed as silicone oils. Linear-polysiloxanes are also obtained by ring-opening polymerization of cyclic oligosiloxanes. On the other hand, sol–gel reactions of tri- and tetra-functional silanes afford final

products with different structures including cyclic, linear, ladder, and cubic structures (Figure 5) [6,9,54]. The final products acquired from tri- and tetra-functional silanes exhibit a mixture of these structures. To fine-tune the properties of siloxane materials, identification, isolations, and characterizations of these structures are considered important.

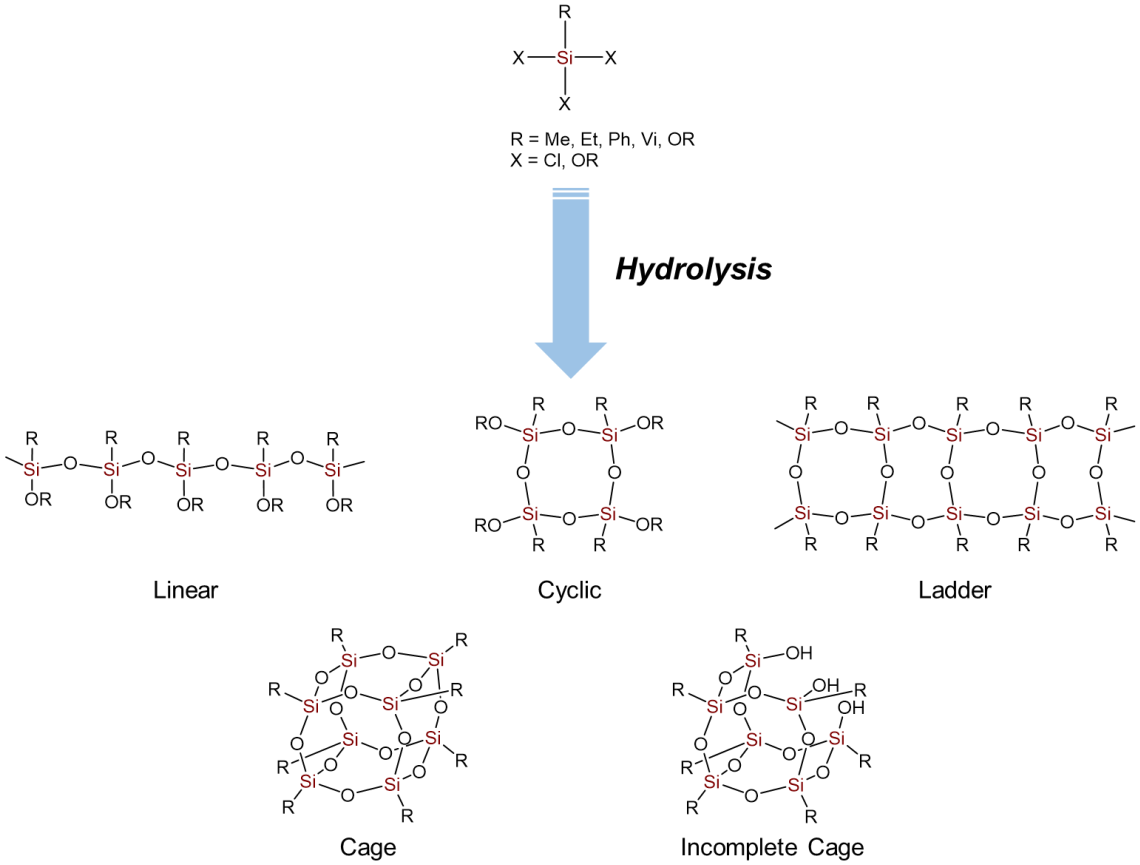

Figure 5. Structures of the hydrolysis–condensation products of tri- and tetra-functional silanes.

1.5 Organic–inorganic hybrid materials

Organic–inorganic hybrid materials are composed of organic and inorganic components,

demonstrating the potentials for novel functions and applications because of the combined advantages of each component [55,56]. Sanchez *et al.* proposed a classification for organic–inorganic hybrid materials based on the hybridization of organic and inorganic components, ranging from a 0.1 to several nanometers in length [57,58]. Class I hybrid materials are generally fabricated by mixing organic and inorganic components and characterized by weak interactions, such as van der Waals force, hydrogen bonding, coordination bonding, and electrostatic forces, between the organic and inorganic segments. Contrarily, class II hybrid materials are typically synthesized by copolymerization of inorganic/organic monomers or polymers and characterized by stronger interactions including covalent and ionic bondings. Classifications of class I and II hybrid materials are depicted in Figure 6.

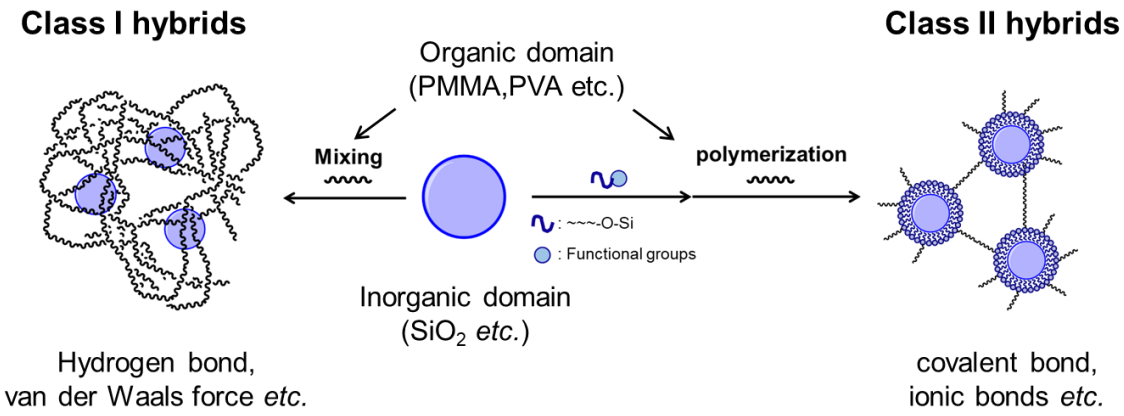

Figure 6. Classifications of class I and II hybrid materials.

1.5.1 Origin of organic–inorganic hybrid materials

Organic–inorganic hybrid materials have originated several centuries ago, and Maya blue pigment,

which is prepared from a clay mineral (palygorskite) and natural dye (indigo) [59], is the oldest organic–inorganic hybrid material used in Mesoamerica from AD 300 to 1500. Maya blue pigment exhibits high chemical stability against acids, bases, and many organic reagents, high thermal stability, even at high temperatures and high humidities in Central America, and very high toughness and resistance against weathering and biodegradation. However, the preparation of organic–inorganic pigments is difficult because of inadequate dispersion of organic dyes in inorganic matrices.

1.5.2 Sol–gel syntheses of organic–inorganic hybrid materials

In 1984, Schmidt *et al.* reported sol–gel-prepared contact lenses, which consisted of an organic–inorganic hybrid material [60]. This material was synthesized by hydrolysis–condensation using epoxysilane, methacryloxy silane, and titanium alkoxide. In this hybrid, the inorganic components were bonded to the organic components by covalent bonding; hence, this hybrid is classified as class II hybrid. These hybrid materials demonstrate the features of both inorganic and organic substances and are termed ORMOCER [61]. This study is believed to be the first report of organic–inorganic hybrid materials fabricated by the sol–gel method. In the same year, Avnir *et al.* reported a study on the preparation of silica gel films containing rhodamine 6G as a fluorescent molecule [62]. This film comprised fixed rhodamine 6G molecules without aggregation such that their fluorescence properties

would not be lost and are classified as class I hybrids. These studies reveal that the sol–gel method is suitable for the fabrication of organic–inorganic hybrid materials because of be solution method which can mix molecular level of each component. Thereafter, organic–inorganic hybrid materials, such as Ormosils [63] and Ceramers [64], synthesized by the sol–gel method were reported by Mackenzie and Wilks. In the 1990s, Chujo *et al.* made a breakthrough using the approach of intermolecular interaction to disperse organic and inorganic domains [65]. Recently, element blocks and element-block polymers have also been proposed by Chujo in the field of materials science as a novel concept for the synthesis of new materials [66]. An element block is a structural unit consisting of several groups of elements [66].

1.5.3 Organic–inorganic hybrid materials with siloxane molecules

In section 1.5.2, I introduced hybrid materials containing organic and inorganic compounds prepared by the sol–gel method. These materials exhibit outstanding properties as compared to those of the organic compound alone; however, they suffer from many problems, for instance, (i) large inorganic domains (generally, with sizes more than 10 nm), (ii) difficulty in regulating the sizes and structures of inorganic domains, (iii) difficulty in controlling the number of coupling reagents on the inorganic domain surfaces, and (iv) difficulty in the purification of inorganic domains.

Therefore, numerous researchers have focused on structural regulated siloxane molecules as

element blocks because these compounds demonstrate various advantages such as (a) solubilities in organic solvents, (b) uniform sizes and shapes, (c) control over the number of functional groups depending on the structure of molecules, and (d) easy purification rather than that of modern inorganic domains. Particularly, cage-type compounds have attracted considerable attention because of their advantages including high thermal, mechanical, and chemical stabilities in addition to homogeneous shapes and possibility of introducing various functional groups into them.

1.5.4 Synthesis of cage siloxanes for organic–inorganic hybrid materials

Polyhedral oligomeric silsesquioxanes (POSSs) are highly regulated cage-like structures with the general formula $[RSiO_{1.5}]_n$ and have been isolated n = 6, 8, 10, 12, 14, and 18 [54,67]. Many researchers have reported various polymerizations of cage-type oligosiloxanes: (i) cross-linking of a cage octasilicate with dichlorosilane [68], (ii) polymerization of alkoxylated cage octasilicate by the sol–gel reaction and producing of the xero gel [69], (iii) dehydrogenative condensation between Si–H and Si–OH groups of a cage siloxane and application of the resulting polymer membrane for gas separation [70], and (IV) polymerization of methacrylate-functionalized POSS by radical polymerization [71]. These hybrid materials exhibit excellent properties such as porosity and high thermal stability, attributed to the presence of cage siloxanes.

1.5.5 Synthesis of incomplete cage siloxanes for organic–inorganic hybrid materials

Recently, incomplete cage siloxanes have attracted significant attention as potential starting materials for organic–inorganic hybrid materials. As incomplete cage siloxanes with different number of functional groups (that is, two, three, and four silanol groups) can be synthesized, functionality control is possible. For example, a one-dimensional hybrid material was constructed by the condensation of $[Si_8O_{11}(C_6H_{11})_8(OH)_2]$ with bis(dimethylamino)octamethyltetrasiloxane ($Me_2N(SiMe_2O)_3SiMe_2NMe_2$), and thermal stability of this material was higher than that of the dimethylsiloxane polymer prepared by $Me_2N(SiMe_2O)_3SiMe_2NMe_2$ [72]. Naka *et al.* and Kunitake *et al.* have reported many organic–inorganic hybrid materials using incomplete cage siloxanes [73] and double-decker-type cage siloxanes [74], respectively. These hybrid materials demonstrate high transparencies, high thermal stabilities, and organic properties (*e.g.*, flexibilities and light weights) arising from the reduced symmetry structures as compared to those of cage siloxanes.

1.5.6 Synthesis of ladder siloxanes for organic–inorganic hybrid materials

Ladder siloxanes exhibit excellent thermal and chemical stabilities due to their double-chain silsesquioxane structures. In 1960s, Brown prepared a ladder phenyl silsesquioxane for the first time [75,76]. Nevertheless, currently, this report is questionable. Then, Gunji, Unno, and Kaneko, which are Japanese researchers, reported the synthesis of ladder siloxanes; however, synthesis of ladder

siloxanes is still challenging. Consequently, almost no studies have been reported on the applications of ladder siloxanes for the construction of organic–inorganic hybrid materials. Kaneko *et al.* have constructed some organic–inorganic hybrid materials using ladder silsesquioxanes. Because these silsesquioxanes comprise ion pairs on terminal groups, several characteristics, such as chiral induction molecule [77], dispersive agent [78], and proton conductor [79], can be endowed by converting the ion pair or the terminal group.

1.5.7 Synthesis of non-silicon cage compounds for organic–inorganic hybrid materials

Zrconium- or titanium-oxo clusters are the most famous non-silicon cage compounds for the synthesis of organic–inorganic hybrid materials [80]. For instance, the organic–inorganic hybrid material formed by hydrgen bonding between a polymer bearing a thiourea group and titanium-oxo cluster with pyrrolidone demonstrated better mechanical properties because the cluster acted as a cross-linker [81]. Furthermore, Sanchez *et al.* fabricated organic–inorganic hybrid materials by mixing ORMOCER and $[Ti_6O_4(OR)_8(OCCPh)_8]$, and the refractive index of the hybrid material with *ca.* 2.2 mol% cluster was higher (1.575) than that of ORMOCER alone (1.552) [82]. Another type of organic–inorganic hybrid materials, namely, titanium phosphonate clusters composed of titanoxane (Ti–O–Ti) and phosphatitanoxane (Ti–O–P) bonds, was reported by Gunji and Hayami. Degradation and glass transition temperatures of the hybrids were higher than those of pristine organic polymers [83,84].

1.6 Aims of this thesis

As mentioned in the previous sections, siloxane materials are important in our lives. Nevertheless, the siloxane chemistry mainly suffers from two problems:

(1) Only a few studies have been reported on the hydrolyzabilities of linear alkoxy oligosiloxanes, which are achieved by the initial sol–gel reactions of alkoxysilanes under acidic conditions, and even steric hindrance dominates the sol–gel reactions of alkoxysilanes. If the reactivity of an intermediate is not known, the mechanisms of the sol–gel reactions of alkoxysilanes may not be understood.

(2) Relationships between the structures and properties of organic–inorganic hybrid materials have not been understood because differentiation of the various structures generated by the sol–gel reactions of polyfunctional alkoxysilanes is difficult due to the polyfunctionalities of these alkoxysilanes.

Aims of this thesis were as follows: (i) synthesis and characterization of linear ethoxy oligosiloxanes, (ii) application of the hydrolyzates of linear ethoxy oligosiloxanes for the formation of organic–inorganic hybrid materials, and (iii) dimensional control of organic–inorganic hybrid materials using cage silsesquioxanes. Via (i), I revealed the hydrolyzabilities of linear alkoxy oligosiloxanes and provided the essential understanding of the sol–gel reactions of alkoxysilanes. Via (ii), I demonstrated the relationships between the structures and properties of organic–inorganic hybrid materials using the different polymer structures obtained by the hydrolysis of linear alkoxy oligosiloxanes. By achieving (iii), I established dimensional control of organic–inorganic hybrid materials

1.7 Overview of this thesis

In this thesis, the synthesis of structurally regulated oligosiloxanes and their application to organic–inorganic hybrids were investigated in the following three categories:

1. Hydrolysis and condensation behaviors of TEOS, hexaethoxydisiloxane (HEDS), and octaethoxytrisiloxane (OETS) (chapter 2).

2. Preparation and properties of polydimethylsiloxane elastomers cross-linked with the hydrolyzates of TEOS, HEDS, and OETS (chapter 3).

3. Syntheses of coordination polymers using an acetylacetonato-terminated polyhedral oligomeric silsesquioxane and properties of these polymers (chapter 4).

References

1. F. W. Clarke, H. S. Washington, The composition of the earth's crust. Vol. 127. US Government Printing Office (1924).

2. F. S. Kipping, *Proc. Chem. Soc*., **20**, 15 (1904).

3. F. W. G. Fearon, High performance polymers, edit. R. Seymour and G. Kirsenbaum, Elsevier (1986).

4. E.G. Rochow, Silicon and silicones, Springer-Verlag (1987).

5. L. Rozes, C. Sanchez, *Chem. Soc. Rev.*, **40**, 1006–1030 (2011). https://doi.org/10.1039/C0CS00137F

6. R. H. Baney, M. Itoh, A. Sakakibara, T. Suzuki, *Chem. Rev.*, **95**, 1409–1430 (1995). https://doi.org/10.1021/cr00037a012

7. A. Colas, J. Curtis, Handbook of polymer applications in medicine and medical devices, Elsevier, pp. 131–143 (2013). https://doi.org/10.1016/B978-0-323-22805-3.00007-4

8. Y. Sugioka, M. Yokota, T. Pude, Y. Suda, H. Takikawa, H. Tanoue, H. Ue, Y. Umeda, K. Shimizu, *Jpn. J. Appl. Phys.*, **50**, 08JF08 (2011). https://doi.org/10.1143/JJAP.50.08JF08

9. Y. Abe, T. Gunji, *Prog. Polym. Sci.,* **29**, 149–182 (2004). https://doi.org/10.1016/j.progpolymsci.2003.08.003

10. K. Matsumoto, S. Shimada, K. Sato, *Chem. Eur. J.*, **25**, 920–928 (2019). https://doi.org/10.1002/chem.201803565

11. R. Wakabayashi, K. Kuroda, *ChemPlusChem*, **78**, 764–774 (2013). https://doi.org/10.1002/cplu.201300027

12. G. Hreczycho, K. Kuciński, P. Pawluć, B. Marciniec, *Organometallics*, **32**, 5001–5004 (2013). https://doi.org/10.1021/om400581g

13. B. Marciniec, P. Pawluć, G. Hreczycho, A. Macina, M. Madalska, *Tetrahedron Lett.*, **49**, 1310–1313 (2008). https://doi.org/10.1016/j.tetlet.2007.12.091

14. H. Sakurai, H. Nozaki, S. Yamamoto, J. Tsuji, R. Noyori, Application of organosilicon compounds to organic synthesis (Eds.), Kagaku Zokan, vol. 105. Kagaku Dojin (1985), pp. 33–40.

15. R. J. P Corriu, C. Guerin, *Adv. Organomet. Chem.*, **20**, 265–312 (1982). https://doi.org/10.1016/S0065-3055(08)60523-7

16. D. Seyferth, *Organometallics*, **20**, 4978– 4992 (2001). https://doi.org/10.1021/om0109051

17. N. Fukaya, S. J. Choi, T. Horikoshi, H. Kumai, M. Hasegawa, H. Yasuda, K. Sato, J. -C. Choi, *Chem. Lett.*, **45**, 828–830 (2016). https://doi.org/10.1246/cl.160329

18. W. S. Putro, V. Y. Lee, K. Sato, J. -C. Choi, N. Fukaya, *ACS Omega*, **6**, 35186–35195 (2021). https://doi.org/10.1021/acsomega.1c05138

19. E. G. Rochow, U.S. Pat. Appl. US 2,473,260, 1949.

20. I. Hasegawa, S. Sakka, *Bull. Chem. Soc. Jpn.*, **61**, 4087–4092 (1988). https://doi.org/10.1246/bcsj.61.4087

21. J. Goubeau, D. Paulin, *Chem. Ber.*, **93**, 1111–1116 (1960). https://doi.org/10.1002/cber.19600930519

22. Y. Abe, H. Tanaka, N. Shikano, T. Gunji, *Nippon Kagaku Kaishi*, **2001**, 157–162 (2001). https://doi.org/10.1246/nikkashi.2001.157

23. R. M. Pike, E. B. Moynaham, *Inorg. Chem.*, **6**, 168–169 (1967). https://doi.org/10.1021/ic50047a043

24. J. Goubeau, E. Heubach, *Chem. Ber.*, **93**, 1117–1125 (1960). https://doi.org/10.1002/cber.19600930520

25. G. Cogliati, R. Lanz, E. Mezi, *EUR-2780.e* 269 (1965).

26. M. Ebelmen, *Ann. Chim. Phys.*, **16**, 129 (1846).

27. W. Geffcken, E. Berger, Dtsch. Reichspatent 736 411 (1939), Jenaer Glaswerk Schott & Gen, Jena, GDR.

28. R. Roy, *J. Am. Ceram. Soc.*, **39**, 145–146 (1956). https://doi.org/10.1111/j.1151-2916.1956.tb14180.x

29. D. C. Bradley, *Progr. Inorg. Chem.* **2**, 303 (1960).

30. D. C. Bradley in F. G. A. Stone and W A. G. Graham: Inorganic Polymers. Academic Press, New York 1962, p. 410; Coord. Chem. Rev. 2, 299 (1967).

31. D. C. Bradley, *Coord. Chem. Rev.*, **2**, 299–318 (1967). https://doi.org/10.1016/S0010-8545(00)80126-5

32. R. C. Mehrotra, *Inorg. Chim. Acta*, **1**, 99–112 (1967). https://doi.org/10.1016/0073-8085(67)80023-8

33. Y. Abe, I. Kijima, *Bull. Chem. Soc. Jpn*., **43**, 466–469 (1970). https://doi.org/10.1246/bcsj.43.466

34. H. Schröder, Oxide layers deposited from organic solutions. In: Haas G, Thun RE, editors. Physics of thin films, vol. 6. New York: Academic; 1969. p. 87–141.

35. K. S. Mazdiyasuni, R. T. Dolloff, J. S. Smith, *J. Am. Ceram. Soc.*, **52**, 523–526 (1969). https://doi.org/10.1111/j.1151-2916.1969.tb09157.x

36. H. Dislich, *Angew. Chem., Int. Ed. Engl.*, **10**, 363–370 (1971). https://doi.org/10.1002/anie.197103631

37. H. K. Schmidt, E. Geiter, M. Mennig, H. Krug, C. Becker, R. -P. Winkler, *J. Sol-Gel Sci. Technol.*, **13**, 397–404 (1998). https://doi.org/10.1023/A:1008660909108

38. C. A. Milea, C. Bogatu, A. Dută, *Bull. Transiv. Univ. Braşov, series I*, **4**, 59–66 (2011).

39. C. J. Brinker, W. S. George, Sol-gel science: the physics and chemistry of sol-gel processing. Academic press, 2013.

40. T. Gunji, Tokyo University of Science, Doctoral dissertations, p110 (1992). https://doi.org/10.11501/3071196

41. T. Gunji, I. Sopyan, Y. Abe, *J. Polym. Sci., Part A: Polym. Chem.*, **32**, 3133–3139 (1994). https://doi.org/10.1002/pola.1994.080321613

42. W. G. Klemperer, V. V. Mainz, S. D. Ramamurthi, F. S. Rosenberg, *Mater. Res. Soc. Symp. Proc.*, **121**, 15–24 (1988). https://doi.org/10.1557/PROC-121-15

43. R.K. Iler, The chemistry of silica, Wiley, New York (1979).

44. Y. Abe, H. Mizono, *J. Chem. Soc. Jpn., Chem. Ind. Chem.*, **1981**, 1152–1158 (1981). https://doi.org/10.1246/nikkashi.1981.1152

45. T. Gunji, Y. Nagao, T. Misono, Y. Abe, *J. Polym. Sci., Part A: Polym. Chem.*, **30**, 1779–1787 (1992). https://doi.org/10.1002/pola.1992.080300901

46. J. Cihlář, *Colloids Surf., A*, **70**, 239–251 (1993). https://doi.org/10.1016/0927-7757(93)80298-S

47. M. T. Harris, R. R. Brunson, C. H. Byers, *J. Non-Cryst. Solids*, **121**, 397–403 (1990). https://doi.org/10.1016/0022-3093(90)90165-I

48. M. I. Tejedor-Tejedor, L. Paredes, M. A. Anderson, *Chem. Mater.*, **10**, 3410–3421 (1998). https://doi.org/10.1021/cm980146l

49. J. C. Echeverría, P. Moriones, G. Arzamendi, J. J. Garrido, M. J. Gil, A. Cornejo, V. Martínez-Merino, *J. Sol-Gel Sci. Technol.*, **86**, 316–328 (2018). https://doi.org/10.1007/s10971-018-4637-7

50. M. Mazúr, V. Mlynárik, M. Valko, P. Pelikán, *Appl. Magn. Reson.*, **18**, 187–197 (2000). https://doi.org/10.1007/BF03162110

51. R. A. Assink, B. D. Kay, *J. Non-Cryst. Solids*, **99**, 359–370 (1988). https://doi.org/10.1016/0022-3093(88)90441-3

52. N. Ueda, T. Gunji, Y. Abe, *J. Sol-Gel Sci. Technol.*, **48**, 163–167 (2008). https://doi.org/10.1007/s10971-008-1808-y

53. I. Abe, Y. Sato, R. Hayami, K. Yamamoto, S. Tsukada, T. Gunji, *Mater. Technol.*, **40**, 50–56 (2023). https://doi.org/10.51045/materialtechnology.40.6_50

54. Y. Sato, R. Hayami, T. Gunji, *J. Sol-Gel Sci. Technol.*, **104**, 36–52 (2022). https://doi.org/10.1007/s10971-022-05920-y

55. S. W. Kuo, *J. Polym. Res.*, **29**, 69 (2022). https://doi.org/10.1007/s10965-021-02885-4

56. M. Gon, K. Tanaka, Y. Chujo, *Polym. J.*, **50**, 109–126 (2018). https://doi.org/10.1038/pj.2017.56

57. F. Mammeri, E. L. Bourhis, L. Rozes, C. Sanchez, *J. Mater. Chem.*, **15**, 3787–3811 (2005). https://doi.org/10.1039/B507309J

58. C. Sanchez, B. Julián, P. Belleville, M. Popall, *J. Mater. Chem.*, **15**, 3559–3592 (2005). https://doi.org/10.1039/B509097K

59. M. Sánchez del Río, P. Martinetto, C. Reyes-Valerio, E. Dooryhée, M. Suárez, *Archaeometry*, **48**, 115–130 (2006). https://doi.org/10.1111/j.1475-4754.2006.00246.x

60. G. Philipp, H. Schmidt, *J. Non-Cryst. Solids*, **63**, 283–292 (1984). https://doi.org/10.1016/0022-3093(84)90407-1

61. H. Schmidt, *J. Sol-Gel Sci. Technol.*, **1**, 217–231 (1994). https://doi.org/10.1007/BF00486165

62. D. Avnir, D. Levy, R. Reisfeld, *J. Phys. Chem.*, **88**, 5956–5959 (1984). https://doi.org/10.1021/j150668a042

63. J. D. Mackenzie, E. P. Bescher, *J. Sol-Gel Sci. Technol.*, **13**, 371–377 (1998). https://doi.org/10.1023/A:1008600723220

64. H. H. Huang, B. Orler, G. L. Wilkes, *Polym. Bull.*, **14**, 557–564 (1985). https://doi.org/10.1007/BF00271615

65. T. Saegusa, Y. Chujo, *J. Macromol. Sci., Part A: Pure Appl. Chem.*, **27**, 1603-1612 (1990). https://doi.org/10.1080/00222339009351504

66. Y. Chujo, K. Tanaka, *Bull. Chem. Soc. Jpn.*, **88**, 633–643 (2015). https://doi.org/10.1246/bcsj.20150081

67. M. Hunsicker, A. Ankur, B. Morgenstern, M. Zimmer, D. Scheschkewitz, *Chem. - Eur. J.*, in press. https://doi.org/10.1002/chem.202303640

68. I. Hasegawa, *J. Sol-Gel Sci. Technol.*, **5**, 93–100 (1995). https://doi.org/10.1007/BF00487725

69. Y. Hagiwara, A. Shimojima, K. Kuroda, *Chem. Mater.*, **20**, 1147–1153 (2008). https://doi.org/10.1021/cm0716194

70. T. Gunji, T. Shioda, K. Tsuchihira, H. Seki, T. Kajiwara, Y. Abe, *Appl. Organomet. Chem.*, **24**, 545–550 (2010). https://doi.org/10.1002/aoc.1562

71. J. D. Lichtenhan, Y. A. Otonari, M. J. Carr, *Macromolecules*, **28**, 8435–8437 (1995). https://doi.org/10.1021/ma00128a067

72. J. D. Lichtenhan, N. Q. Vu, J. A. Carter, J. W. Gilman, F. J. Feher, *Macromolecules*, **26**, 2141–2142 (1993). https://doi.org/10.1021/ma00060a053

73. A. Igarashi, H. Imoto, K. Naka, *Polym. Chem.*, **13**, 1228–1235 (2022). https://doi.org/10.1039/D1PY01709H

74. M. Yoshimatsu, K. Komori, Y. Ohnagamitsu, N. Sueyoshi, N. Kawashima, S. Chinen, Y. Murakami, J. Izumi, D. Inoki, K. Sakai, T. Matsuo, K. Watanabe, M. Kunitake, *Chem. Lett.*, **41**, 622–624 (2012). https://doi.org/10.1246/cl.2012.622

75. J. F. Brown Jr., L. H. Vogt Jr., A. Katchman, J. W. Eustance, K. M. Kiser, K. W. Krantz, *J. Am. Chem. Soc.*, **82**, 6194–6195 (1960). https://doi.org/10.1021/ja01508a054

76. J. F. Brown Jr., *J. Am. Chem. Soc.*, **87**, 4317–4324 (1965). https://doi.org/10.1021/ja00947a017

77. H. Toyodome, Y. Higo, R. Sasai, J. Kurawaki, Y. Kaneko, *J. Nanosci. Nanotechnol.*, **13**, 3074–3078 (2013). https://doi.org/10.1166/jnn.2013.7416

78. T. Arake, K. Shikinaka, T. Sugioka, H. Hashimoto, Y. Sumida, Y. Kaneko, *Polymer*, **54**, 5643–5647 (2013). https://doi.org/10.1016/j.polymer.2013.08.035

79. A. Harada, K. Shikinaka, J. Ohshita, Y. Kaneko, *Polymer*, **121**, 228–233 (2017). https://doi.org/10.1016/j.polymer.2017.06.025

80. G. Kickelbick, D. Holzinger, C. Brick, G. Trimmel, E. Moons, *Chem. Mater.*, **14**, 4382–4389 (2002). https://doi.org/10.1021/cm021216y

81. F. Périneau, S. Pensec, C. Sanchez, C. Creton, L. Rozes, L. Bouteiller, *Polym. Chem.*, **2**, 2785–2788 (2011). https://doi.org/10.1039/C1PY00341K

82. S. Cochet, L. Rozes, M. Popall, C. Sanchez, *Mater. Sci. Eng. C,* **27**, 1401–1405 (2007). https://doi.org/10.1016/j.msec.2006.09.025

83. R. Hayami, K. Wada, Y. Miyase, T. Sagawa, S. Tsukada, K. Yamamoto, T. Gunji, *Polym. J.*, **50**, 1169–1177 (2018). https://doi.org/10.1038/s41428-018-0108-9

84. R. Hayami, K. Wada, I. Nishikawa, T. Sagawa, K. Yamamoto, S. Tsukada, T. Gunji, *Polym. J.*, **49**,

665–669 (2017). https://doi.org/10.1038/pj.2017.34

Chapter 2

Hydrolysis and condensation behaviors of tetraethoxysilane, hexaethoxydisiloxane, and octaethoxytrisiloxane

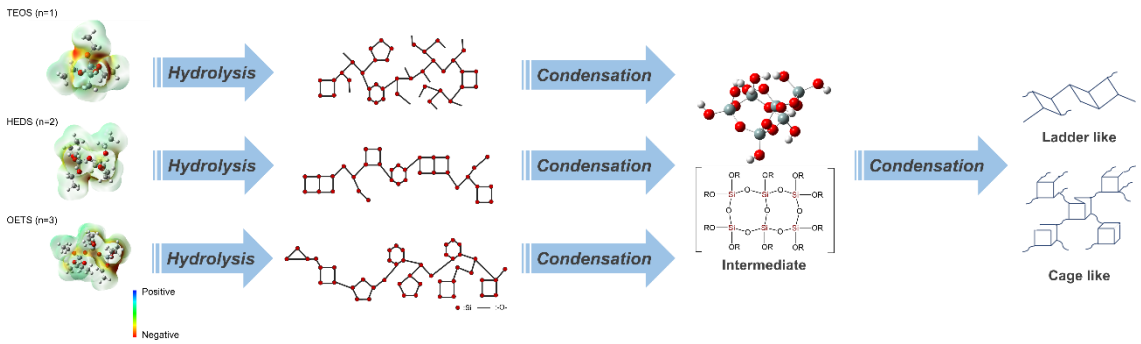

1 Introduction

During the initial hydrolysis–condensation of tetraethoxysilane (TEOS), linear oligosiloxanes, such as disiloxane and trisiloxane, are formed under acidic conditions. Subsequently, various species including long linear components, cyclic components, and randomly condensed structural oligomers and polymers are produced. Properties of low-molecular-weight polysiloxanes also differ according to the molecular weights and proportions of $Si(OSi)_n(OR)_{4-n}$ (n = 1–4; Q^n) in them [1,2]. Therefore, hydrolysis and condensation behaviors of alkoxysilanes can be hypothesized to depend on the structure of the raw material. Although hydrolyzates of hexaethoxydisiloxane (HEDS) and octaethoxytrisiloxane (OETS) have been identified by ^{29}Si nuclear magnetic resonance (NMR) spectroscopy [3–5], the hydrolysis–condensation behaviors of HEDS and OETS have not been investigated. Therefore, in this chapter, I report the hydrolysis–condensation behaviors of TEOS, HEDS, and OETS in detail based on instrumental analysis of the following two aspects: (i) estimation of hydrolyzability by adjusting the molar ratio on a monomer basis (hydrolysis section) and (ii) assessment of condensation ability by altering the molar ratio on the OEt group basis (H_2O) and Si basis (EtOH and HCl) (condensation). Furthermore, hydrolysis and condensation were conducted under acidic conditions based on the information provided in section 1.4.1 of chapter 1. Moreover, the reactivity of tetraisocyanatosilane and synthesis of an alkoxy-substituted isocyanatosilane from

tetraisocyanatosilane using a new synthetic method for alkoxydisiloxanes and trisiloxanes (Scheme 1) are reported.

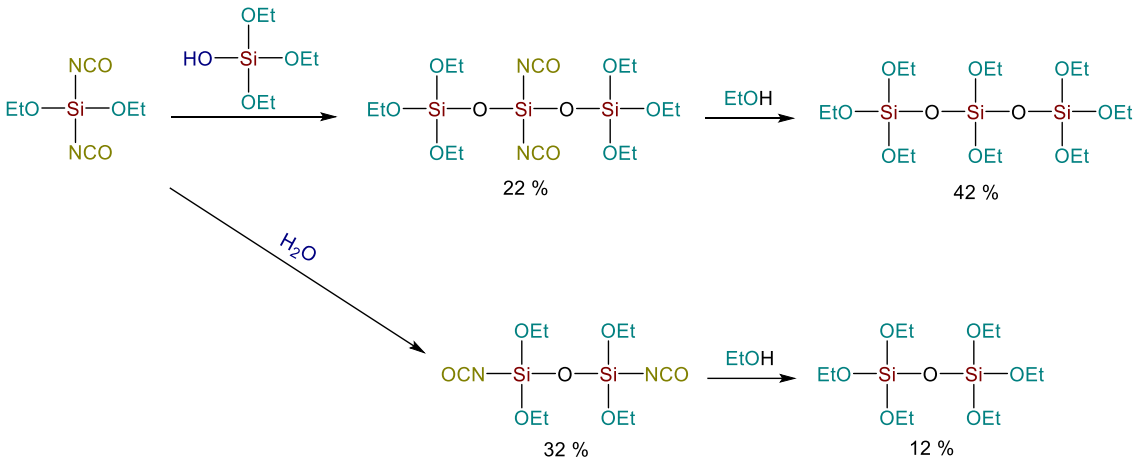

Scheme 1. Synthesis of alkoxydisiloxanes and trisiloxanes.

2 Experimental section

2.1 Measurements

Gas chromatography (GC) was performed using a GC-390 instrument (GL Science, Japan) equipped with an SE-30 capillary column (Agilent, USA) and a thermal conductivity detector. Helium was employed as the carrier gas. Column temperature was programmed as follows: injection temperature of 250 °C, isothermal state at 80 °C for 2 min, heating up to 200 °C at a rate of 10 °C min^{-1}, heating up to 280 °C at a rate of 20 °C min^{-1}, and holding at a final temperature of 280 °C for 2 min. GC/mass spectrometry (MS) (GC/MS) was conducted using a GCmate™ GC/MS double-focusing mass spectrometer (JEOL, Japan). Helium was used as the carrier gas. Column temperature was programmed as follows: injection temperature of 280 °C, isothermal state at 80 °C for 2 min, heating

up to 200 °C at a rate of 10 °C min^{-1}, heating up to 280 °C at a rate of 20 °C min^{-1}, and holding at a final temperature of 280 °C for 20 min. NMR spectra were recorded using a JEOL resonance JNM-ECZ 400 spectrometer (^{1}H: 400 MHz, ^{13}C: 100 MHz, and ^{29}Si: 80 MHz). Chemical shifts are reported in ppm relative to the residual chloroform in chloroform-*d* ($CDCl_3$) (^{1}H: 7.26 ppm), chloroform (^{13}C: 77.16 ppm), and tetramethylsilane ($^{29}Si\{^{1}H\}$: 0.00 ppm) as internal standards. For $^{29}Si\{^{1}H\}$ NMR spectroscopy, chromium(III) acetylacetonate was added to the sample as a paramagnetic relaxation agent. Fourier transform infrared (FTIR) spectra were acquired using an FTIR-6100 spectrophotometer (JASCO, Japan) using the neat method, in which the sample was sandwiched between two KBr crystal disks. High-resolution electrospray ionization time-of-flight MS (HR-ESI-TOF MS) was performed using JEOL JMS-T100CS AccuTOF CS. Molecular weights of the oligomers and polymers were determined by gel permeation chromatography (GPC) using an LC-20AD HPLC prominent liquid chromatograph (Shimadzu, Japan) attached to a PLgel 5-μm Mixed-D column. Tetrahydrofuran (THF) was utilized as an eluent (1 mL min^{-1}), and RID-20A was used as a detector at 40 °C. Molecular simulations of ethoxysilane oligomers were conducted using quantum chemical calculations. Optimized structures, electrostatic potential (ESP) maps, dipole moments, and solvation-free energies for TEOS, HEDS, and OETS were evaluated at the B3LYP/6-31 G(d,p) level of theory using Gaussian 16 [6].

2.2 Materials

Ethanol (EtOH), THF, toluene, and diethyl ether were purified using standard processes and stored over activated molecular sieves. Tetraisocyanatosilane was provided by Matsumoto Fine Chemical Co., Ltd. (Japan). Ammonium carbonate ($(NH_4)_2CO_3$) and molecular sieves were purchased from Kanto Chemical Co., Inc. (Japan). Anhydrous sodium sulfate, *N*,*N*-dimethylformamide (DMF), and 6 M hydrochloric acid (HCl aq.) were procured from FUJIFILM Wako Pure Chemical Corporation (Japan). TEOS, thionyl chloride ($SOCl_2$), chloro(trimethyl)silane, and chromium(III) acetylacetonate were purchased from Tokyo Chemical Industry Co., Ltd. (Japan). TEOS and tetraisocyanatosilane were purified by distillation (106.5–111.0 °C under 160 mmHg and 133.5–136.5 °C under 123 mmHg, respectively).

2.3 Synthesis of diethoxydiicocyanatosilane (DEDIS)

According to a previous procedure [7], a mixture of ethanol (9.2 g, 0.2 mol) and diethyl ether (40 mL) was added dropwise to a mixture of tetraisocyanatosilane (19.62 g, 0.1 mol) and diethyl ether (160 mL) at 0 °C. Then, a mixture was stirred at room temperature for 10 min followed by stirring at 40 °C overnight (o.n.). After the reaction, the solvent was evaporated. DEDIS was obtained as a colorless liquid (18.4 g, 91%) by distillation (77.2–78.1 °C under 23 mmHg).

^{1}H NMR (400 MHz, $CDCl_3$): δ (ppm) 3.88 (q, *J* = 6.0 Hz, CH_2, 4H), 1.25 (t, *J* = 6.0 Hz, CH_3, 6H).

^{29}Si NMR (80 MHz, $CDCl_3$): δ (ppm) −93.2.

2.4 Synthesis of chloro(triethoxy)silane (CTES)

According to a previous procedure [8,9], a mixture of $SOCl_2$ (59.8 g, 0.50 mol) and DMF (0.5 mL) was cooled in an ice bath, and TEOS (104 g, 0.50 mol) was slowly introduced dropwise into the abovementioned mixture followed by stirring for 1 h in the ice bath and then for o. n. at room temperature. Subsequently, the volatiles were evaporated under reduced pressure, followed by distillation under reduced pressure (67.0–68.8 °C under 76 mmHg), affording 89.3 g (92% yield) CTES as a colorless liquid.

^{1}H NMR (400 MHz, $CDCl_3$): δ (ppm) 3.90 (q, 6H, J = 6.0 Hz, CH_2), 1.26 (t, 9H, J = 6.0 Hz, CH_3).

^{29}Si NMR (80 MHz, $CDCl_3$): δ (ppm) −70.1.

2.5 Synthesis of triethoxysilanol (TESOL)

According to a previous procedure [8,9], CTES (9.98 g, 0.05 mol) dissolved in THF (100 mL) was added dropwise to a mixture of THF (as-received) (250 mL), $(NH_4)_2CO_3$ (24.22 g, 0.25 mol), and water (0.90 g, 0.05 mol) in an ice bath. Thereafter, the mixture was stirred for 1 h at ca. 23 °C. After filtration, the volatiles were removed under reduced pressure, followed by vacuum

distillation (b.p.: 56.3–61.2 °C under 3.1 mmHg), providing 6.8 g (76% yield) TESOL as a colorless liquid.

^{1}H NMR (400 MHz, $CDCl_3$): δ (ppm) 4.50 (s, 1H, OH), 3.83 (q, 6H, J = 6.0 Hz, CH_2), 1.21 (t, 9H, J = 6.0 Hz, CH_3).

^{13}C NMR (125 MHz, $CDCl_3$): δ (ppm) 18.0 (CH_3), 59.4 (CH_2).

^{29}Si NMR (100 MHz, $CDCl_3$): δ (ppm) −78.7.

FTIR (neat, cm^{-1}): 3403 (νO-H), 2976, 2929, 2895 (νC-H), 1170 (ρCH_3), 1103 (νSi-O-C), 966 (νC-C), 905 (νSi-O-H).

2.6 Synthesis of 1,1,3,3-tetraethoxy-1,3-diisocyanatodisiloxane (TEDIDS)

A solution of water (0.18 g, 0.01 mol) and THF (20 mL) was introduced dropwise into a solution of DEDIS (4.04 g, 0.02 mol) and THF (20 mL) at 0 °C. The solution was stirred at 0 °C for 2 h followed by stirring at room temperature or 85 °C for a specified time. The solution was dried over anhydrous sodium sulfate followed by filtration and evaporation. TEDIDS was isolated by distillation.

TEDIDS: colorless liquid; yield: 13–32%; b.p.: 54.8–58.9 °C under 0.25 mmHg; ^{1}H NMR (400 MHz, $CDCl_3$): δ (ppm) 3.90–3.85 (m, 8H, CH_2), 1.28–1.23 (m, 12H, CH_3); ^{29}Si NMR (80 MHz, $CDCl_3$): δ (ppm) −94.6.

2.7 Synthesis of 1,1,1,5,5,5-hexaethoxy-3,3-diisocyanatotrisiloxane (HEDITS)

A solution of TESOL and THF (20 mL) was added dropwise to a solution of DEDIS (4.04 g, 0.02 mol) and THF (20 mL) at 0 °C. Then, the solution was stirred at 0 °C for 2 h, followed by stirring at room temperature for a set time. After completion of this reaction, the solvent was evaporated, and HEDITS was obtained by distillation.

HEDITS: colorless liquid; yield: 24–44%; 100.8–104.8 °C under 1.3 mmHg; ^{1}H NMR (400 MHz, $CDCl_3$): δ (ppm) 3.88–3.77 (m, 12H), 1.23–1.16 (m, 18H); ^{13}C NMR (100 MHz, $CDCl_3$): δ (ppm) 122.5 (NCO), 59.0 (CH_2), 17.6 (CH_3); ^{29}Si NMR (80 MHz, $CDCl_3$): δ (ppm) −88.8, −89.0; IR (cm^{-1}): 2978, 2929, 2894, 2290, 1169, 1103, 1081; HRMS (HR-ESI-TOF) m/z: Calcd. for $C_{14}H_{31}N_2O_{10}Si_3$: 471.1208 $[M+H]^+$; Found: 471.1459.

2.8 Synthesis of HEDS and OETS

Based on the alcoholysis of isocyanatosilane [10], TEDIDS (2 mmol) and HEDITS (1.5 mmol) were separately dissolved in THF (1 mL). Subsequently, 20 equiv. EtOH against oligosiloxane was separately introduced into the resulting solutions followed by refluxing for o.n. After the reaction, the solvents were evaporated followed by distillation to separately achieve HEDS and OETS.

HEDS: colorless liquid; yield: 12%; b.p.: 51.4–54.2 °C under 0.5 mmHg; ^{1}H NMR (400 MHz, $CDCl_3$):

δ (ppm) 3.83 (q, J = 6.0 Hz, 12H, CH_2), 1.20 (t, J = 6.0 Hz, 18H, CH_3); ^{13}C NMR (100 MHz, $CDCl_3$): δ (ppm) 59.2 (CH_2), 18.1 (CH_3); ^{29}Si NMR (80 MHz, $CDCl_3$): δ (ppm) −88.8.

OETS: colorless liquid; yield: 42%; b.p.: 90.2–90.5 °C under 0.3 mmHg; ^1H NMR (400 MHz, $CDCl_3$): δ (ppm) 3.79–3.74 (m, 16H), 1.15–1.11 (m, 24H); ^{13}C NMR (100 MHz, $CDCl_3$): δ (ppm) 59.3 (CH_2), 59.2 (CH_2), 18.1 (CH_3), 18.6 (CH_3); ^{29}Si NMR (80 MHz, $CDCl_3$): δ (ppm) −89.0, −96.2.

2.9 Initial hydrolysis of ethoxysilane monomers

HCl aq. was slowly added to an EtOH solution of an ethoxysilane monomer (TEOS, HEDS, or OETS) in an ice bath, and the HCl:H_2O:EtOH:monomer molar ratio was 0.1:2:10:1. After stirring the mixture in an ice bath for 10 min, chloro(trimethyl)silane (equal to the molar amount of H_2O) was introduced into the mixture to stop hydrolysis. Thereafter, the acquired mixture was poured into a mixture of hexane/THF (1/2 v/v) followed by washing twice with water and twice with brine. The organic layer was dried over anhydrous sodium sulfate followed by filtration and evaporation. The obtained residue was characterized by MS and $^{29}Si\{^1H\}$ NMR spectroscopy.

2.10 Hydrolysis behaviors of ethoxysilane monomers

HCl aq. was slowly added to an EtOH solution of an ethoxysilane monomer (TEOS, HEDS, or OETS) in an ice bath, and the HCl:H_2O:EtOH:monomer molar ratio was 0.1:2:10:1. After stirring the mixture

in an ice bath for 10 min, the acquired mixture was brought to room temperature. Then, the mixture was aged for GPC and $^{29}Si\{^{1}H\}$ NMR spectroscopy.

2.11 Condensation of ethoxysilane monomers

HCl aq. was slowly introduced into an EtOH solution of an ethoxysilane monomer (TEOS, HEDS, or OETS) in an ice bath, and the HCl:Si, H_2O:OEt, and EtOH:Si molar ratios were 0.1, 0.5, and 4, respectively. After stirring in an ice bath for 10 min, the mixture was brought to room temperature and maintained at this temperature for 24 h. Thereafter, the acquired mixture was poured into a mixture of hexane/THF (1/2 v/v) followed by washing twice with water and twice with brine. The organic layer was dried over anhydrous sodium sulfate followed by filtration and evaporation. The obtained residue was characterized by GPC and $^{29}Si\{^{1}H\}$ NMR spectroscopy. Subsequently, it was distilled under reduced pressure to achieve a distillate (LS) and a residue (HS) with low and high molecular weights, respectively. The residue was characterized by GPC and $^{29}Si\{^{1}H\}$ NMR spectroscopy. In contrast, the distillate was characterized by MS, GPC, and $^{29}Si\{^{1}H\}$ NMR spectroscopy.

3 Results and discussion

3.1 Reactivity of DEDIS

DEDIS was used as the raw material for the selective syntheses of HEDS and OETS. Substitution

reactivities of isocyanatosilanes are lower than those of chlorosilanes and higher than those of the corresponding alkoxysilanes [11–14]. We have previously reported the synthesis of partially alkoxy-substituted isocyanatosilanes by the reaction of tetraisocyanatosilane with an alcohol and isolation of these isocyanatosilanes [10] as isocyanatosilanes are easier to handle than chlorosilanes. However, to date, the reactivities of alkoxy-substituted isocyanatosilanes have not been investigated. In this section, the reactivities of DEDIS with water and silanol are discussed.

To prepare TEDIDS, hydrolysis–condensation of DEDIS was performed according to Scheme 2; the corresponding results are presented in Table 1. TEDIDS yield depended on the reaction temperature and time. When condensation was conducted at 85 °C for 3 h (Entry 1), the TEDIDS yield was 13% because condensation was favored to form oligosiloxanes which have higher numbered silicon atoms. When the reaction was performed at room temperature (23 °C) for 3 h (Entry 2), the TEDIDS yield was maximum (32%). Nevertheless, the TEDIDS yield decreased to 28% when the reaction was conducted for 16 h (Entry 3). The TEDIDS yield attained via the ethanolysis of hexa(isocyanato)disiloxane acquired from tetraisocyanatosilane was 11% [11]; in contrast, the TEDIDS yield obtained via the ethanolysis of DEDIS achieved from tetra(isocyanate)silane was 29%. Hence, this method is useful for synthesizing disiloxanes containing isocyanate and alkoxy groups.

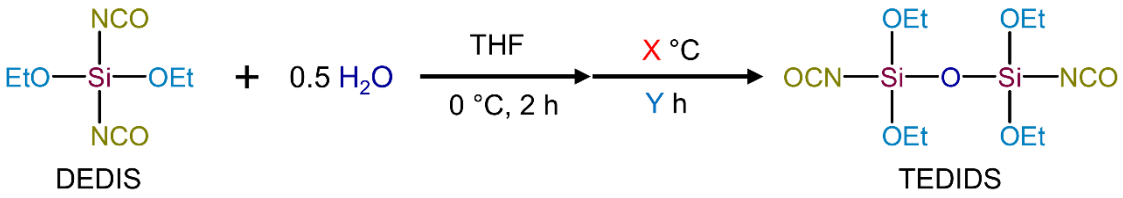

Scheme 2. Synthesis of TEDIDS via the hydrolysis of DEDIS.

Table 1 Synthetic conditions and TEDIDS yields

Entry	Temperature[a] (°C)	Time[b] (h)	Yield (%)
1	85	3	12
2	23	3	32
3	23	16	28

[a]Corresponding to “X” in Scheme 2

[b]Corresponding to “Y” in Scheme 2

Reaction between DEDIS and TESOL was monitored by GC/MS for 8 h (Figure 1), and a strong signal attributed to ethanol was observed, indicating that the reaction proceeded between Si–OH and Si–OEt rather than between Si–OH and Si–NCO. Signals of DEDIS, triethoxy(isocyanato)silane (TEIS), and TEOS were noticed, implying the reaction of DEDIS with ethanol. Additionally, the signals of 1,3,3,3-tetraethoxy-1,1-diisocyanatodisiloxane (TE-1,1-DIDS) and HEDS were identified, supporting the ethanolysis of TE-1,1-DIDS and/or condensation between TEOS and TESOL or between TEIS and TESOL. Signals of HEDITS and OETS were also observed. Moreover, although

several other signals were noticed, the corresponding structures could not be determined either because the molecular ion peak could not be identified or because of the presence of many plausible isomers. Reaction between DEDIS and TESOL produced TE-1,1-DIDS and ethanol, whereas reaction between TE-1,1-DIDS and TESOL furnished HEDITS and ethanol (Scheme 3). As the generated ethanol attacked Si–NCO, the reaction mixture was a complex because of the formation of various compounds during ethanolysis. HEDITS in the reaction mixture was isolated by distillation because the reactive isocyanato group was protected by two bulky triethoxysiloxy groups. The isolated yield of HEDITS depended on the reaction time and additional molar amount of TESOL (Table 2). Isolated yield of HEDITS initially increased (Entries 1 and 2) and then decreased (Entry 3) owing to ethanolysis and siloxane bond formation. When the molar ratio was set to 2 (Entry 3), HEDITS could not be isolated by distillation because the distillate comprised several by-products. HEDS and OETS were acquired in 12 and 42% yields by the ethanolysis of TEDIDS and HEDITS, respectively. To obtain more information on the identification of HEDITS, isopropoxylation in the presence of triethylamine of HEDITS without catalyst was considered. However, this reaction afforded a complicated mixture.

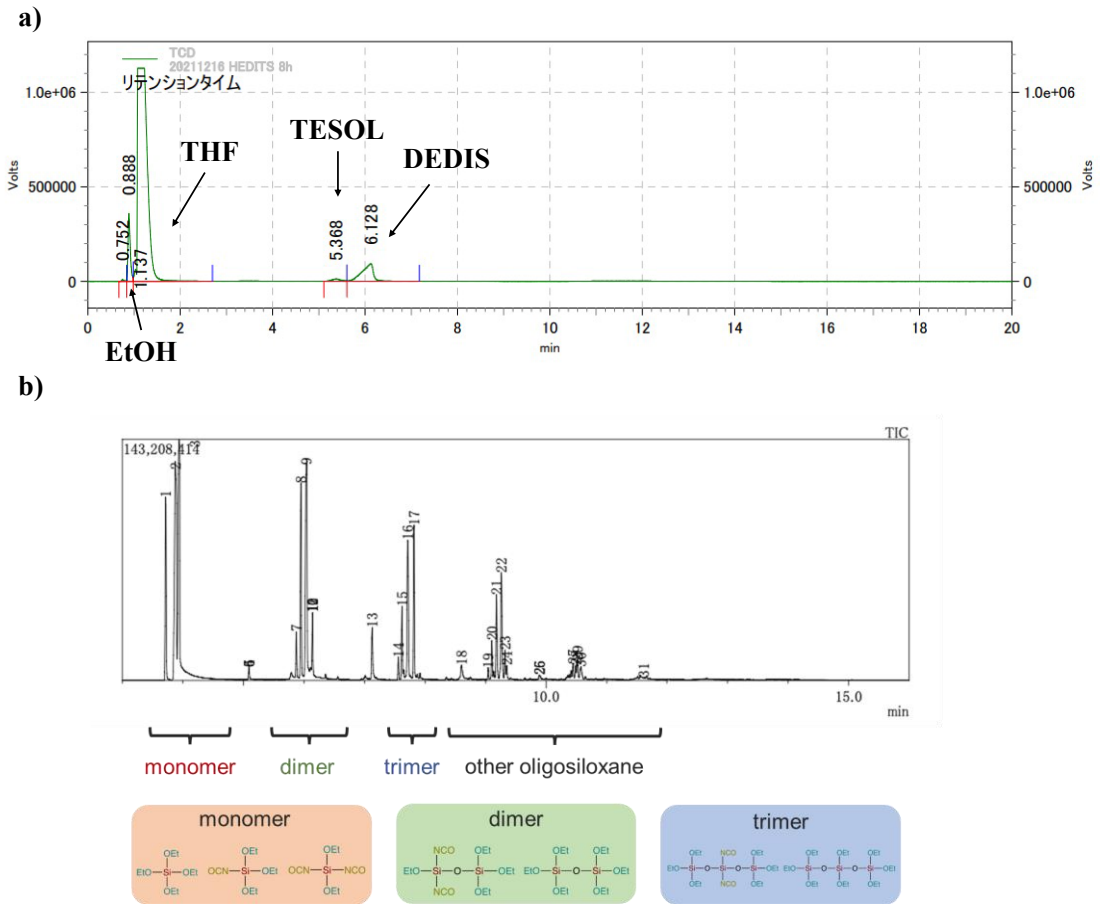

Figure 1. GC traces of the reaction solution of HEDITS monitored for 8 h via a) GC and b) GC/MS.

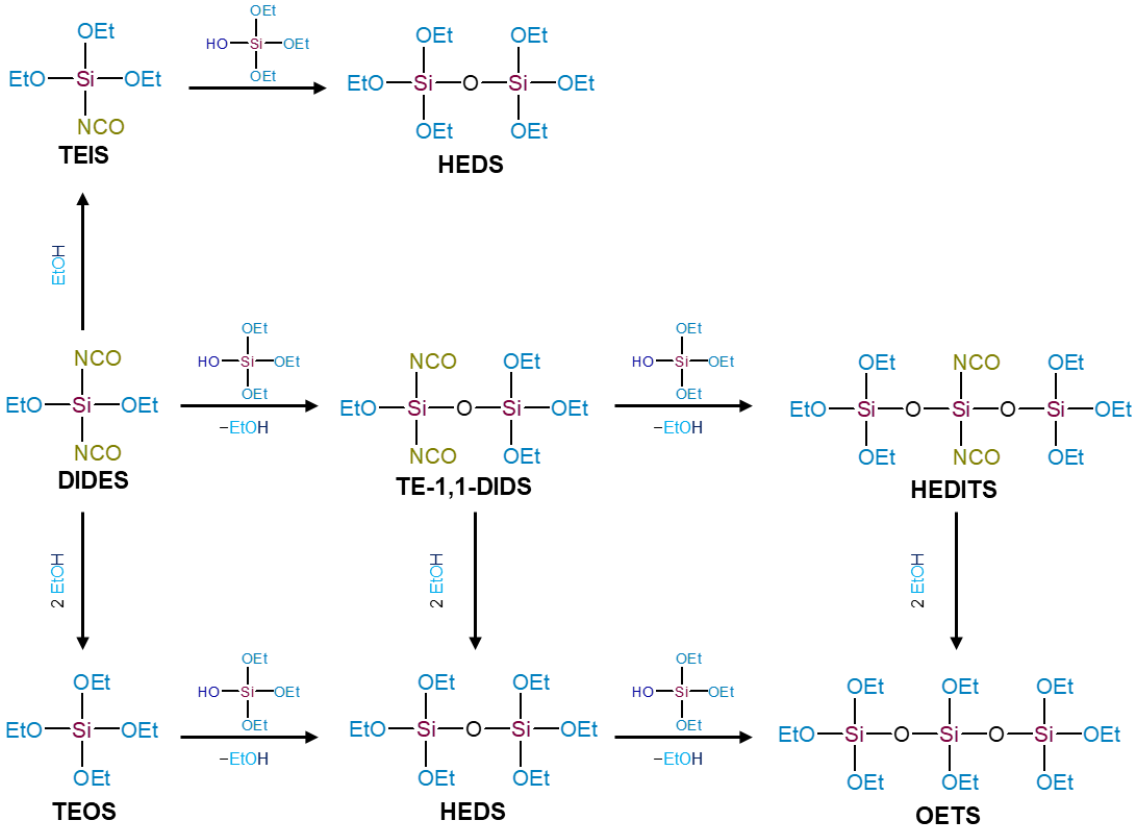

Scheme 3. Reaction between DEDIS and TESOL.

Table 2 Isolated yields of HEDITS obtained by the reaction of DEDIS with TESOL

Entry	TESOL (equiv.)	Time (day)	Isolated yield of HEDITS (%)	
			Based on DEDIS	Based on TESOL
1	1	0.67	18	36
2	1	2.00	22	44
3	1	3.00	12	24
4	2	0.67	– [a]	

[a]Complicated mixture

^{29}Si NMR spectra of tetraisocyanatosilane, DEDIS, TEDIDS, HEDITS, HEDS, and OETS are shown in Figure 2. Chemical shift of the Q^1 unit for $-OSi(OEt)_3$ appeared at −88.8 ppm. In contrast, the chemical shift of the Si atom bound to the isocyanate group was irregular. Generally, the chemical shift is influenced by the shielding effects of $p(X)\pi \rightarrow d(Si)\pi$ and $p(X)\pi \rightarrow \sigma^*(Si–Y)$ and bonding angles around the Si atom [15,16]. Signal of tetraisocyanatosilane emerged in the high magnetic field due to the shielding effect of $p(N)\pi \rightarrow d(Si)\pi$ [10,17,18]. Chemical shifts of DEDIS, TEDIDS, and HEDITS were observed at lower magnetic fields than that for tetraisocyanatosilane.

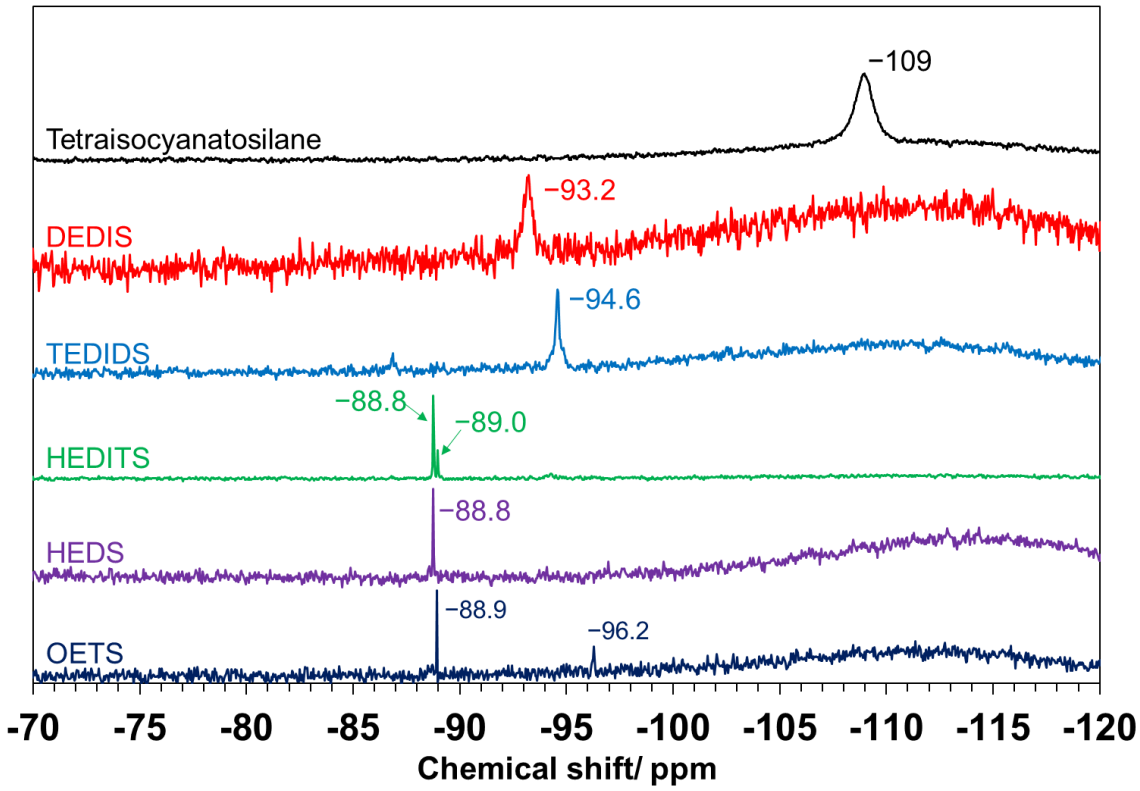

Figure 2. ^{29}Si NMR spectra of tetraisocyanatosilane, DEDIS, TEDIDS, HEDITS, HEDS, and OETS.

FTIR spectra of DEDIS, TEDIDS, HEDITS, HEDS, and OETS are shown in Figure 3, and the assignments are presented in Table 3. Absorption bands were assigned based on the vibrational frequencies of tetraisocyanatosilane, triethoxysilane, and tetraethoxysilane (TEOS) [19–23]. Spectra of all siloxanes except for that of DEDIS exhibited the υSiOSi peak at approximately 795 cm^{-1}. Spectra of DEDIS, TEDIDS, and HEDITS demonstrated a band corresponding to υNCO at approximately 2285 cm^{-1}, which was not observed for HEDS and OETS.

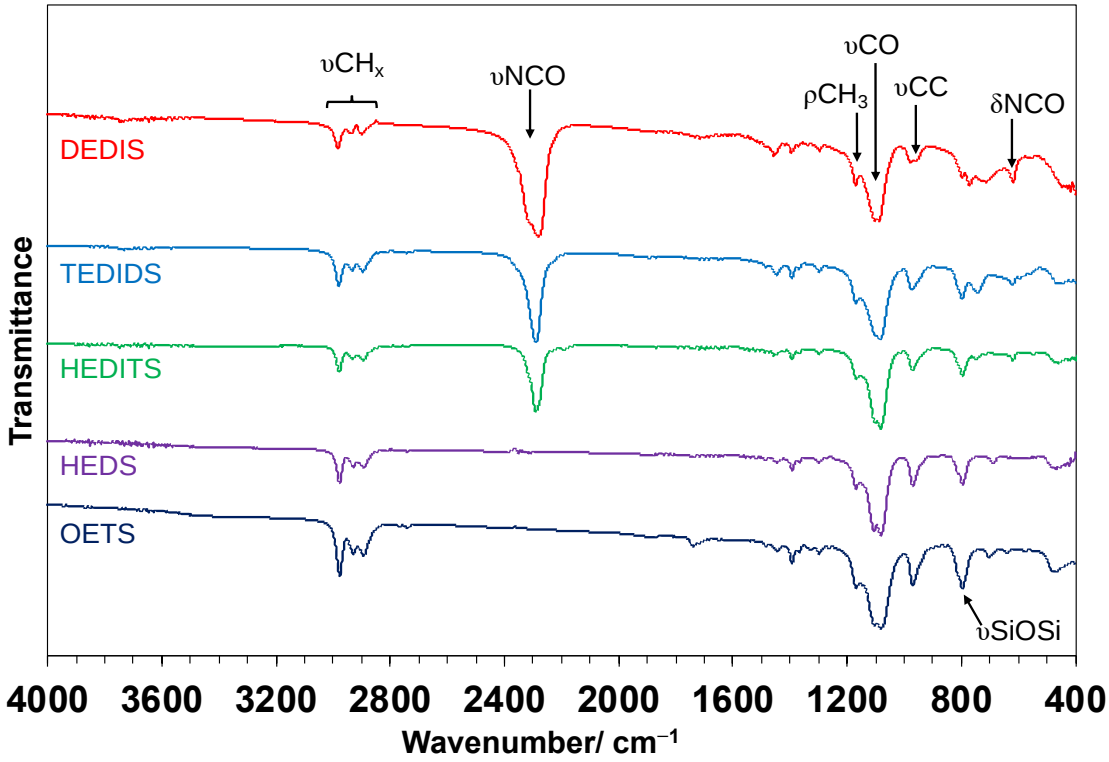

Figure 3. FTIR spectra of DEDIS, TEDIDS, HEDITS, HEDS, and OETS acquired using the neat method.

Table 3 FTIR assignments of DEDIS, TEDIDS, HEDITS, HEDS, and OETS

Wavenumber (cm^{-1})[a]					Assignment[b]
DEDIS	TEDIDS	HEDITS	HEDS	OETS	
2983m	2980m	2980m	2978m	2977m	$\upsilon_{as}CH_3$
2940w	2930w	2930w	2930w	2930w	$\upsilon_{s}CH_2$
2901w	2897w	2895w	2893w	2893w	$\upsilon_{s}CH_3$
2281s	2289s	2291s	–	–	υNCO
1453w	1447w	1449w	1445w	1443w	δCH_3
1394vw	1394vw	1394vw	1394vw	1394vw	δCH_2
1299vw	1297vw	1295vw	1297vw	1297vw	δCH_2
1172m	1171m	1169m	1170m	1169m	ρCH_3
1105s	1104s	1103s	1106s	1105s	υCO
1086s	1081s	1082s	1082s	1080s	υCO
980w	975w	971w	970m	970m	υCC, ρCH_3
–	796m	795m	795m	796m	υ_{s}SiOSi
771m	–	–	–	–	
–	740w	746vw	–	–	
–	–	–	688vw	703vw	
618w	619vw	618vw	–	–	δNCO
–	459w	468w	473w	477w	δSiOSi
448w	447sh	448sh	447sh	448sh	δCCO

[a]s: strong, m: middle, w: weak, vw: very weak, and sh: shoulder

[b]υ: stretching, δ: scissoring, ρ: rocking, as: asymmetric, and s: symmetric

3.2 Hydrolysis–condensation of TEOS, HEDS, and OETS

Reaction between alkoxysilanes and water is a well-known competitive reaction involving hydrolysis and condensation. The rate of hydrolysis is higher than that of condensation [24,25], and condensation slows down at low temperatures (<0 °C) [26]. At first, I performed hydrolysis of ethoxysilane monomers (TEOS, HEDS, and OETS) with the HCl:H_2O:EtOH:monomer molar ratio of 0.1:2:10:1 at 0 °C for 10 min. To examine hydrolysis during 10 min at 0 °C, silanol in the

hydrolyzed ethoxysilanes was capped using chlorotrimethylsilane [27,28], and the structures of TEOS–TMS, HEDS–TMS, OETS–TMS were estimated by MS and $^{29}Si\{^{1}H\}$ NMR spectroscopy. Furthermore, to investigate hydrolysis, hydrolysis of ethoxysilane monomers was performed at 0 °C for 10 min followed by aging at room temperature (23 °C). Hydrolyzates of the ethoxysilane oligomers were analyzed by ^{29}Si NMR spectroscopy and GPC. Next, I conducted the condensation of ethoxysilane monomers with the HCl/Si, H_2O/OEt, and EtOH/Si molar ratios of 0.1, 2, and 4, respectively. The reaction was investigated at 0 °C for 10 min and then at room temperature for 24 h followed by isolation of the polymer by trimethylsilylation of chlorotrimethylsilane [27,28]. C_{TEOS}, C_{HEDS}, and C_{OETS}, which are isolated polymer from TEOS, HEDS, and OETS, respectively, were calculated by GPC and $^{29}Si\{^{1}H\}$ NMR spectroscopy. Moreover, Cs were separated into the low- and high-molecular-weight components LS and HS by vacuum distillation, respectively. LS and HS were also characterized by GPC, MS, and $^{29}Si\{^{1}H\}$ NMR spectroscopy. These processes are depicted in Figure 4.

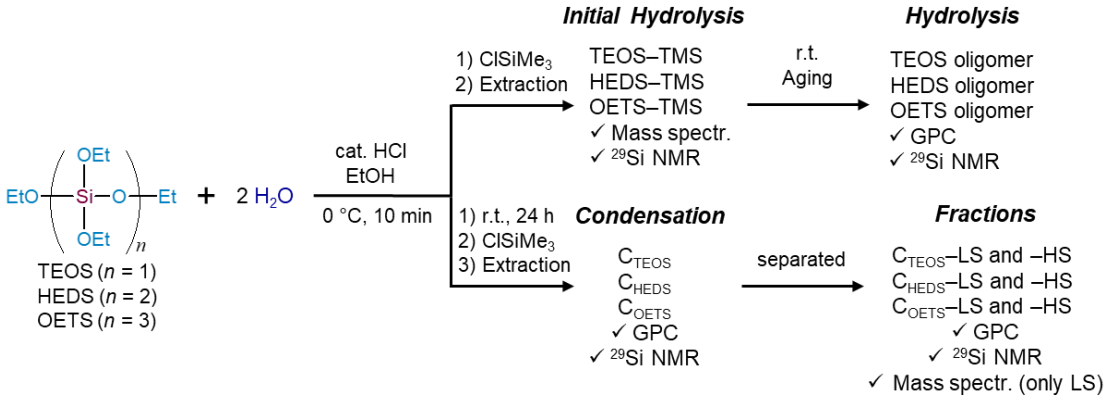

Figure 4. Experimental procedures for the hydrolysis and condensation of ethoxy oligosiloxanes.

3.2.1 Initial hydrolyzates of TEOS, HEDS, and OETS

Progress of trimethylsilylation was confirmed by the appearance of the adsorption bands corresponding to δSi–Me (at approximately 1250 cm^{-1}) and ρSi–Me (at approximately 840 cm^{-1}) and absence of the band related to υSi–OH (at approximately 950 cm^{-1}) in the FTIR spectrum (Figure 5) [22,29,30]. No υSi–O–Si adsorption band was observed at 1200–1100 or 1040–1000 cm^{-1}; hence, the main structures of ethoxysilane–TMSs were attributed to their linear, branched, and cyclic forms [22,31]. Mass spectra of the ethoxysilane–TMSs are shown in Figure 6 (the attribution results are provided in Table S1). TEOS–TMS was verified to be a mixture of linear (from trimer to octamer) and cyclic (from tetramer to heptamer) oligosiloxanes, and the primary components were trimers, tetramers, and pentamers. This result was similar to that of the general hydrolysis of TOES under acidic conditions [27,32]. HEDS–TMS was confirmed to be a mixture of linear (from dimer to octamer) and cyclic (from tetramer to heptamer) oligosiloxanes, and the main components were tetramers. Peak intensities of the mass spectra of the oligosiloxanes with an even number of Si atoms in the primary structure were higher than those for the oligosiloxanes with an odd number of Si atoms, indicating that rearrangement hardly proceeded. Main structure of OETS–TMS consisted of trimers. $^{29}Si\{^{1}H\}$ NMR spectra of ethoxysilane–TMSs are depicted in Figure 7, and the corresponding

assignments are presented in Table 4. M^1/Q ratio was in the following order: TEOS–TMS > HEDS–TMS > OETS–TMS, which was consistent with the relationship between the amount of water added and number of alkoxy groups (H_2O/OEt = 0.50 for TEOS, 0.33 for HEDS, and 0.25 for OETS). Degrees of M^1 for TEOS–, HEDS–, and OETS–TMSs were 47.0, 56.3, and 72.8%, respectively. Compositions of the siloxane unit structures a, b, c, d, and e (Table 5) were determined based on the signal areas of the $^{29}Si\{^1H\}$ NMR spectra of ethoxysilane–TMSs (Figure 8). The unit a was ascribed to the end group, whereas the units b, c, and d were attributed to the linear or cyclic structures. The unit e was ascribed to the branched structure. These results verified that ethoxysilane–TMSs mainly comprised the unit a, as shown in Figure 5 (TEOS–TMS: 58.1%, HEDS–TMS: 70.6%, and OETS–TMS: 56.7%) without the Q^4 signal.

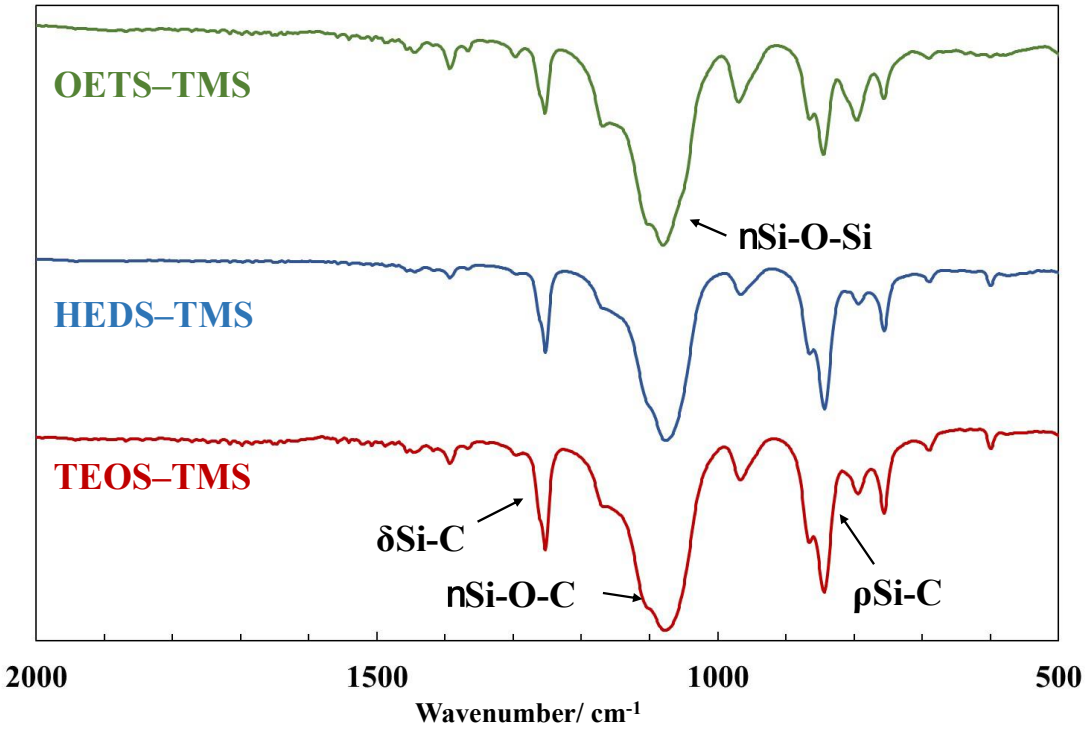

Figure 5. FTIR spectra of top) OETS–TMS, middle) HEDS–TMS, and bottom) TEOS–TMS (neat method).

a) TEOS–TMS

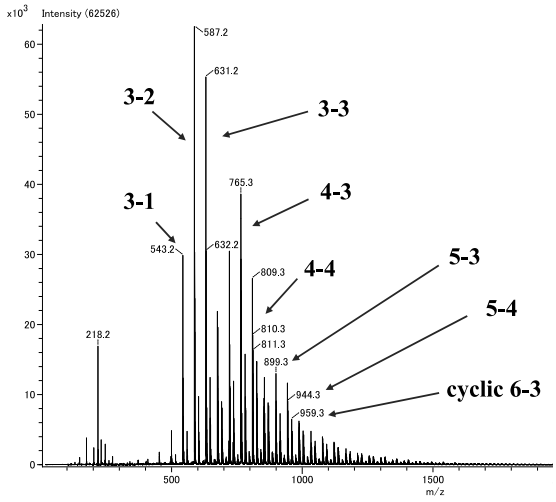

b) HEDS–TMS

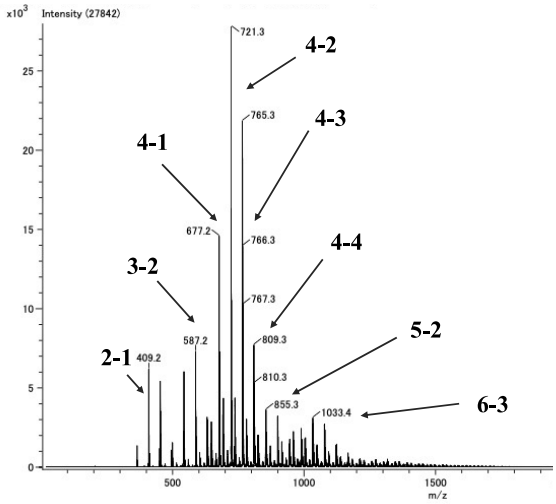

c) OETS–TMS

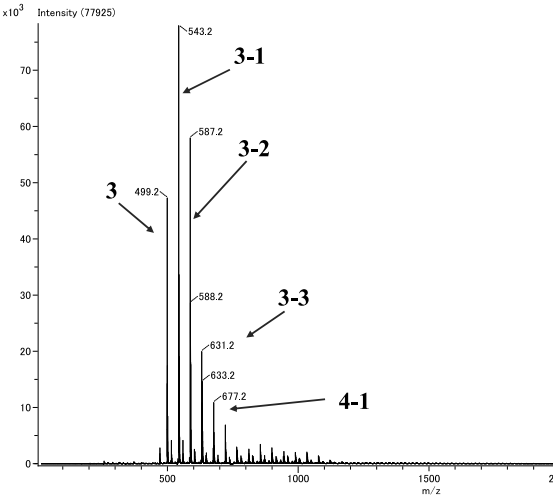

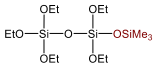

2-1
(409.2)

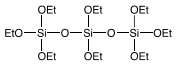

3
(499.2)

$Si_3O_2(OEt)_7(OSiMe_3)_1$
3-1
(543.2)

$Si_3O_2(OEt)_6(OSiMe_3)_2$
3-2
(587.2)

$Si_3O_2(OEt)_5(OSiMe_3)_3$
3-3
(631.2)

$Si_4O_3(OEt)_9(OSiMe_3)_1$
4-1
(677.2)

$Si_4O_3(OEt)_8(OSiMe_3)_2$
4-2
(721.3)

$Si_4O_3(OEt)_7(OSiMe_3)_3$
4-3
(765.3)

$Si_4O_3(OEt)_6(OSiMe_3)_4$
4-4
(809.3)

$Si_5O_4(OEt)_{10}(OSiMe_3)_2$
5-2
(855.3)

$Si_5O_4(OEt)_9(OSiMe_3)_3$
5-3
(899.3)

$Si_5O_4(OEt)_8(OSiMe_3)_4$
5-4
(944.3)

$Si_6O_6(OEt)_9(OSiMe_3)_3$
cyclic 6-3
(959.3)

$Si_6O_5(OEt)_{11}(OSiMe_3)_3$
6-3
(1033.4)

Figure 6. ESI-MS spectra of a) TEOS–TMS, b) HEDS–TMS, and c) OETS–TMS detected as $[M + Na]^+$.

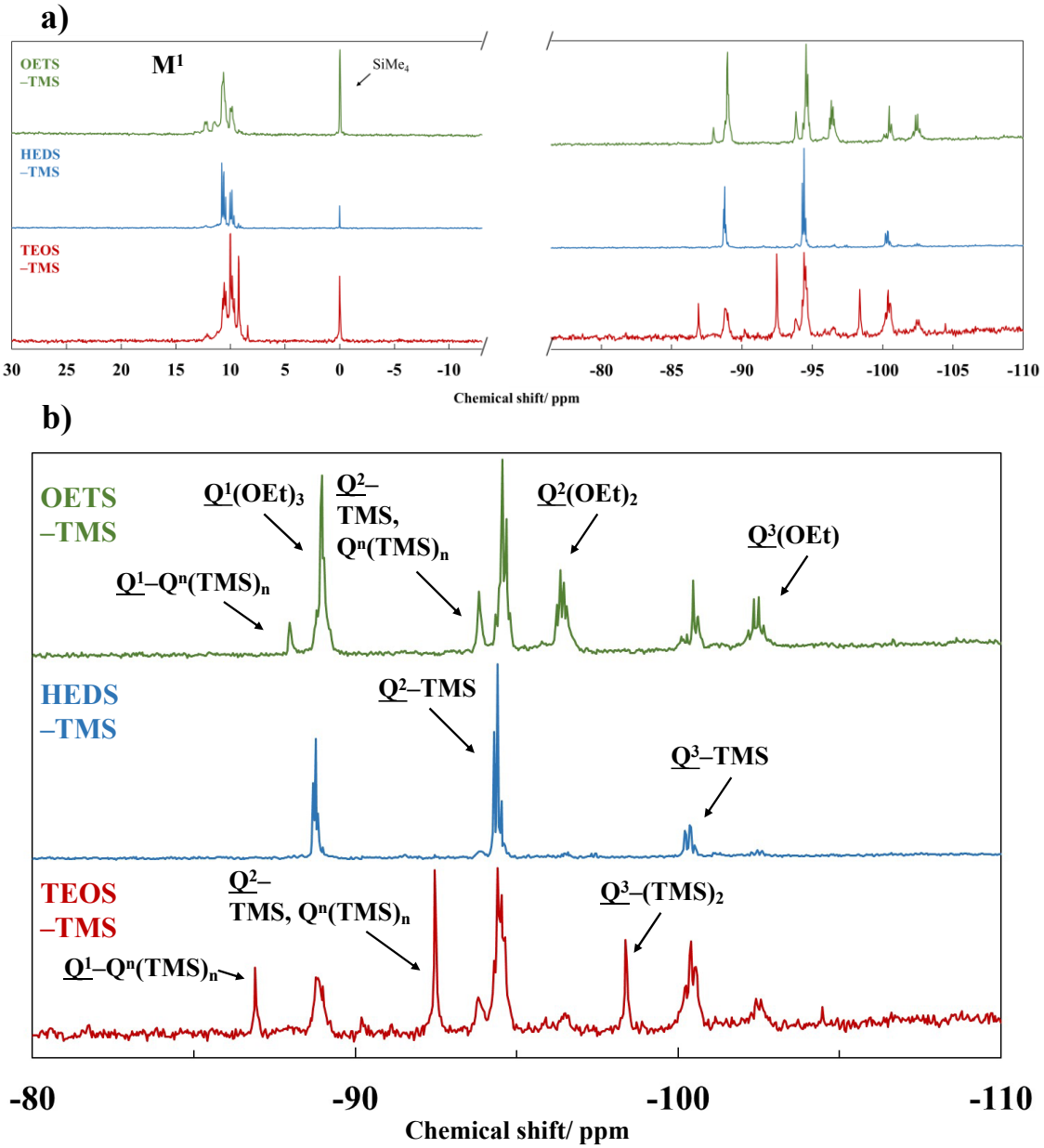

Figure 7. $^{29}Si\{^1H\}$ NMR spectra of TEOS–, HEDS–, and OETS–TMSs: a) from 30 to -110 ppm region and b) from -80 to -110 ppm region.

Table 4 Assignments for the $^{29}Si\{^1H\}$ NMR spectra of ethoxysilane–TMSs

Q^n unit	Chemical shift of Q^n unit prepared from linear ethoxy oligosiloxanes/ppm

	TEOS–TMS	HEDS–TMS	OETS–TMS
monomer	−81.9	−88.8	−88.9, −96.2
M^1	10.7–8.4	11.1–10.0	13.3–9.9
$Q^1(OEt)_3$	−88.8	−88.7–88.9	−88.9
Q^1–$Q^n(TMS)_n$	-86.9	−88.0	
$Q^2(OEt)_2$	−95.9–−96.5	−96.6–−97.5	−96.2–−96.5
Q^2–TMS	from −94.3 to −94.6, −93.8, −92.5	from −94.3 to −94.5, −93.9	−94.6–−94.7, 93.8
$Q^3(OEt)$	−102.4–−102.6	−101.2–−102.5	−102.3–−102.5
Q^3–(TMS)	−100.2–−100.6	−100.2–−100.5	−100.1–−100.5
Q^3–$(TMS)_2$	−98.4		

Table 5 Relative ratios of the siloxane unit structures for ethoxysilane–TMSs

ethoxysilane–TMS	M^1/M^1Q^a ratio (%)	Ratio of structural units[b] (%)				
		a	b	c	d	e
TEOS–TMS	47.0	58.1	9.1	9.0	16.4	7.5
HEDS–TMS	56.3	70.6	5.5	0	15.7	8.2
OETS–TMS	72.8	56.7	19.3	0	11.0	13.0

[a]Calculated based on the $^{29}Si\{^1H\}$ NMR spectra

[b]Evaluated based on the signal areas of the $^{29}Si\{^1H\}$ NMR spectra

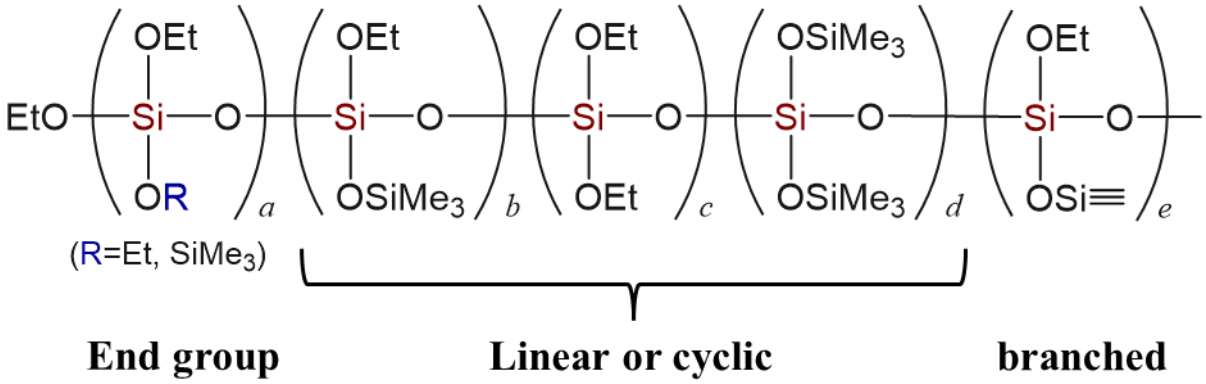

Figure 8. Structures of ethoxysilane–TMSs.

3.2.2 $^{29}Si\{^{1}H\}$ NMR spectra of the hydrolyzates of TEOS, HEDS, and OETS

GPC traces of the hydrolyzates after 1 h of reaction initiation are depicted in Figure 9. The traces were different for different monomers. $^{29}Si\{^{1}H\}$ NMR spectra of ethoxysiloxane oligomers are shown in Figure 10. Structures of the oligomers were estimated based on the hydrolysis–condensation of ethoxysilane and isolated specific structural monomer [5,22,33–40]. Spectrum of the hydrolyzate of TEOS after 1 h of reaction demonstrated main signals attributed to $Q^1(OEt)_2(OH)$ (−86.2 ppm), four-membered cyclic $Q^2(OEt)(OH)$ (−92.7 ppm), four-membered cyclic $Q^2(OEt)_2$ (−95.1 ppm), and five- or six-membered cyclic $Q^2(OEt)_2$ (−95.4 ppm) and minor signals related to linear Q^2 (−96 ppm) and silanol-terminated species (−85.5 ppm). Signal of the Q^1 unit disappeared after 24 h. After 7 days of reaction, the intensities of the four-membered cyclic Q^2 signals decreased, and signals appeared from −99 to −105 ppm in the Q^3 unit region, corresponding to cyclic Q^3–OH (−99.7 ppm), Q^3–OH (−100.5 ppm), cyclic Q^3 (−101.5 ppm), cage-type Q^3 such as open and complete cages (−102.3 ppm), and Q^3–OEt (−103.2 ppm). After 14 days, the intensities of the signals decreased, and unclear broad signals were noticed in the Q^2 (−92–−97 ppm), Q^3 (−99–−105 ppm), and Q^4 (−110 ppm) regions. Molecular weight of the TEOS oligomer increased over time (from 1600 to 2400 Da), and after 14 days of reaction, the TEOS oligomer was primarily composed of Q^3 structures.

Spectrum of the hydrolyzate of HEDS after 1 h of reaction initiation exhibited the signals attributed to $Q^1(OEt)(OH)_2$ (−84.0 ppm), $Q^1(OEt)_2(OH)$ (−86.1 and −86.2 ppm), $Q^1(OEt)_3$ (−88.7 ppm), cyclic $Q^2(OEt)(OH)$ (−92.7 ppm), four-membered cyclic $Q^2(OEt)_2$ (−95.1 ppm), five- or six-membered cyclic $Q^2(OEt)_2$ (−95.4 ppm), and linear Q_2 (−96.3 ppm), verifying that the HEDS oligomer acquired after 1 h of reaction initiation mainly consisted of four-membered cyclic Q^2 and end-terminated Q^1. After 24 h of reaction, the signals corresponding to Q^1 units disappeared, and the signal of four-membered cyclic Q^2 became strong. Small signals due to cyclic Q^3 (−101.2 and −101.5 ppm) were observed. After 7 days of reaction, the signal intensity of the four-membered cyclic Q^2 decreased, whereas that of the Q^3 unit increased. Spectrum of the HEDS oligomer after 14 days of reaction was similar to that after 7 days of reaction, and the Q^4 unit was barely formed. Molecular weight of the HEDS oligomer changed from 1300 to 1800 Da from 1 h to 14 days of reaction, respectively, and the HEDS oligomer acquired after 14 days of reaction was primarily composed of four-membered cyclic Q^2, cyclic Q^3, and Q^3 structures; linear Q^2 and six-membered cyclic Q^2 were also present in the oligomer.

Hydrolysis–condensation behavior of OETS was different from those of TEOS and HEDS. Spectrum of the hydrolyzate of OETS after 1 h of reaction initiation demonstrated the signals related to three-membered cyclic $Q^2(OEt)(OH)$ (−85.5 and −85.7 ppm), $Q^1(OEt)_2(OH)$ (−86.2 ppm), three-membered cyclic $Q^2(OEt)_2$ (−87.7 and −87.9 ppm), $Q^1(OEt)_3$ (−88.7 and −88.9 ppm), cyclic

Q^2(OEt)(OH) (−92.7 ppm), Q^2(OEt)(OH) (−93.6 ppm), four-membered cyclic $Q^2(OEt)_2$ (−95.1 ppm), and linear Q^2 (−96.2 ppm). After 24 h of reaction, the signal intensities of four-, five-, and six-membered cyclic $Q^2(OEt)_2$ (−95.1, −95.4, and −95.6 ppm, respectively) increased, whereas those of Q^1 and three-membered cyclic Q^2 decreased. After 7 days of reaction, cyclic Q^3–OH (−100.5 ppm), Q^3–OH (−101.5 ppm), cage-type Q^3 including open and complete cages (−102.3 ppm), cyclic Q^3–OEt (−103.2 ppm), and Q^3–OEt (−104.5 ppm) were generated, and the contents of Q^1–OH and three-membered cyclic Q^2 decreased. After 14 days of reaction, the signals of Q^1–OH and three-membered cyclic Q^2 disappeared, signal intensities of the Q^3 structures increased, and the content of four-membered cyclic Q^2 decreased. Moreover, the signal of end-terminated $Q^1(OEt)_3$ was observed. After 14 days of reaction, the OETS oligomer mainly comprised four-, five-, or six-membered cyclic Q^2, linear Q^2, various Q^3, and end-terminated $Q^1(OEt)_3$. These assignments are presented in Table 5.

Figure 11 depicts the changes in the area ratios of the structures in the $^{29}Si\{^1H\}$ NMR spectra of TEOS, HEDS, and OETS oligomers over time. Contents of cyclic and linear structures reached up to approximately 50 and 20%, respectively. Area ratios of these structures decreased with an increase in the area ratio of the branched structure. Schematics of the estimated structures generated by linear ethoxysilane oligomers are shown in Figure 12.

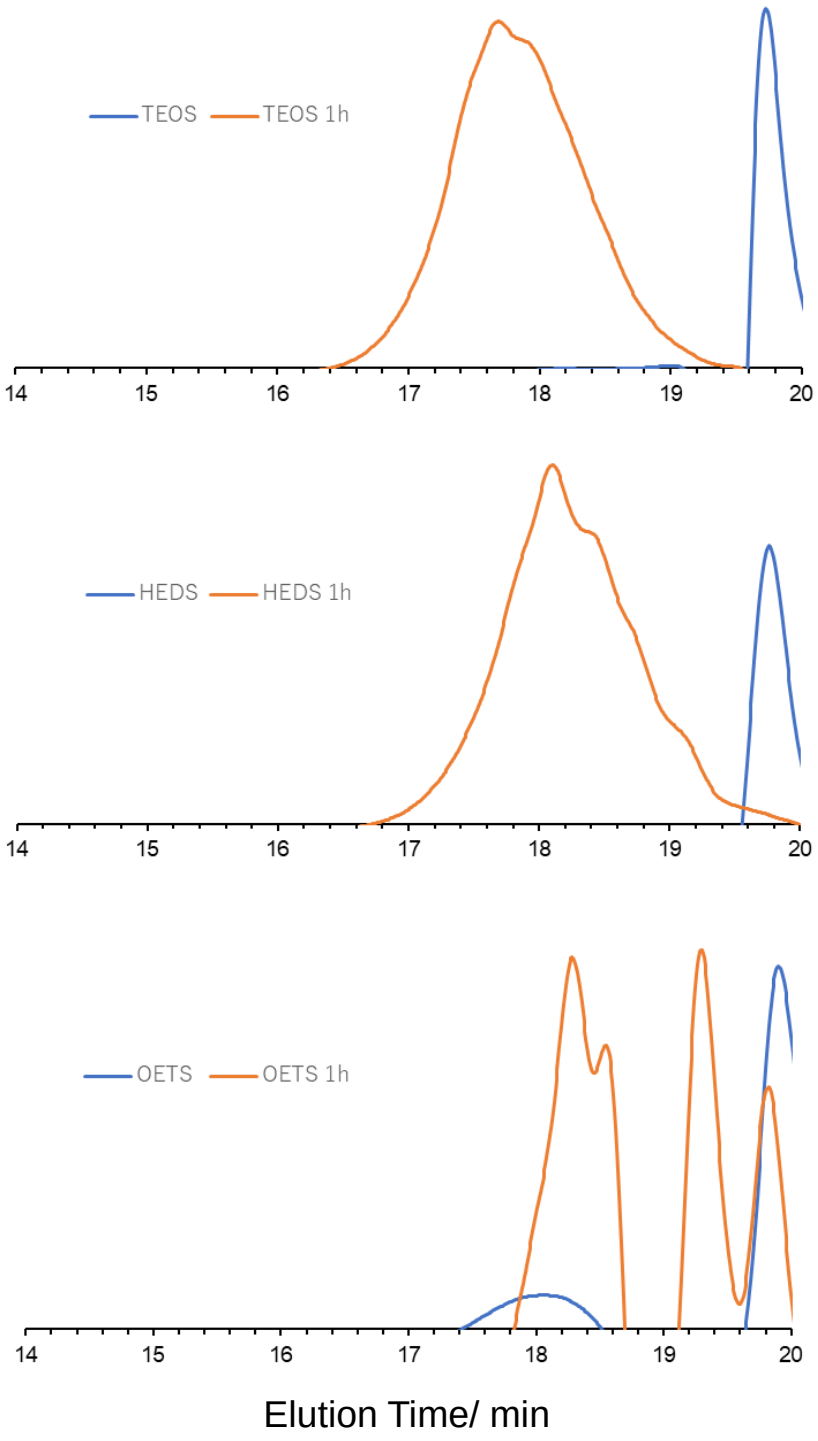

Figure 9. GPC charts of monomers and oligomers after 1 h of reaction initiation.

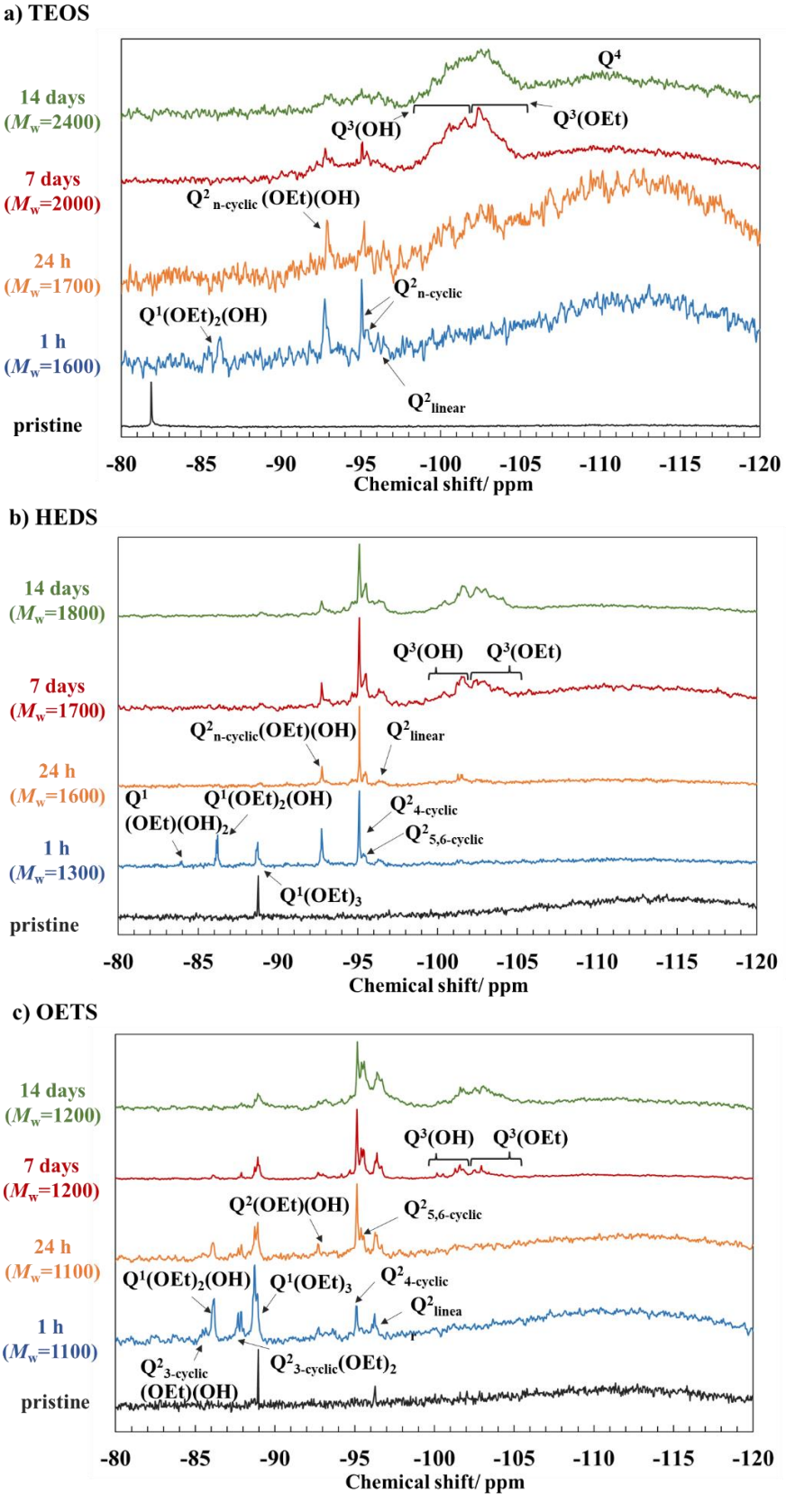
a) TEOS
14 days
(M_w=2400)
7 days
(M_w=2000)
24 h
(M_w=1700)
1 h
(M_w=1600)
pristine
Q⁴
Q³(OH)
Q³(OEt)
Q² n-cyclic (OEt)(OH)
Q²n-cyclic
Q¹(OEt)₂(OH)
Q²linear
-80 -85 -90 -95 -100 -105 -110 -115 -120
Chemical shift/ ppm
b) HEDS
14 days
(M_w=1800)
7 days
(M_w=1700)
24 h
(M_w=1600)
1 h
(M_w=1300)
pristine
Q³(OH) Q³(OEt)
Q²n-cyclic(OEt)(OH)
Q²linear
Q¹ (OEt)(OH)₂
Q¹(OEt)₂(OH)
Q²4-cyclic
Q²5,6-cyclic
Q¹(OEt)₃
-80 -85 -90 -95 -100 -105 -110 -115 -120
Chemical shift/ ppm
c) OETS
14 days
(M_w=1200)
7 days
(M_w=1200)
24 h
(M_w=1100)
1 h
(M_w=1100)
pristine
Q³(OH) Q³(OEt)
Q²(OEt)(OH)
Q²5,6-cyclic
Q¹(OEt)₂(OH)
Q¹(OEt)₃
Q²4-cyclic
Q²linea
Q²3-cyclic (OEt)(OH)
Q²3-cyclic(OEt)₂
-80 -85 -90 -95 -100 -105 -110 -115 -120
Chemical shift/ ppm

Figure 10. $^{29}Si\{^{1}H\}$ NMR spectra of the hydrolyzates of a) TEOS, b) HEDS, and c) OETS.

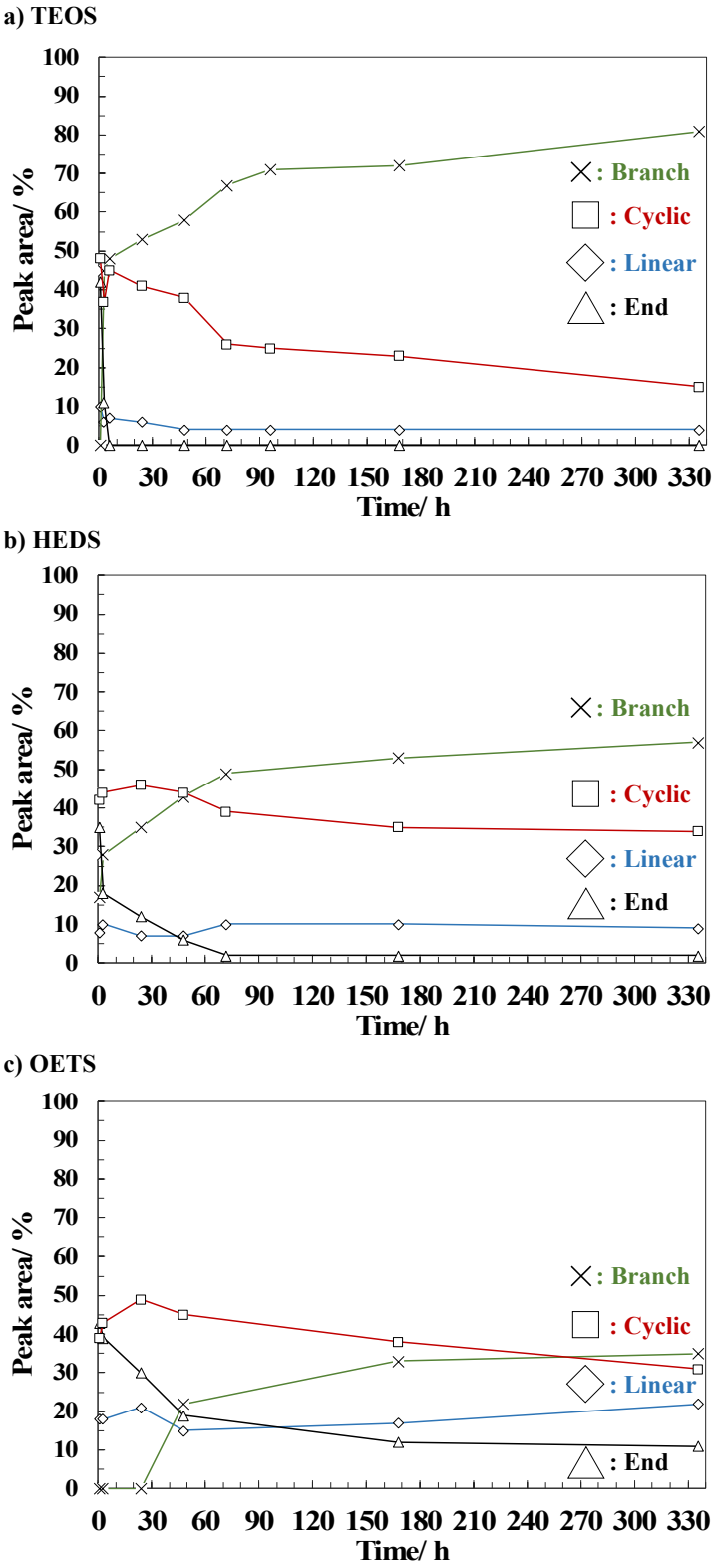

Figure 11. Variations of the peak area ratios of structures with time in the $^{29}Si\{^{1}H\}$ NMR spectra of the hydrolyzates of a) TEOS, b) HEDS, and c) OETS (△: End group, ◇: Linear structure, □: Cyclic structure, and ×: Branched structure).

Table 6 Assignments for the $^{29}Si\{^{1}H\}$ NMR spectra of ethoxysiloxane oligomers

Q^n unit	Chemical shift of Q^n unit/ppm		
	TEOS oligomer	HEDS oligomer	OETS oligomer
monomer	−81.9	−88.8	−88.9, −96.2
$Q_1(OEt)_3$		−88.7	−88.7, −88.9
$Q_1(OEt)_2(OH)$	−85.5, −86.2	−86.1, −86.2	−86.2
$Q_1(OEt)(OH)_2$		−84.0	
Q^2_{linear}	−96.1, −96.4	−96.3	−96.2
$Q^2_{5,6\text{-cyclic}}$	−95.4	−95.4	−95.4, −95.6
$Q^2_{4\text{-cyclic}}$	−95.1	−95.1	−95.1
$Q^2_{linear}(OEt)(OH)$			−93.6
$Q^2_{n\text{-cyclic}}(OEt)(OH)$	−92.7	−92.7	−92.7
$Q^2_{3\text{-cyclic}}(OEt)_2$			−87.7, −87.9
$Q^2_{3\text{-cyclic}}(OEt)(OH)$			−85.7, −85.5
$Q^3(OEt)$	−101.5–−103.8	−102.4–−103.8	−102.5–−103.4
$Q^3(OH)$	−99.4–−101.5	−100.4–−101.5	−100.2–−101.6
Q^4	−110.7		

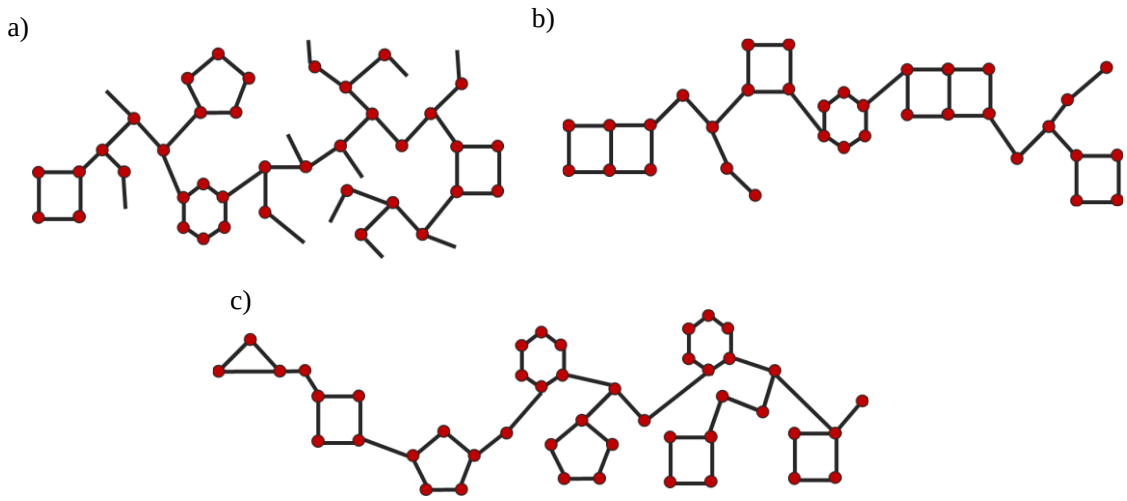

Figure 12. Schematics of the estimated oligomer structures obtained from a) TEOS, b) HEDS, and c) OETS.

3.2.3 Condensates of TEOS, HEDS, and OETS

Condensation ability was evaluated by adjusting the molar ratio on OEt group basis (H_2O) and Si basis (EtOH, HCl). For example, to produce HEDS from 2 mol TEOS, 1 mol water is required. Therefore, if TEOS is hydrolyzed using 2 mol water, 4 mol EtOH, and 0.1 mol HCl, HEDS should be hydrolyzed using 3 mol water, 8 mol EtOH, and 0.2 mol HCl, whereas OETS should be hydrolyzed using 4 mol water, 12 mol EtOH, and 0.3 mol HCl, respectively.

Condensates of linear ethoxy oligosiloxanes (Cs) were isolated by silylation followed by extraction. Results of the synthesis of Cs are provided in Table 7.

Table 7. Synthesis of Cs

monomer	GPC result[a]		OEt/Si-Me_3[b]	Ratio of siloxane units[c](%)					DC[d] (%)
	$M_w \times 10^{-3}$	M_w/M_n	ratio	Q^0	Q^1	Q^2	Q^3	Q^4	
C_{TEOS}	3.2	1.3	1.2	0	0	16	53	31	79
C_{HEDS}	3.7	1.2	1.2	0	0	16	51	33	79
C_{OETS}	3.7	1.3	1.2	0	0	14	48	38	81

a Calculated based on standard polystyrene

b Calculated based on ^{1}H NMR spectra

c Calculated based on the Q^n signal area of ^{29}Si NMR spectra

d DC(%)=$0/4Q^0+1/4Q^1+2/4Q^2+3/4Q^3+4/4Q^4$

Cs was isolated as a viscous liquid. Weight-average molecular weight (M_w), polydispersity (M_w/number-average molecular weight (M_n)), and QEt/Si–Me_3 ratio were ca. 3500, approximately 1.3, and 1.2, respectively. Trimethylsilylation was confirmed by the appearance of the adsorption bands corresponding to δSi–Me (1254 cm^{-1}) and ρSi–Me (846 cm^{-1}) in the FTIR spectra (Figure 13) [22,29,30]. No υSi–O–Si adsorption band was noticed at 1200–1100 or 1040–1000 cm^{-1}; hence, the main structures of ethoxysilane–TMSs were attributed to their linear, branched, and cyclic forms [22,31].

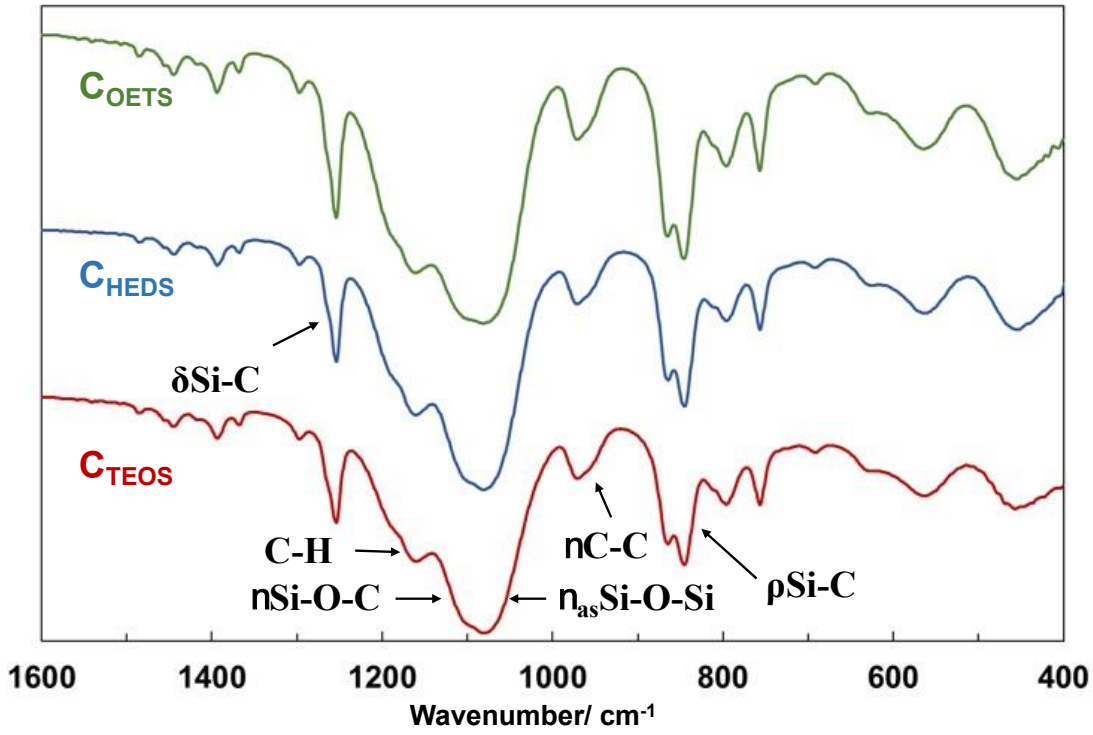

Figure 13. FTIR spectra of top) C_{OETS}, middle) C_{HED}, and bottom) C_{TEOS} (neat method).

^{29}Si NMR spectra of Cs are depicted in Figure 14.

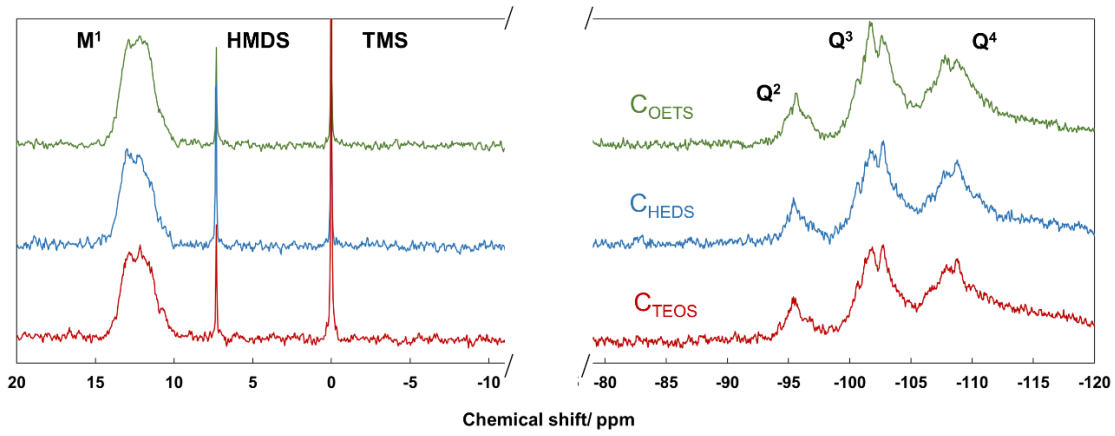

Figure 14. ^{29}Si{^{1}H} NMR spectra of Cs.

Signals at approximately 12.5, -95, -102.5, and -108 ppm in the ^{29}Si{^{1}H} NMR spectra were ascribed to the Me_3SiO (M^1), $(EtO)_2SiO_2$ (Q^2), $EtOSiO_3$ (Q^3), and SiO_4 (Q^4) units, respectively. Nevertheless,

hexamethyldisiloxane (HMDS), which was acquired by the hydrolysis of chlorotrimethylsilane, was formed because its signal was observed at 7.3 ppm [41]. Q_n region was primarily occupied by Q_3 and Q_4 units.

To gain more information, Cs were separated into LS and HS by vacuum distillation [42]. These results are presented in Table 8, and the $^{29}Si\{^1H\}$ NMR spectra are shown in Figure 15.

Table 8. Fractions of Cs

Product	LS or HS	Bp (℃/ Torr)	GPC result[a]		OEt/Si-Me_3[b]	Ratio of siloxane units[c](%)					DC[d] (%)	Yield (%)
			$M_w\times10^{-3}$	M_w/M_n	ratio	Q^0	Q^1	Q^2	Q^3	Q^4		
C_{TEOS}	LS	122.5–147.1/ 0.12	2.1	1.2	1.2	0	0	22	50	28	77	30
	HS		4.1	1.3	1.2	0	0	11	43	46	84	70
C_{HEDS}	LS	72.5–138.0/ 0.14	2.2	1.1	1.2	0	0	17	49	35	80	40
	HS		4.9	1.2	1.2	0	0	9	45	46	84	60
C_{OETS}	LS	129.0–135.0/ 0.34	2.2	1.1	1.2	0	0	19	48	33	79	20
	HS		5.5	1.4	1.2	0	0	11	49	44	86	80

a Calculated based on standard polystyrene

b Calculated based on ^1H NMR spectra

c Calculated based on the Q^n signal area of ^{29}Si NMR spectra

d $DC(\%)=0/4Q^0+1/4Q^1+2/4Q^2+3/4Q^3+4/4Q^4$

Boiling points of Cs–LS were ca. 120–150 °C/ 0.1–0.3 Torr except for the case of C_{HEDS}–LS. C_{HEDS}–LS is believed to contain four-membered cyclic derivatives, as described later. In the $^{29}Si\{^1H\}$ NMR spectra of Cs–LS and –HS, the signals at approximately 12.5, -95, -102.5, and -108 ppm were attributed to the M^1, Q^2, Q^3, and Q^4 units, respectively. M_w, M_w/M_n, QEt/Si–Me_3 ratio, and DC of Cs–LS were ca. 2000, ca. 1.1, 1.2, and ca. 80, respectively, whereas M_w, M_w/M_n, QEt/Si–Me_3 ratio, and DC of Cs –HS were ca. 5000, ca. 1.3, 1.2, and ca. 85, respectively. Because QEt/Si–Me_3 ratios of Cs–LS and Cs–HS were similar, Cs were estimated to be appropriately separated. Cs comprised Q^3 and Q^4 structures regardless of LS and HS. Cs–LS and Cs–HS yields differed depending on the starting materials.

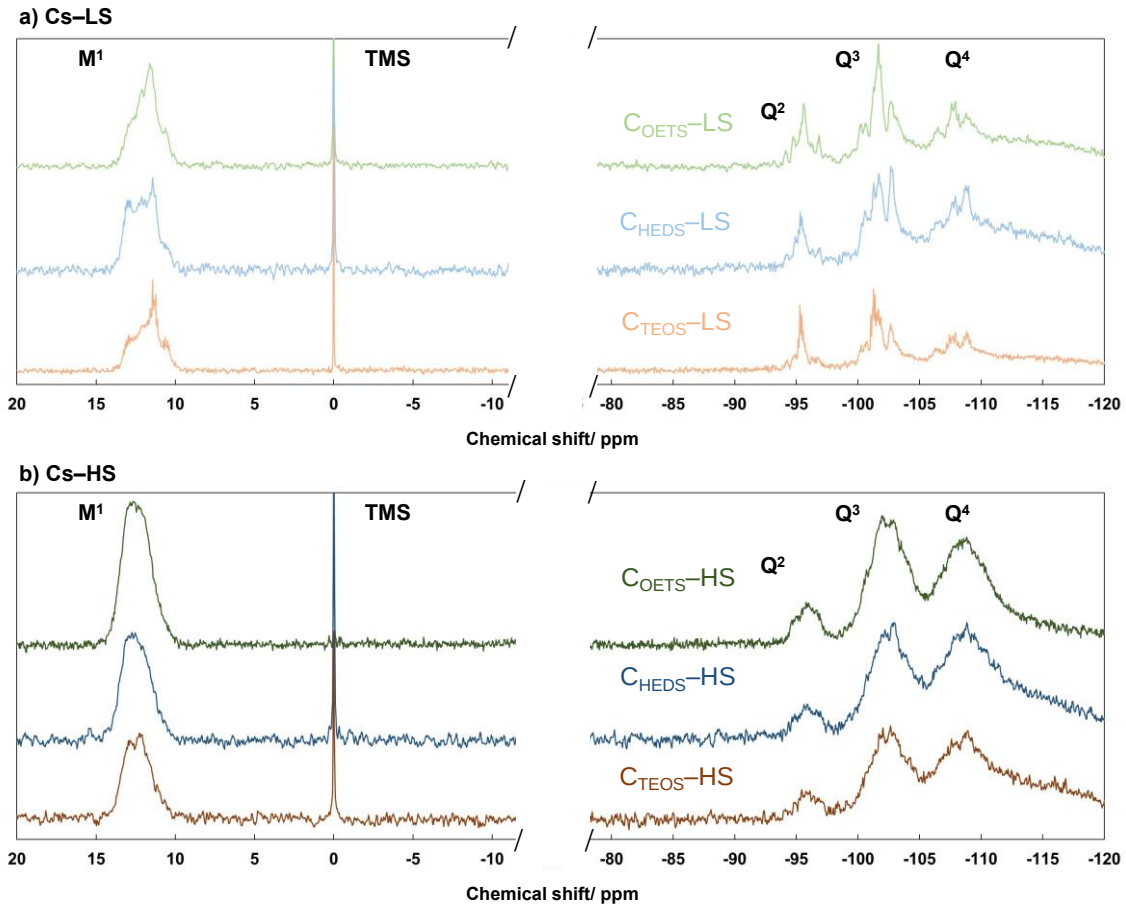

Figure 15. $^{29}Si\{^{1}H\}$ NMR spectra of a) Cs–LS and b) Cs–HS.

ESI-MS of Cs–LS was conducted, and the corresponding results are depicted in Figure 16 (Attribution results are provided in Table S2). Cs–LS was predicted to be mainly composed of short ladder structures comprising some isomers. Short ladder structures were hypothesized to primarily consist of six-membered ladder structures because of the integral ratio of the $^{29}Si\{^{1}H\}$ NMR spectrum and ring strains of cyclic siloxanes. However, abundance ratios of the isomers related to short ladder structures may differ depending on the starting materials. Four-membered cyclic structure was verified only in the case of C_{HEDS}–LS, whereas five-membered cyclic structure or branched four-membered

cyclic structure was observed in the case of only C_{HEDS}–LS. Branched short, long ladder, and cage-like structures were confirmed as other minor products. These results suggested that Cs were composed of broken ladder and incomplete cage structures similar to those of the condensates of silicic acid [42], methyltrialkoxysilane [43,44], and trichlorosilane [45]. Itoh *et al.* [45] and Hayami *et al.* [46] proposed that siloxane and metalloxane cage compounds were formed via (i) condensations of cyclic compounds with each other, (ii) addition of monomer or dimer to open-cage and ladder structures, and (iii) rearrangement of polymer and cage-like compound. These results may indicate that the key formation route of siloxane cage compounds is addition of cyclic compounds to ladder and open-cage structures, which are formed via ladder structures.

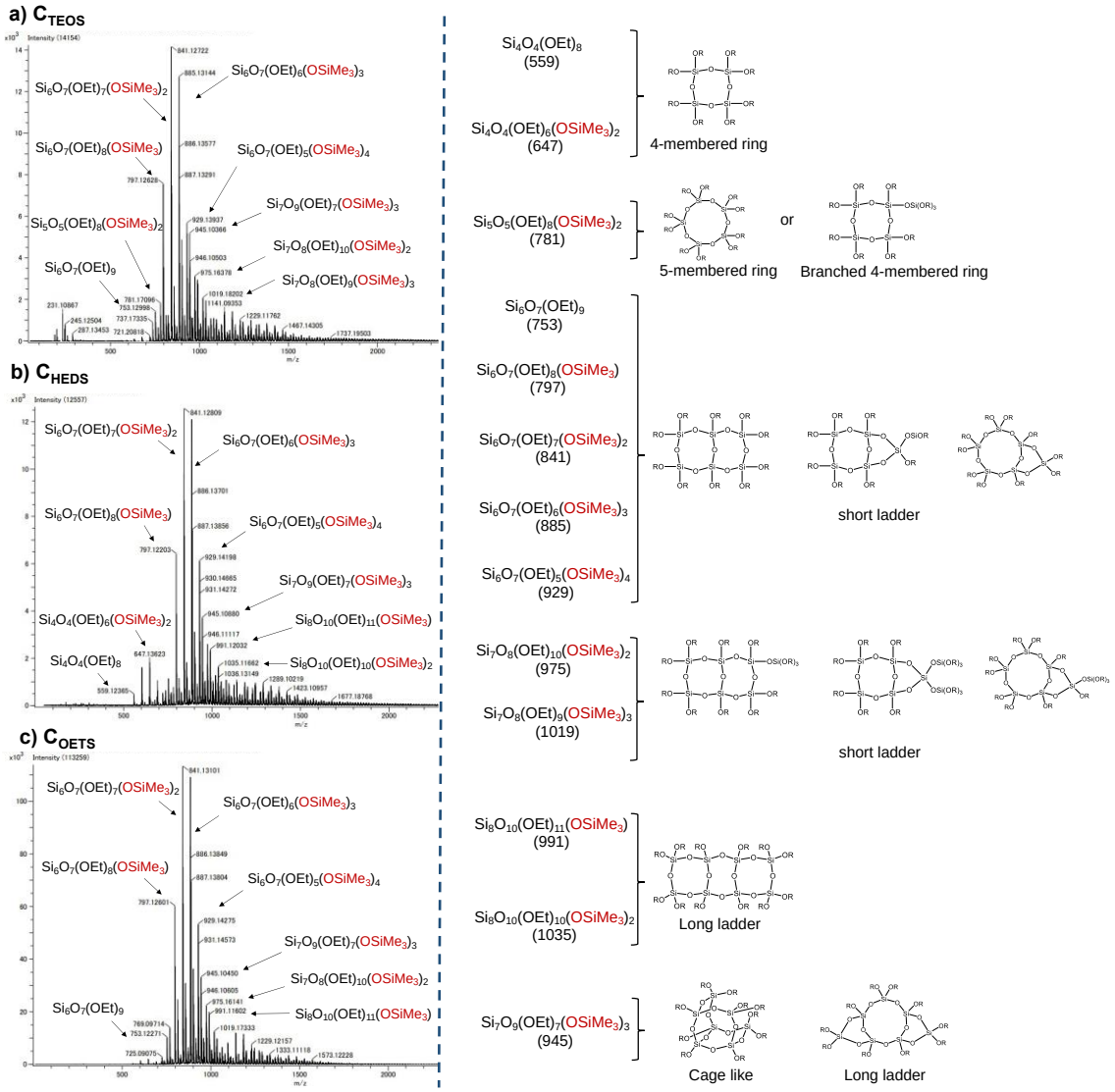

Figure 16. ESI-MS spectra of a) C_{TEOS}, b) C_{HEDS}, and c) C_{OETS} detected as $[M + Na]^+$.

3.2.4 Proposed hydrolysis–condensation mechanisms of TEOS, HEDS, and OETS

Herein, I propose possible mechanisms of hydrolysis–condensations of TEOS, HEDS, and OETS (Scheme 4). Linear and cyclic oligosiloxanes were generated in the initial stage. Then, these oligosiloxanes developed into a network-type polymer containing a cyclic siloxane, polymer

consisting of four-membered cyclic siloxanes, and polymer comprising cyclic siloxanes for TEOS, HEDS, and OETS, respectively. These precursors finally afforded polymers with broken ladder or cage structures via an intermediate with a six-membered cyclic structure.

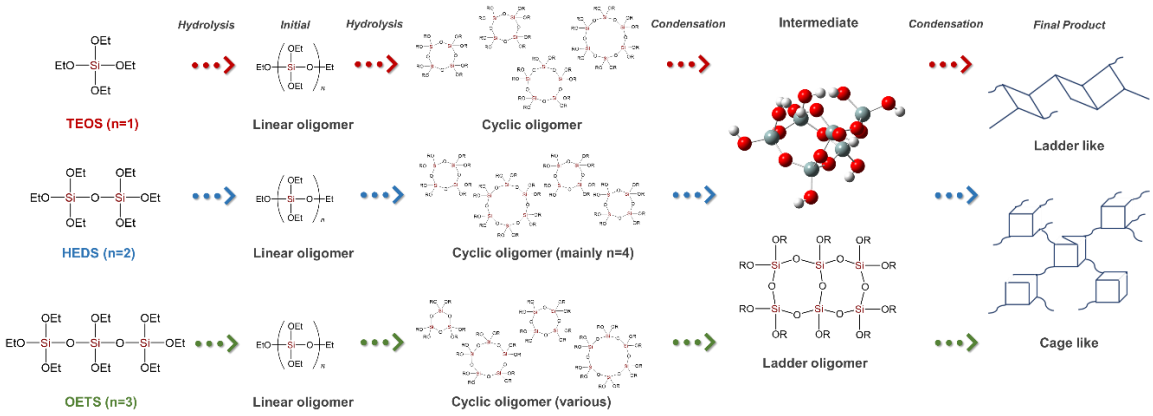

Scheme 4. Possible hydrolysis–condensation mechanisms of TEOS, HEDS, and OETS.

3.2.5 Computational study of ethoxysiloxane monomers

Optimized structures with their ESP maps and dipole moments were calculated using density functional theory (DFT) to supplement the reactivities of the ethoxysilane monomers (Figure 17). When siloxane bonding was extended, the dipole moment of the optimized structure increased (TEOS: 0.11 D, HEDS: 1.07 D, and OETS: 3.86 D). Optimized HEDS and OETS structures demonstrated that the electron density was high on the O atoms of the siloxane bond and alkoxy group. Particularly, OETS exhibited high electron density on the O atom of the alkoxy group arranged on one side of the

molecule. These electron densities may affect the reactivities of the monomers [47–49].

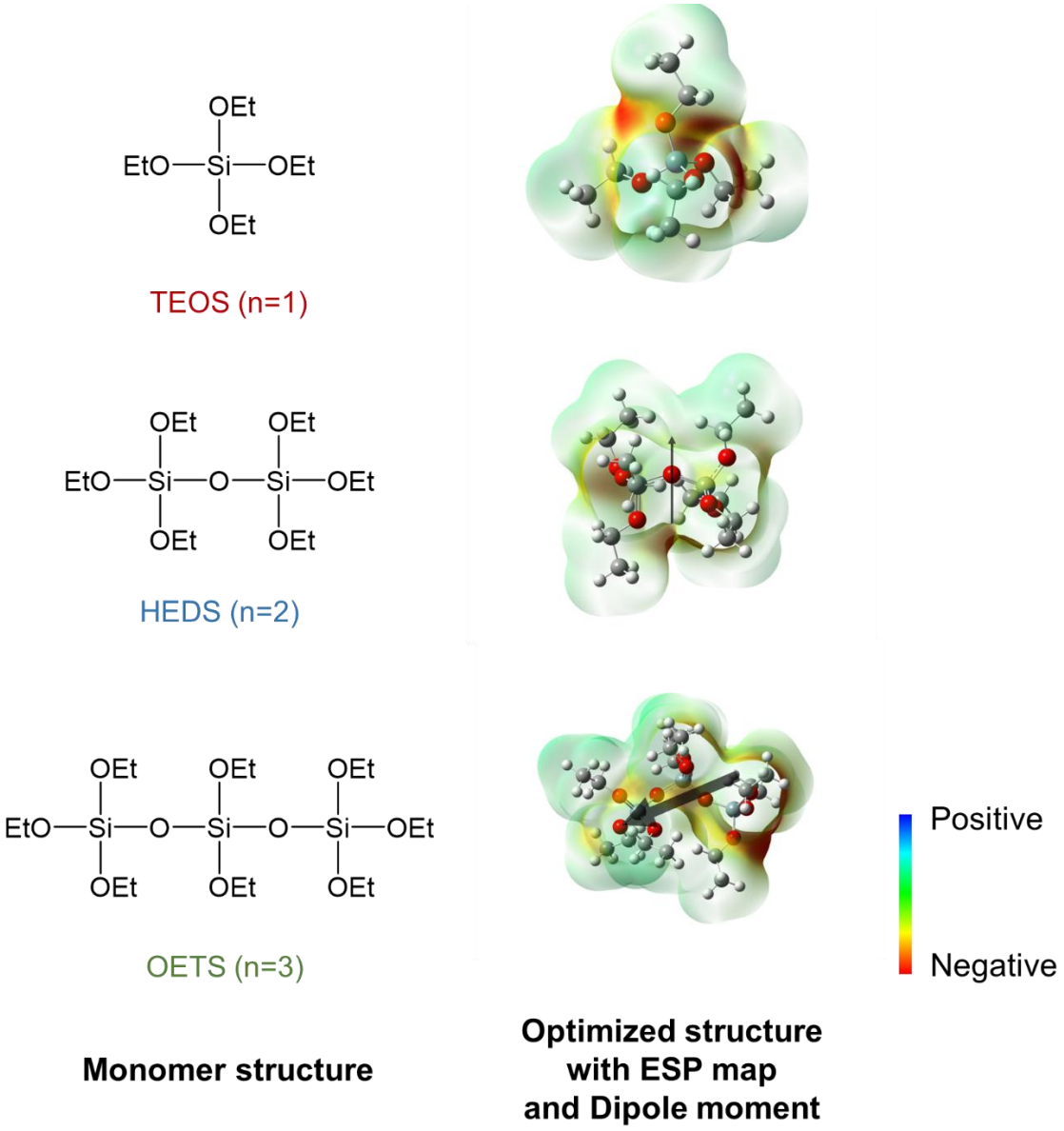

Figure 17. ESP maps and dipole moments for TEOS, HEDS, and OETS evaluated using DFT calculation (B3LYP/6-31 G(d,p)).

4 Conclusion

HEDS and OETS were synthesized in total yields of 3.5 and 8.4%, respectively, from DEDIS by regulating the functionality. Hydrolyzates of TEOS, HEDS, and OETS were trimethylsilylated and analyzed by MS, GPC, and NMR spectroscopy. Linear and cyclic oligosiloxanes were produced in the initial stage. Polymer structure given by TEOS was estimated to be a network-type polymer containing a cyclic siloxane. HEDS produced that polymer mainly consisted of four-membered cyclic siloxanes. OETS gave that polymer primarily comprised cyclic siloxanes. These precursors finally furnished ladder or cage-like polymers via an intermediate with a six-membered cyclic structure. Additionally, the electron densities of the ethoxysilane monomers calculated using DFT calculation were examined. Optimized HEDS and OETS structures demonstrated high electron densities on the O atoms in the siloxane bond and alkoxy group. These results suggest that electron density may affect the reactivities of TEOS, HEDS, and OETS.

References

1. Y. Abe, R. Shimano, K. Arimitsu, T. Gunji, *J. Polym. Sci., Part A: Polym. Chem.*, **41**, 2250–2255 (2003). https://doi.org/10.1002/pola.10739

2. T. Gunji, Y. Hayashi, A. Komatsubara, K. Arimitsu, Y. Abe, *Appl. Organomet. Chem.*, **26**, 32–36 (2012). https://doi.org/10.1002/aoc.1861

3. J. Sanchez, A. McCormick, *J. Phys. Chem.*, **96**, 8973–8979 (1992).

https://doi.org/10.1021/j100201a051

4. J. Sanchez, A. V. McCormick, *J. Non-Cryst. Solids*, **167**, 289–294 (1994). https://doi.org/10.1016/0022-3093(94)90251-8

5. C. C. Lin, J. D. Basil, *Mater. Res. Soc. Symp. Proc.*, **73**, 585–590 (1986). https://doi.org/10.1557/PROC-73-585

6. M. J. Frisch, G. W. Trucks, H. B. Schlegel, G. E. Scuseria, M. A. Robb, J. R. Cheeseman, G. Scalmani, V. Barone, G. A. Petersson, H. Nakatsuji, X. Li, M. Caricato, A. V. Marenich, J. Bloino, B. G. Janesko, R. Gomperts, B. Mennucci, H. P. Hratchian, J. V. Ortiz, A. F. Izmaylov, J. L. Sonnenberg, D. Williams-Young, F. Ding, F. Lipparini, F. Egidi, J. Goings, B. Peng, A. Petrone, T. Henderson, D. Ranasinghe, V. G. Zakrzewski, J. Gao, N. Rega, G. Zheng, W. Liang, M. Hada, M. Ehara, K. Toyota, R. Fukuda, J. Hasegawa, M. Ishida, T. Nakajima, Y. Honda, O. Kitao, H. Nakai, T. Vreven, K. Throssell, J. A. Montgomery Jr., J. E. Peralta, F. Ogliaro, M. J. Bearpark, J. J. Heyd, E. N. Brothers, K. N. Kudin, V. N. Staroverov, T. A. Keith, R. Kobayashi, J. Normand, K. Raghavachari, A. P. Rendell, J. C. Burant, S. S. Iyengar, J. Tomasi, M. Cossi, J. M. Millam, M. Klene, C. Adamo, R. Cammi, J. W. Ochterski, R. L. Martin, K. Morokuma, O. Farkas, J. B. Foresman, D. J. Fox, Gaussian˜16 Revision C.01 (2016).

7. Y. Abe, K. Motoyama, T. Kobayashi, S. Iwasaki, T. Gunji, *Nippon Kagaku Kaishi*, 973–974 (1996). https://doi.org/10.1246/nikkashi.1996.969

8. V. V. Kazakova, O.B Gorbatsevich, S. A. Skvortsova, N. V. Demchenko, A. M. Muzafarov, *Russ.*

Chem. Bull., **54**, 1350–1351 (2005). https://doi.org/10.1007/s11172-005-0409-y

9. K. Yamamoto, T. Shimoda, Y. Sato, T. Nakaya, J. Ohshita, T. Gunji, *J. Sol-Gel Sci. Technol.*, **104**, 724–734 (2022). https://doi.org/10.1007/s10971-022-05806-z

10. T. Gunji, A. Setogawa, K. Asakura, Y. Abe, *Bull. Chem. Soc. Jpn.*, **71**, 2967–2972 (1998). https://doi.org/10.1246/bcsj.71.2967

11. Y. Abe, T. Kanemaru, T. Yamazaki, Y. Nagao, T. Misono, *Nippon Kagaku Kaishi*, **1991**, 1094–1101 (1991). https://doi.org/10.1246/nikkashi.1991.1094

12. Y. Kondo, K. Miyao, Y. Aya, N. Yoshino, *J. Oleo Sci.*, **53**, 143–151 (2004). https://doi.org/10.5650/jos.53.143

13. H. Sakurai, H. Nozaki, S. Yamamoto, J. Tsuji, R. Noyori, Application of organosilicon compounds to organic synthesis (Eds.), Kagaku Zokan, vol. 105. Kagaku Dojin (1985), pp. 33–40.

14. R. J. P. Corriu, C. Guerin, *Adv. Organomet. Chem.*, **20**, 265–312 (1982). https://doi.org/10.1016/S0065-3055(08)60523-7

15. H. Oberhammer, J. E. Boggs, *J. Am. Chem. Soc.*, **102**, 7241–7244 (1980). https://doi.org/10.1021/ja00544a011

16. F. Dankert, C. von Hänisch, *Eur. J. Inorg. Chem.*, **2021**, 2907–2927 (2021). https://doi.org/10.1002/ejic.202100275

17. Y. Abe, A. Ito, Y. Kuno, Y. Nagao, H. Misono, *Nippon Kagaku Kaishi*, **1992**, 649–656 (1992).

https://doi.org/10.1246/nikkashi.1992.649

18. V. P. Kozyukov, V. D. Sheludyakov, V. F. Mironov, *Russ. Chem. Rev.*, **42**, 662–677 (1973). https://doi.org/10.1070/RC1973v042n08ABEH002704

19. J. O. Jensen, *Spectrochim. Acta A Mol. Biomol. Spectrosc.*, **59**, 937–947 (2003). https://doi.org/10.1016/S1386-1425(02)00280-9

20. F. A. Miller, G. L. Carlson, *Spectrochim. Acta*, **17**, 977–989 (1961). https://doi.org/10.1016/0371-1951(61)80033-7

21. W. E. Newton, E. G. Rochow, *J. Chem. Soc. A*, **1970**, 2664–2668 (1970). https://doi.org/10.1039/J19700002664

22. Y. Sato, R. Hayami, T. Gunji, *J. Sol-Gel Sci. Technol.*, **104**, 36–52 (2022). https://doi.org/10.1007/s10971-022-05920-y

23. F. Rubio, J. Rubio, J. L. Oteo, *Spectrosc. Lett.*, **31**, 199–219 (1998). https://doi.org/10.1080/00387019808006772

24. R. A. Assink, B. D. Kay, *J. Non-Cryst. Solids*, **99**, 359–370 (1988). https://doi.org/10.1016/0022-3093(88)90441-3

25. B. D. Kay, R. A. Assink, *J. Non-Cryst. Solids*, **104**, 112–122 (1988). https://doi.org/10.1016/0022-3093(88)90189-5

26. T. Gunji, Tokyo University of Science, Doctoral dissertations, p110 (1992).

https://doi.org/10.11501/3071196

27. T. Gunji, I. Sopyan, Y. Abe, *J. Polym. Sci., Part A: Polym. Chem.*, **32**, 3133–3139 (1994). https://doi.org/10.1002/pola.1994.080321613

28. C. W. Lentz, *Inorg. Chem.*, **3**, 574–579 (1964). https://doi.org/10.1021/ic50014a029

29. D. H. Flagg, T. J. McCarthy, *Macromolecules*, **49**, 8581–8592 (2016). https://doi.org/10.1021/acs.macromol.6b01852

30. W. Liang, X. Ge, J. Ge, T. Li, T. Zhao, X. Chen, Y. Song, Y. Cui, M. Khan, J. Ji, X. Pang, R. Liu, *Polymers*, **10**, 1254 (2018). https://doi.org/10.3390/polym10111254

31. G. Cruz-Quesada, M. Espinal-Viguri, M. V. López-Ramón, J. J. Garrido, *Gels*, **8**, 677 (2022). https://doi.org/10.3390/gels8100677

32. W. G. Klemperer, V. V. Mainz, S. D. Ramamurthi, F. S. Rosenberg, *Mater. Res. Soc. Symp. Proc.*, **121**, 15–24 (1988). https://doi.org/10.1557/PROC-121-15

33. M. Mazúr, V. Mlynárik, M. Valko, P. Pelikán, *Appl. Magn. Reson.*, **18**, 187–197 (2000). https://doi.org/10.1007/BF03162110

34. A. Depla, D. Lesthaeghe, T. S. van Erp, A. Aerts, K. Houthoofd, F. Fan, C. Li, V. V. Speybroeck, M. Waroquier, C. E. A. Kirschhock, J. A. Martens, *J. Phys. Chem. C*, **115**, 3562–3571 (2011). https://doi.org/10.1021/jp109901v

35. J. Brus, J. Karhan, P. Kotlík, *Collect. Czech. Chem. Commun.*, **61**, 691–703 (1996). https://doi.org/10.1135/cccc19960691

36. R. J. Hook, *J. Non-Cryst. Solids*, **195**, 1–15 (1996). https://doi.org/10.1016/0022-3093(95)00508-0

37. N. Ueda, T. Gunji, Y. Abe, *Mater. Technol.*, **26**, 162–169 (2008).

38. R. Hayami, K. Wada, I. Nishikawa, T. Sagawa, K. Yamamoto, S. Tsukada, T. Gunji, *Polym. J.*, **49**, 665–669 (2017). https://doi.org/10.1038/pj.2017.34

39. L. W. Kelts, N. J. Armstrong, *J. Mater. Res.*, **4**, 423–433 (1989). https://doi.org/10.1557/JMR.1989.0423

40. S. A. Myers, R. A. Assink, D. A. Loy, K. J. Shea, *J. Chem. Soc., Perkin Trans.*, **2**, 545–549 (2000). https://doi.org/10.1039/A906569E

41. S. Suda, M. Iwaida, K. Yamashita, T. Umegaki, *J. Non-Cryst. Solids*, **176**, 26–32 (1994). https://doi.org/10.1016/0022-3093(94)90207-0

42. T. Gunji, Y. Nagao, T. Misono, Y. Abe, *J. Polym. Sci., Part A: Polym. Chem.*, **30**, 1779–1787 (1992). https://doi.org/10.1002/pola.1992.080300901

43. H. -J. Kim, J. -K. Lee, S. -J. Park, H. W. Ro, D. Y. Yoo, D. Y. Yoon, *Anal. Chem.*, **72**, 5673–5678 (2000). https://doi.org/10.1021/ac0003899

44. H. W. Ro, E. S. Park, C. L. Soles, D. Y. Yoon, *Chem. Mater.*, **22**, 1330–1339 (2010). https://doi.org/10.1021/cm901771y

45. M. Itoh, F. Oka, M. Suto, S. D. Cook, N. Aune, *Int. J. Polym. Sci.*, **2012**, 1–17, (2012). https://doi.org/10.1155/2012/526795

46. R. Hayami, T. Gunji, *J. Sol-Gel Sci. Technol.*, **100**, 205–223 (2021). https://doi.org/10.1007/s10971-021-05652-5

47. H. Saito, Y. Nishio, M. Kobayashi, Y. Sugahara, *J. Sol-Gel Sci. Technol.*, **57**, 51–56 (2011). https://doi.org/10.1007/s10971-010-2323-5

48. K. Yamamoto, I. Saito, Y. Amaike, T. Nakaya, J. Oshita, T. Gunji, *J. Sol-Gel Sci. Technol.*, Online Published (2023). https://doi.org/10.1007/s10971-022-06017-2

49. G. J. McIntosh, *Phys. Chem. Chem. Phys.*, **15**, 3155–3172 (2013). https://doi.org/10.1039/C3CP43399D

Chapter 3

Preparation and properties of polydimethylsiloxane elastomers cross-linked with hydrolyzates of tetraethoxysilane, hexaethoxydisiloxane, and octaethoxytrisiloxane

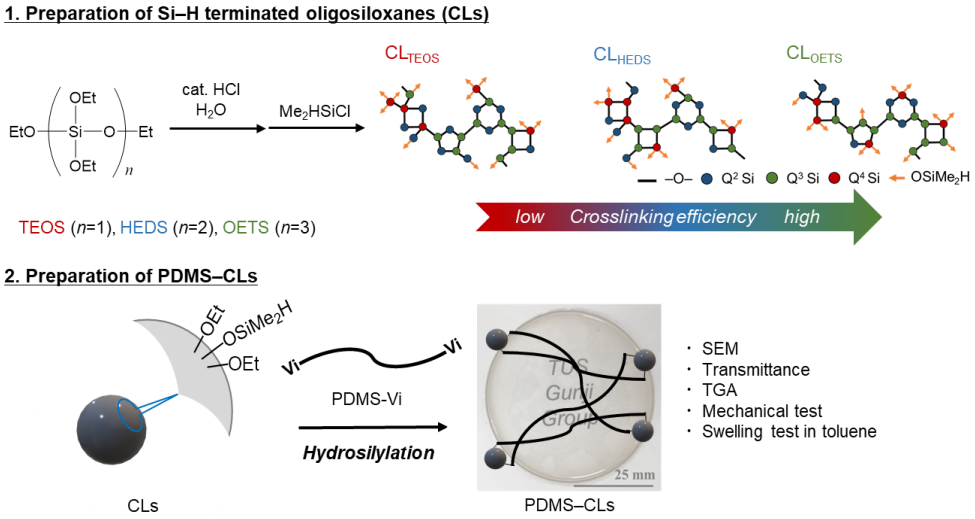

1 Introduction

In chapter 2, I discussed the hydrolysis–condensation of ethoxysilanes, formed in the early stages of the sol–gel reaction of tetraethoxysilane (TEOS). My findings indicate that TEOS, hexaethoxydisiloxane (HEDS), and octaethoxytrisiloxane (OETS) produce polymers with distinct characteristics: network-type polymers containing cyclic siloxanes, polymers comprising cyclic siloxanes with four silicon atoms, and polymers containing various cyclic siloxanes, respectively. These results shed light on the structural and chemical variations in the starting materials during the reaction. This type of findings suggests potential applications of the hydrolyzates derived from ethoxysilanes as inorganic components in organic–inorganic hybrid materials. Moreover, the structure of the inorganic segment is considered important to fine-tune the properties of polydimethylsiloxane (PDMS)-based hybrid materials [1].

In this chapter, I investigated the differences between the cross-linking abilities and physical

properties of PDMS silicone elastomers with different oligosiloxane cross-linkers. PDMS silicone elastomers were prepared as follows: Si–H-terminated oligosiloxanes (CLs) were separately synthesized by hydrolysis–condensation of ethoxysiloxanes (TEOS, HEDS, and OETS) followed by silylation with Me_2HSiCl, and then, PDMS silicone elastomers (PDMS–CLs) were fabricated by hydrosilylation between vinyl-terminated PDMS (PDMS–Vi) and CLs (Scheme 1). Structures of CLs were determined by nuclear magnetic resonance (NMR) spectroscopy. Thermal stabilities, swelling behaviors in toluene, and tensile strengths of PDMS–CLs were evaluated by corresponding tests, and differences with respect to CLs were compared.

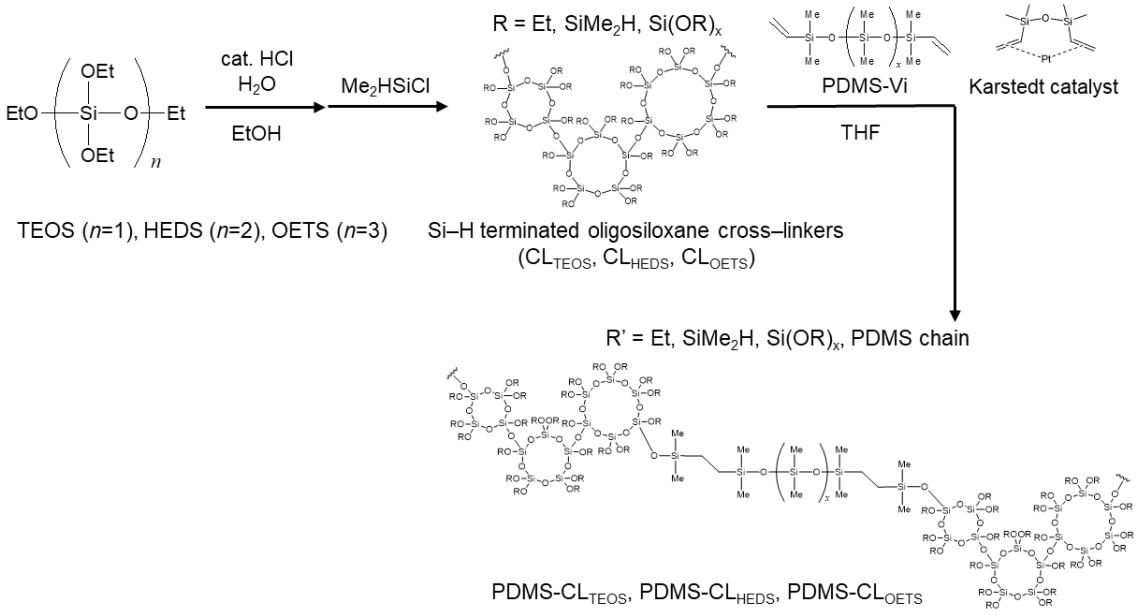

Scheme 1. Schematic of this study.

2 Experimental section

2.1 Measurements

NMR spectra were recorded using a JNM-ECZ 400 spectrometer (JEOL, Japan; ^{1}H: 399.00 MHz and ^{29}Si{^{1}H}: 79.00 MHz). Chemical shifts are reported in ppm relative to residual chloroform in deuterated chloroform ($CDCl_3$) (for ^{1}H: 7.26 ppm) or residual tetrahydrofuran (THF) in THF-d_8 (for ^{1}H: 1.72 ppm) and tetramethylsilane (for ^{29}Si{^{1}H}: 0.00 ppm) as internal standards. For ^{29}Si{^{1}H} NMR spectroscopy, chromium(III) acetylacetonate was added to the sample as a paramagnetic relaxation agent. Fourier transform infrared (FTIR) spectra were obtained using an FTIR-6100 spectrophotometer (JASCO, Japan) via the neat method, in which the sample is sandwiched between two KBr crystal disks, or by the attenuated total reflectance (ATR) method using JASCO ATR PRO 0450-S (ZnSe prism). Thermogravimetric analysis (TGA) was performed using a TG-DTA analyzer 2000SE (Netzsch Japan, Japan) at a heating rate of 10 °C min^{-1} up to 1000 °C under N_2 or air flow. Ultraviolet–visible (UV–Vis) transmittance spectra were recorded by a V-670 UV–VIS/NIR spectrophotometer (JASCO, Japan) equipped with an integrating sphere (ISN-470 type). High-resolution electrospray ionization time-of-flight mass spectrometry (HR-ESI-TOF MS) was conducted using JMS-T100CS AccuTOF CS (JEOL, Japan). Gel permeation chromatography (GPC) was performed using a LC-20AD HPLC prominence liquid chromatograph (Shimadzu, Japan) attached to a Plgel 5-μm Mixed-D column. THF was used as an eluent (1 mL min^{-1}), and RID-20A was employed as the detector at 40 °C. Number-average molecular weight (M_n), weight-average molecular weight

(M_w), and polydispersity (M_w/M_n) were calculated based on standard polystyrene. Scanning electron microscopy (SEM) was conducted using a JCM-6000 (JEOL, Japan) instrument with an accelerating voltage of 15 kV. Tensile strength tests of the samples, which were cut to sizes of 30 mm × 5 mm, were performed by MCT-2150 (A&D, Japan) at a tensile speed of 10 mm/min at approximately 23 °C. Swelling tests were conducted by measuring the solvent uptakes of the samples immersed in toluene for 3 days. Degrees of swelling (DSs) for the samples were evaluated using the following equation:

$$DS\ (\%) = 100 \times (W_a - W_b) / W_b$$

where W_a and W_b denote the weight after and before sample immersion, respectively.

2.2 Materials

Ethanol (EtOH), THF, toluene, and diethyl ether were purified via standard processes and stored over activated molecular sieves. Tetraisocyanatosilane was provided by Matsumoto Fine Chemical Co., Ltd. (Japan). Octamethylcyclotetrasiloxane (D_4) was purchased from Shin-Etsu Chemical (Japan). Ammonium carbonate ($(NH_4)_2CO_3$) and potassium hydroxide (KOH) were procured from Kanto Chemical Co., Inc. (Japan). *N*,*N*-Dimethylformamide (DMF) and 6 M hydrochloric acid (HCl aq.) were purchased from FUJIFILM Wako Pure Chemical Corporation (Japan). TEOS, thionyl chloride ($SOCl_2$), chlorodimethylsilane, and chlorodimethylvinylsilane were acquired from Tokyo Chemical Industry Co., Ltd. (Japan). PDMS–OH (45–85 cSt) and Karstedt catalyst (0.1 M in xylene solution)

were purchased from Sigma-Aldrich (Tokyo, Japan). TEOS were purified by distillation. HEDS and OETS were synthesized according to the methods described in chapter 2. KOH powder was prepared as follows: KOH pellets were dissolved in EtOH and reprecipitated with THF followed by drying under vacuum at 90 °C for 3 h [2].

2.3 Synthesis of Si–H-terminated oligosiloxane cross-linkers (CL_{TEOS}, CL_{HEDS}, and CL_{OETS})

HCl aq. was slowly added to EtOH solutions of ethoxysilane monomers (TEOS, HEDS, and OETS). HCl/Si molar ratio = 0.1 (HCl/TEOS molar ratio = 0.1, HCl/HEDS molar ratio = 0.2, and HCl/OETS molar ratio = 0.3), H_2O/Si–OEt molar ratio = 0.5 (H_2O/TEOS molar ratio = 2, H_2O/HEDS molar ratio = 3, and H_2O/OETS molar ratio = 4), and EtOH/Si molar ratio = 10 (EtOH/TEOS molar ratio = 10, EtOH/HEDS molar ratio = 20, and EtOH/OETS molar ratio = 30). The resulting mixtures were stirred in an ice bath for 10 min. Thereafter, the obtained mixtures were stirred for 3 h at room temperature (approximately 23 °C). Chlorodimethylsilane (equimolar ratio of added H_2O) was added into the resulting mixtures under stirring in an ice bath for 10 min. The acquired mixtures were poured into a mixed solvent of THF/hexane (1/2 v/v) followed by washing twice with water and twice with brine. The organic layers were dried over anhydrous sodium sulfate followed by filtration and evaporation. The resulting CLs were obtained as colorless liquids.

CL_{TEOS}: M_w = 1,500 Da, M_w/M_n = 1.1

CL_{HEDS}: M_w = 1,400 Da, M_w/M_n = 1.1

CL_{OETS}: M_w = 1,200 Da, M_w/M_n = 1.1

2.4 Synthesis of low-molecular-weight dimethylvinylsiloxy-terminated PDMS (Low–PDMS–Vi)

PDMS–OH (4.6 g) was dissolved in 6 mL THF. Then, 4 mL THF solution of vinyldimethylchrolosilane (3 mL) was added to the abovementioned mixture followed by stirring at room temperature for 30 min. After stirring, the resulting mixture was concentrated to half volume followed by reprecipitation with MeOH, and the viscous liquid was acquired. The viscous liquid was dried under vacuum at room temperature, and Low-PDMS–Vi was obtained as a viscous liquid (3.1 g).

^{1}H NMR (400 MHz, $CDCl_3$): δ (ppm) 6.16–5.71 (m, Vi), 0.91 (brs, CH_3).

2.5 Synthesis of dimethylvinylsiloxy-terminated PDMS (PDMS–Vi)

PDMS–Vi was prepared according to a previously reported procedure [2]. Octamethylcyclotetrasiloxane (D_4, 10 g, 34 mmol) and KOH powder (0.17 g, 3 mmol) were placed in a 200 mL four-necked flask equipped with a mechanical stirrer. The mixture was stirred at 180 °C for 2 h at 200 rpm. The resulting viscous liquid was cooled to approximately 23 °C and dissolved in 10 g toluene. Vinyldimethylchlorosilane (1.4 g, 11.8 mol) was added to the abovementioned solution

followed by stirring at approximately 23 °C for overnight. Subsequently, the resulting mixture was washed twice with water and then twice with brine, and the organic layer was dried over $MgSO_4$. After filtration, the solution was poured into MeOH under vigorous stirring, and the viscous liquid was acquired. This viscous liquid was dried under vacuum at 95 °C, and PDMS–Vi was obtained as an opaque viscous liquid (8.4 g, 95%).

^{1}H NMR (400 MHz, $CDCl_3$): δ (ppm) 6.13 (dd, Vi), 5.93 (dd, Vi), 5.73 (dd, Vi), 0.72 (brs, CH_3).

$^{13}C\{^{1}H\}$ NMR (125 MHz, $CDCl_3$): δ (ppm) 1.0 (CH_3).

$^{29}Si\{^{1}H\}$ NMR (100 MHz, $CDCl_3$): δ (ppm) −21.9.

GPC (THF eluent): $M_w = 49000$ g mol^{-1} and $M_w/M_n = 3.3$.

2.6 Model reactions of Low-PDMS–Vi and CL_{TEOS} with the Karstedt catalyst

Low-PDMS–Vi (0.06 g) and CL_{TEOS} (0.04 g) were dissolved in THF-d_8 (0.75 mL) followed by addition of 1 μL Karstedt catalyst (0.1 M in xylene solution). Progress of hydrosilylation was monitored by recording the ^{1}H NMR spectra at specific time intervals.

2.7 Preparation of PDMS-CLs

A 1 g mixture containing PDMS–Vi and CLs (at concentrations of 10, 20, and 40 wt% relative to PDMS–Vi) was dissolved in 4 g THF. To this solution, 10 μL Karstedt catalyst (0.1 M in xylene

solution) was added, and the mixture was stirred for 30 min. Thereafter, the obtained mixture was poured into a 50-mm ϕ Teflon Petri dish. Then, this mixture was cured at 50 °C for 1 day followed by heating at 150 °C for an additional day. The resulting PDMS–CLs were obtained as elastomers.

3 Results and discussion

3.1 Characterizations of CLs

$^{29}Si\{^{1}H\}$ NMR spectra of the hydrolysis condensates of TEOS, HEDS, and OETS before and after silylation are depicted in Figure 1. Before silylation, the spectra of all hydrolysis condensates primarily demonstrated signals corresponding to four-membered cyclic $Q^2(OEt)(OH)$ (−92.7 ppm) and four-membered cyclic $Q^2(OEt)_2$ (−95.1 ppm). Minor signals associated with $Q^1(OEt)_2(OH)$ (approximately −86 ppm), cyclic $Q^2(OH)_2$ (−90.6 ppm), Q^3–OH (from −99.6 to −101 ppm), and Q^3–OEt (from −101.5 to −103 ppm) were also observed [1,3–5]. Small signals due to five- or six-membered cyclic $Q^2(OEt)_2$ (−95.4 ppm) were noticed in the spectra of the hydrolysis condensates of TEOS and OETS before silylation [3,6]. Following silylation, complex signals attributed to the dimethylsiloxyl group emerged between −1 and −5 ppm [3]. All silylated hydrolyzates (CL_{TEOS}, CL_{HEDS}, and CL_{OETS}) included end-group $Q^1(OEt)_3$ (−89.0 ppm), four-membered cyclic $Q^2(OEt)_2$ (−95.3 ppm), and linear $Q^2(OEt)_2$ (−96.5 ppm). Signals of Q^3 and Q^4 units were evident between −99 and −105 ppm and −105 and −110 ppm, respectively; nevertheless, detailed structures of these units could not be determined. To identify

the position of silylation, ethoxylation of the Si—H group was performed using $Zn(OCOCH_3)_2$ as a catalyst [7]; however, this reaction did not proceed. Table 1 provides GPC results, OEt/Si–H ratios, siloxane unit ratios, and degrees of crosslinking (DCs). OEt/Si–H ratios of CLs exhibited no considerable differences.

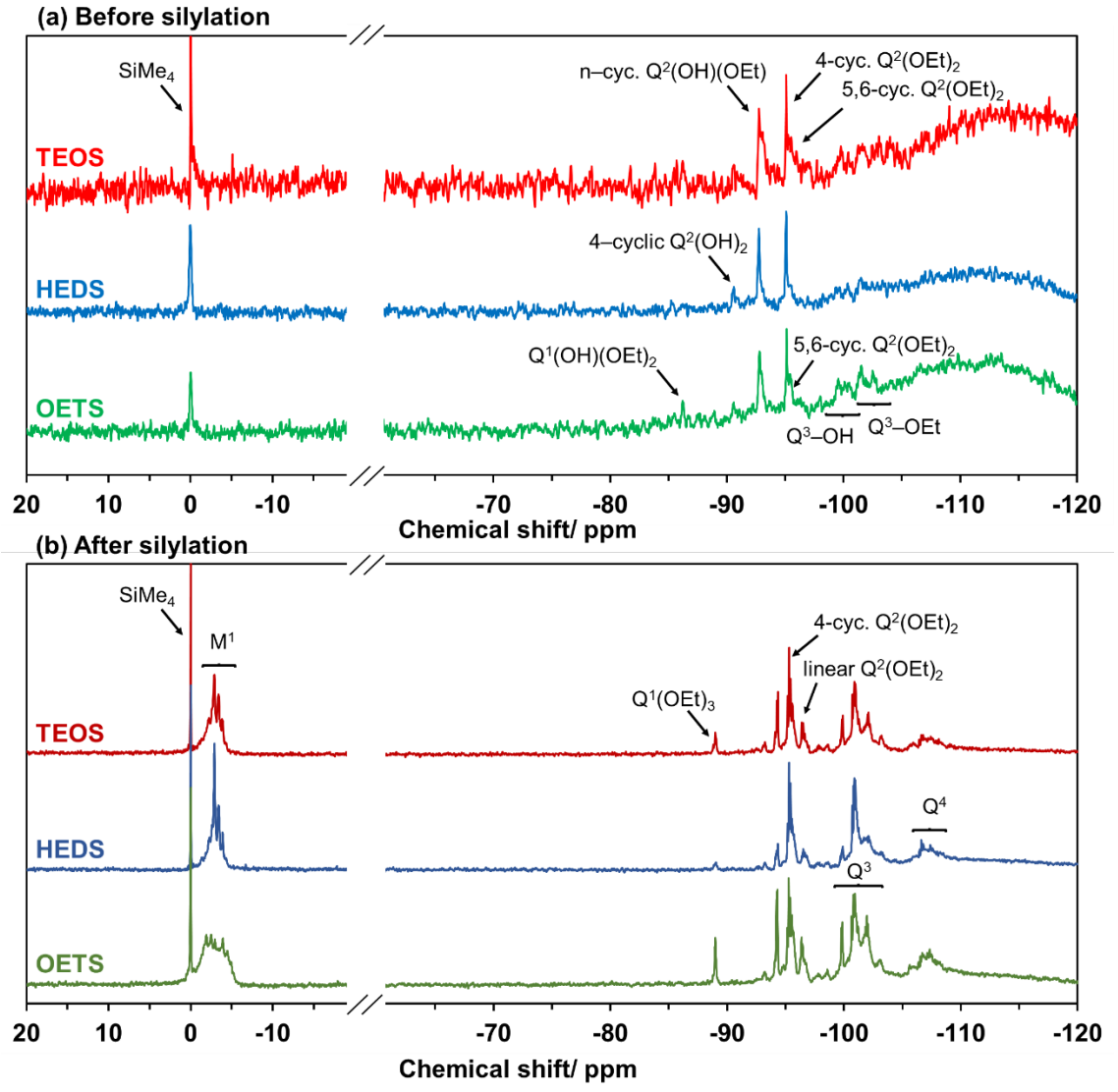

Figure 1. $^{29}Si\{^1H\}$ NMR spectra of the hydrolysis condensates of TEOS, HEDS, and OETS (a) before and (b) after silylation.

Table 1. Synthesis of CLs

monomer	Before/after silylation	GPC result[a]		OEt/Si-H[b]	Ratio of siloxane units[c](%)					DC[d] (%)
		$M_w \times 10^{-3}$	M_w/M_n	ratio	Q^0	Q^1	Q^2	Q^3	Q^4	
CL_{TEOS}	Before				0	11	44	45	0	59
	After	1.5	1.1	4	0	4	36	44	16	68
CL_{HEDS}	Before				0	8	48	44	0	59
	After	1.4	1.1	4	0	2	34	47	17	70
CL_{OETS}	Before				0	9	58	33	0	56
	After	1.2	1.1	4	0	3	36	46	15	68

a Calculated based on standard polystyrene

b Calculated based on ^{1}H NMR spectra

c Calculated based on the Q^n signal area of ^{29}Si NMR spectra

d $DC(\%)=0/4Q^0+1/4Q^1+2/4Q^2+3/4Q^3+4/4Q^4$

FTIR spectra of CLs are shown in Figure 2. Absorption bands due to υSi–H (2139 cm^{-1}), δCH_3 (approximately 1255 cm^{-1}), δSi–Me (approximately 1155 cm^{-1}), υCC (970 cm^{-1}), and ρSi–Me (903 cm^{-1}) were detected, indicating the completion of silylation [3,8]. Absorption bands related to $\upsilon_{as}CH_3$ (approximately 2977 cm^{-1}), υ_sCH_2 (approximately 2930 cm^{-1}), υ_sCH_3 (approximately 2897 cm^{-1}), υCO (approximately 1100 cm^{-1}), υ_{as}Si–O–Si (approximately 1080 cm^{-1}), ρCH_3 in Si–CH_3 (860 cm^{-1}), υ_sSi–O–Si (795 cm^{-1}), and δCCO and δSiOSi (approximately 455 cm^{-1}) were also observed [2,3,9,10].

a)

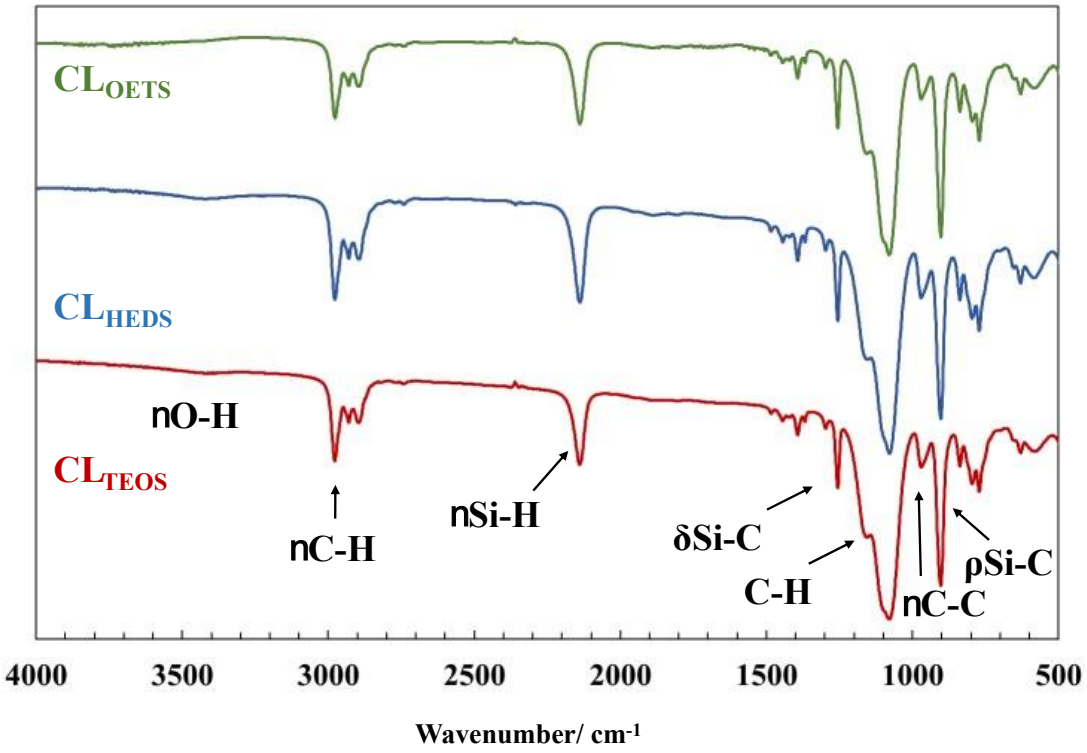
CLOETS
CLHEDS
CLTEOS
nO-H
nC-H
nSi-H
δSi-C
C-H
nC-C
ρSi-C
4000
3500
3000
2500
2000
1500
1000
500
Wavenumber/ cm-1

b)

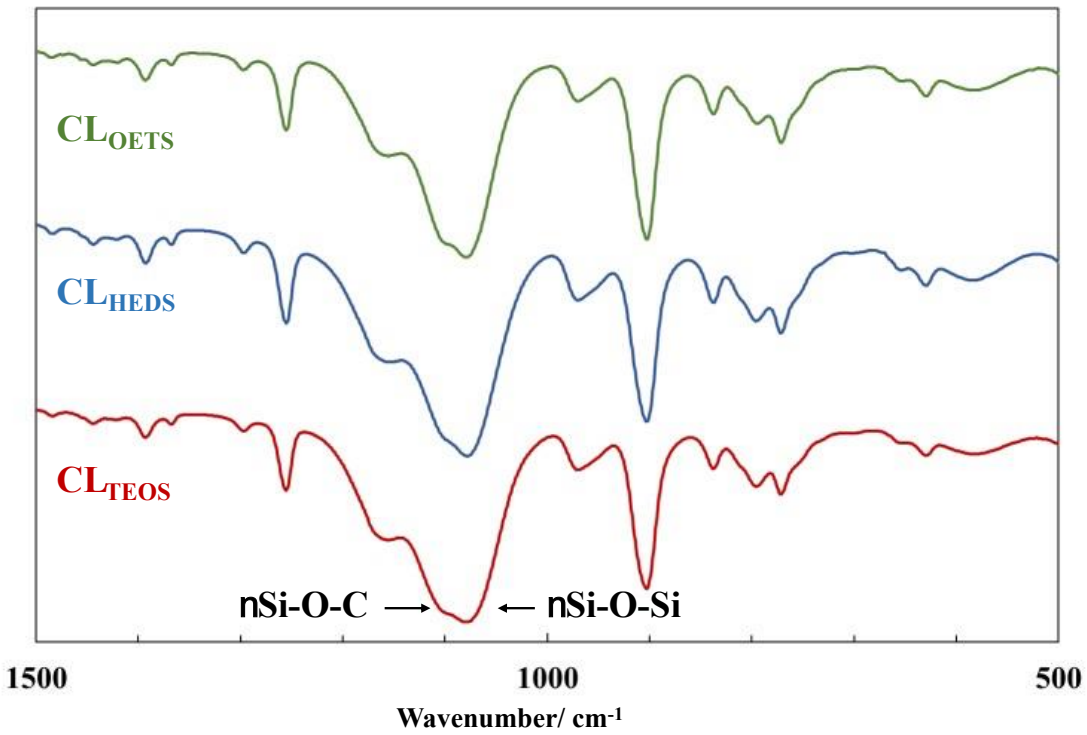
CLOETS
CLHEDS
CLTEOS
nSi-O-C
nSi-O-Si
1500
1000
500
Wavenumber/ cm-1

Figure 2. FTIR spectra of CLs: a) 4000–400 cm^{-1} region and b) 1600–400 cm^{-1} region.

Figure 3 depicts the mass spectra of CLs. These spectra reveal the presence of several chemical species, ranging from trisiloxane to octasiloxane. Nevertheless, precise interpretations of the CL mass spectra are challenging due to the existence of structures with overlapping molecular weights.

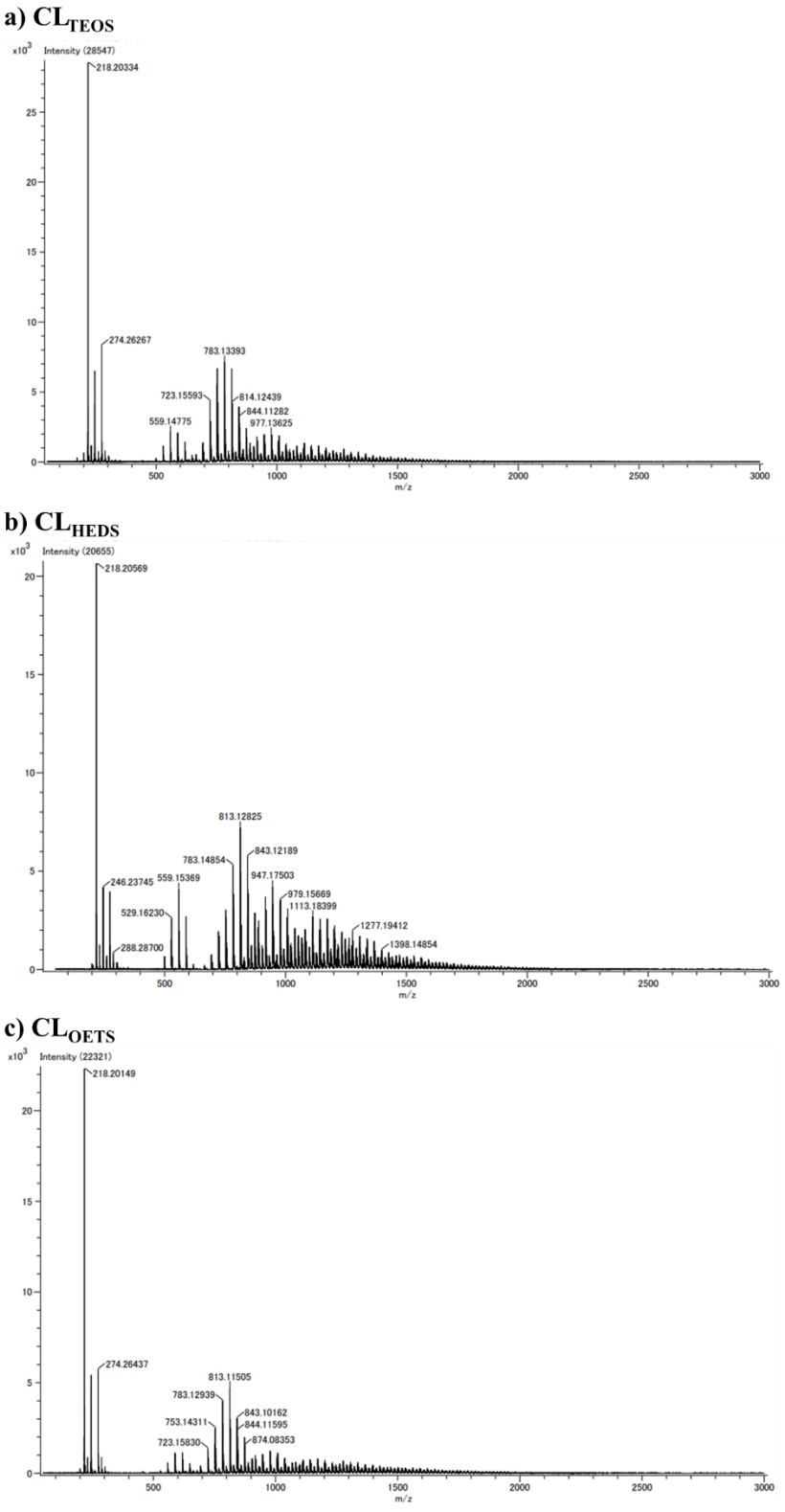

Figure 3. ESI-MS spectra of a) CL_{TEOS}, b) CL_{HEDS}, and c) CL_{OETS}.

Figure 4 shows the schematics of the anticipated structures of CLs. Specifically, CL_{TEOS} primarily consisted of cyclic siloxane derivatives, which were mainly converted from Q^1 and Q^2 to Q^4 owing to silylation. CL_{HEDS} was primarily composed of four-membered cyclic siloxane derivatives, mainly transforming from Q^2 to Q^4 due to silylation. Moreover, CL_{OETS} primarily consisted of cyclic siloxane derivatives, mainly converting from Q^2 to both Q^3 and Q^4 because of silylation.

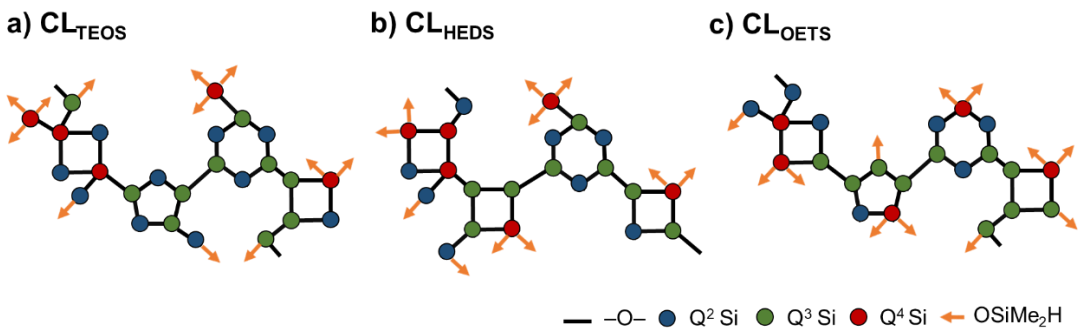

Figure 4. Schematics of the estimated structures of a) CL_{TEOS}, b) CL_{HEDS}, and c) CL_{OETS}.

3.2 Properties of PDMS elastomers cross-linked with CL_{TEOS}, CL_{HEDS}, and CL_{OETS}

To confirm the progress of hydrosilylation between PDMS–Vi and CLs, hydrosilylation between Low-PDMS–Vi and CL_{TEOS} in THF-d_8 as a model reaction was monitored by ^{1}H NMR spectroscopy (Figure 5). Signals originating from vinyl and hydrosilyl groups appeared at 5.7–6.2 and 4.8 ppm, respectively, and the corresponding integral ratios decreased with an increase in time (Figure 4). Signals attributed

to methylene (SiC**H₂**) moieties were detected at 0.55 ppm [11,12], and the corresponding integral ratio increased with an increase in time (Figure 6). This suggests the progress of *β*-addition [12]. After 2 h of reaction initiation, vinyl group was detection limit in the ^{1}H NMR spectrum. These results implied main progression of hydrosilylation between PDMS-Vi and CLs and *β*-addition.

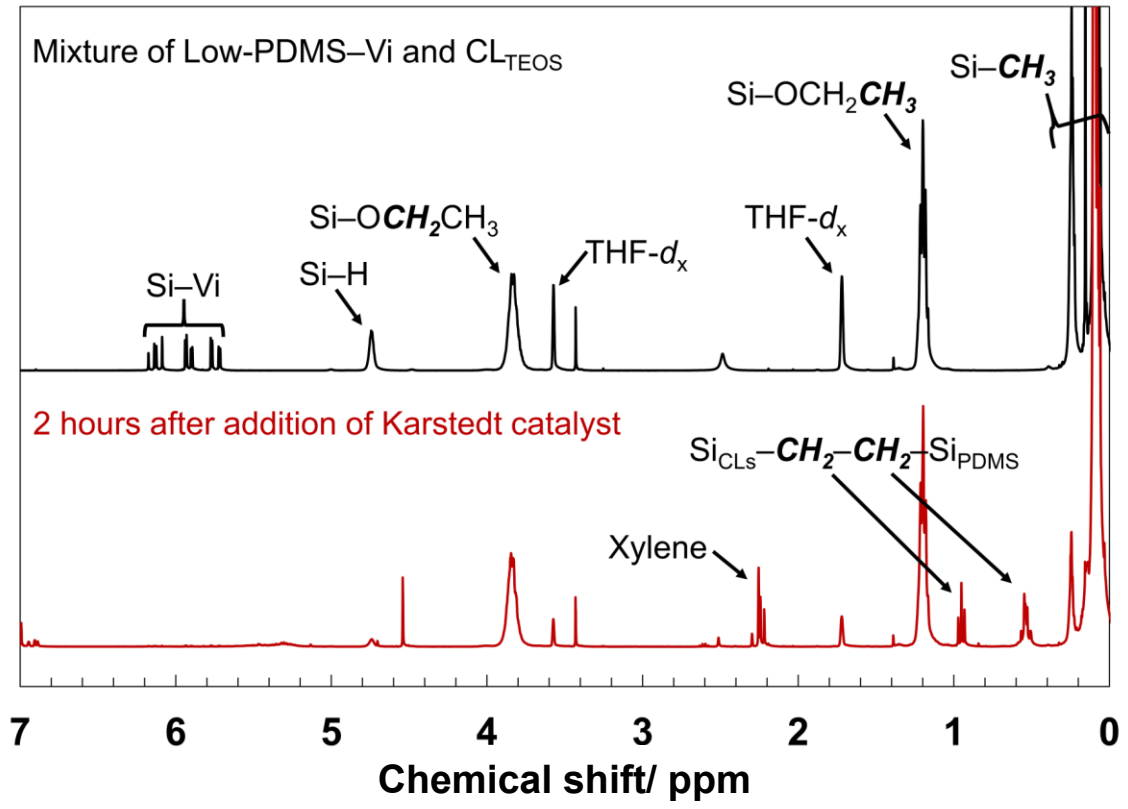

Figure 5. ^{1}H NMR spectra obtained before and after the addition of the Karstedt catalyst to the solution of Low-PDMS–Vi and CL$_{TEOS}$.

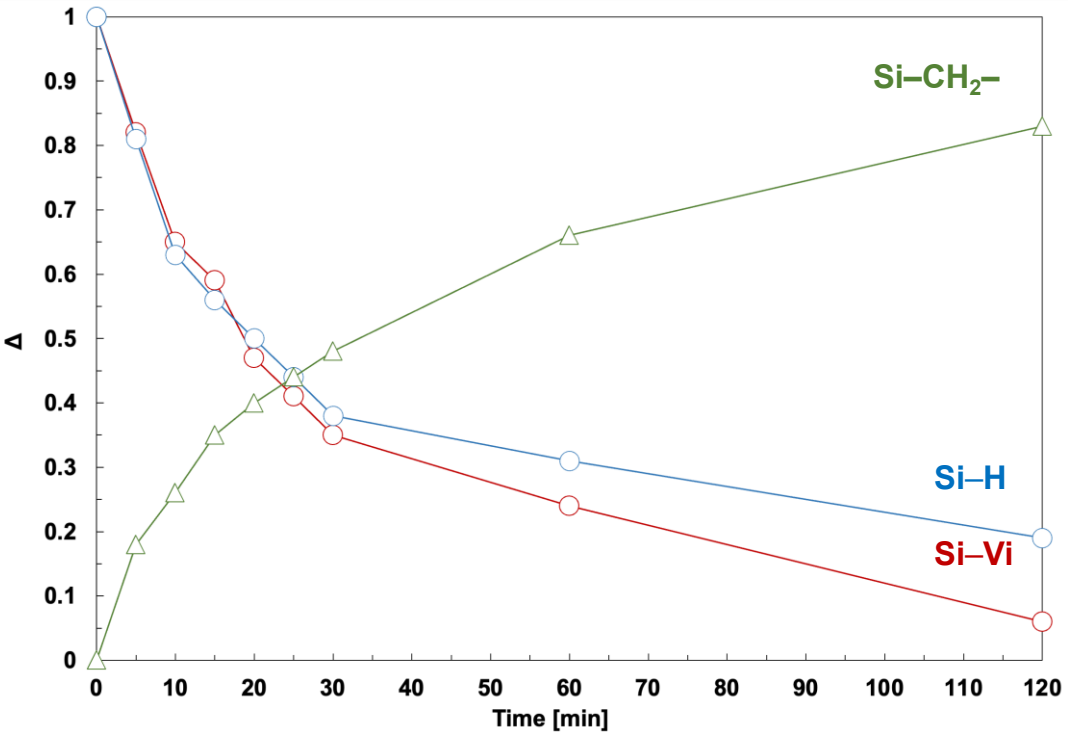

Figure 6. Variation of the integral values of vinyl, hydrosilyl, and methylene groups during hydrosilylation of Low-PDMS–Vi with CL_{TEOS} in the presence of Karstedt catalyst.

Figure 7 depicts the FTIR spectra of PDMS–CLs and PDMS–Vi acquired using the ATR method. Absorption bands related to $\upsilon_{as}CH_3$ (2962 cm^{-1}), $\upsilon_{s}CH_2$ (2903 cm^{-1}), δCH_3 in $Si–CH_3$ (1258 cm^{-1}), ρCH_3 in $Si–CH_3$ (860 cm^{-1}), υSi–C (785 cm^{-1}), and υSi–C (700 cm^{-1}) were observed for the PDMS chain [2,3,9,10]. Strong bands associated with $\upsilon_{as}Si–O–Si$ (1060 cm^{-1}), υO–Si–O (1010 cm^{-1}), $\delta SiCH_3$ and υSiO_4 (780 cm^{-1}), and υSi–O (750 cm^{-1}) emerged, and the υO–Si–O (1010 cm^{-1}) and υSi–O (750 cm^{-1}) bands stemmed from the PDMS chain [9,10,13]. No absorption band corresponding to υSi–H (2139 cm^{-1}) was detected, supporting the progress of hydrosilylation [3,8]. The absorption bands related to ρCH_3 (1160 cm^{-1}), υC–O (1070 cm^{-1}), υC–C (970 cm^{-1}), and ρCH_2 (848 cm^{-1}) were

noticed for the ethoxy group [7,17,18].

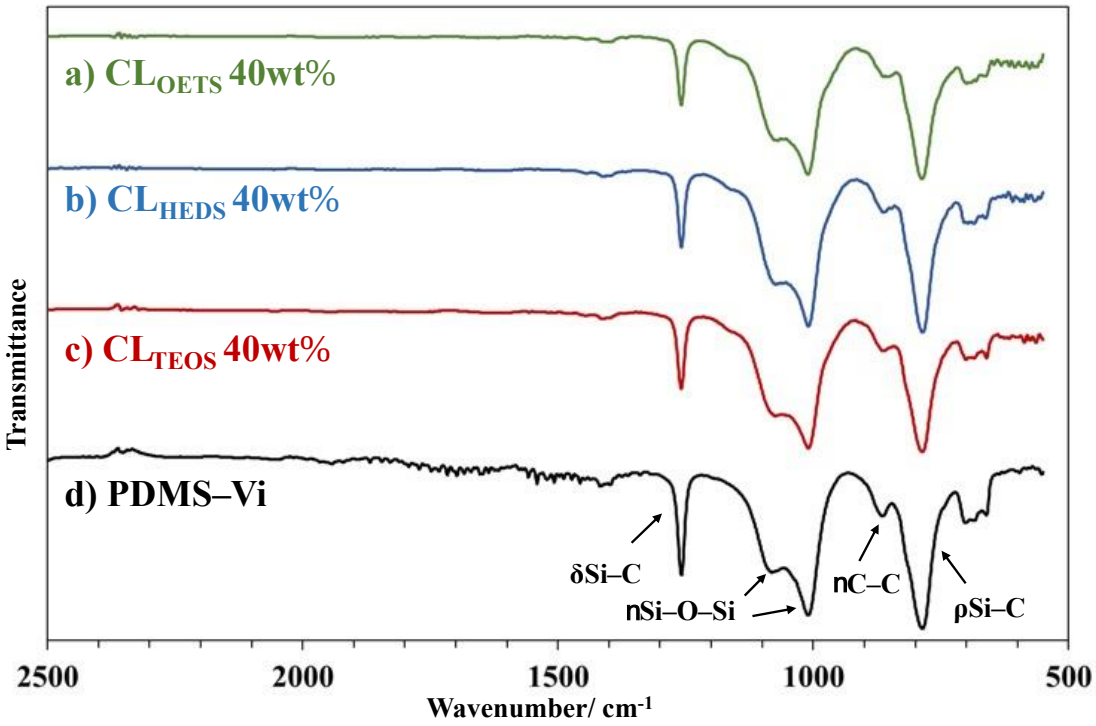

Figure 7. FTIR spectra of a-c) PDMS–CLs with 40 wt% CLs and b) PDMS–Vi acquired via the ATR method.

Surface morphologies of PDMS–CLs with 40 wt% CLs were examined via SEM. Some spherical accumulation domains (1–2 μm) were observed on the surface, which might be ascribed to the aggregation of CLs (Figure 8). Aggregation was noticed in the PDMS–MQ elastomer prepared by condensation of PDMS–OH with the MQ polymer [15].

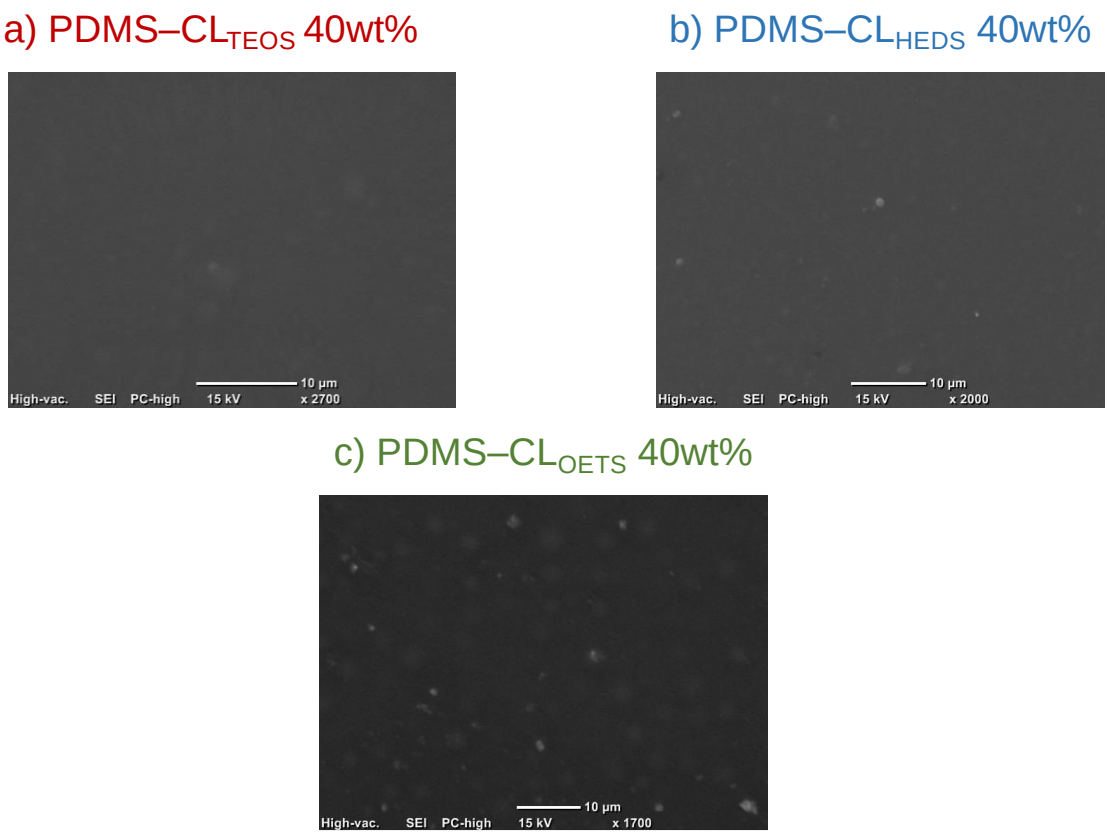

Figure 8. SEM images of a) PDMS–CL$_{TEOS}$ 40 wt%, b) PDMS–CL$_{HEDS}$ 40 wt%, and c) PDMS–CL$_{OETS}$ 40 wt%.

Transmittances, temperatures corresponding to 5% weight loss (T_{d5}), swelling behaviors in toluene, and tensile strengths of PDMS–CLs were assessed. Although PDMS–CLs demonstrated

excellent transparencies (≥80% at 500 nm), their appearance was tinted due to the inclusion of the Pt catalyst (Figure 9) [16]. An elastomer was fabricated without the Karstedt catalyst and employed as a control; however, it was brittle and weak (Figure 9).

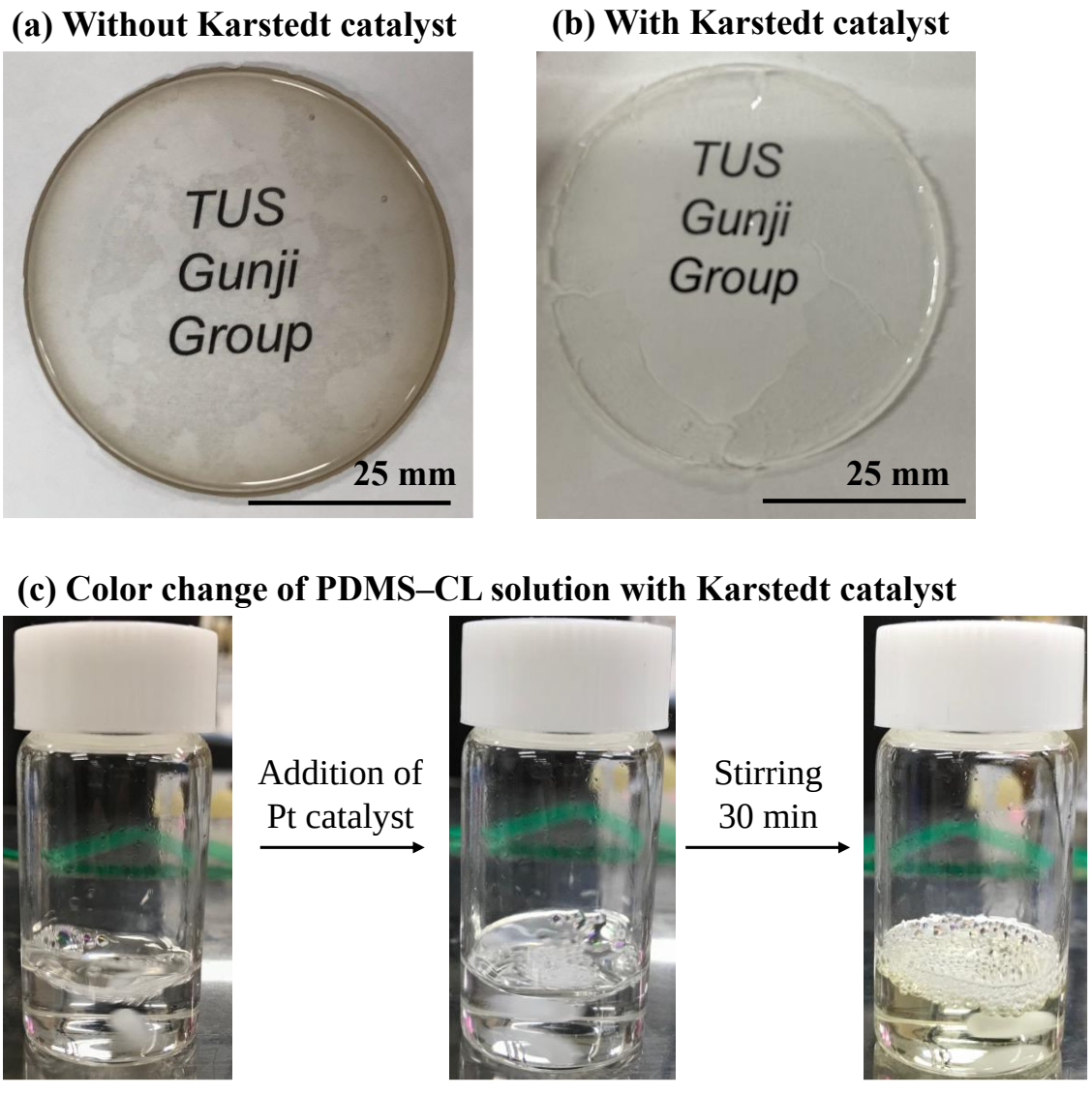

Figure 9. Images of PDMS–CLs without and with Karstedt catalyst and color change of the PDMS-CL solution with the addition of the Karstedt catalyst.

Thermal properties of PDMS–Vi and PDMS–CLs were investigated using TGA under a N_2 atmosphere. TGA profiles of PDMS–Vi and PDMS–CLs are depicted in Figure 10. T_{d5} value of PDMS–Vi was 364 °C, and the residual mass at 1000 °C was 5.5%. This was attributed to the formation of cyclic siloxanes, such as D_3 and D_4, via depolymerization caused by the thermal degradation of PDMS under N_2 flow [17]. T_{d5} values of PDMS–CLs (420–480 °C) were higher than that of PDMS–Vi. Increased crosslinking can inhibit random polymer-main chain degradation [18–21] because PDMS primarily depolymerizes from its chain ends and then undergoes random main-chain degradation at high temperatures in an inert environment [17,19]. Hence, the higher T_{d5} values were attributed to the high crosslinking density. Nevertheless, the T_{d5} values decreased with an increase in the addition amounts of CLs. As ethoxy groups undergo decomposition at 250–350 °C [22,23], decomposition of the ethoxy groups decreased the T_{d5} values. Residual masses for PDMS–CL_{HEDS} and PDMS–CL_{OETS} increased in the following order of the addition amounts of CLs: 20 wt% > 40 wt% > 10 wt%; however, general understanding is that the higher the crosslinking density, the higher the residual mass [24]. We proposed that the inhibition of cyclization of PDMS via thermal degradation and slight decomposition of the ethoxy groups in CLs might affect the residual mass; hence, PDMS–CL 40 wt% exhibited lower residual mass than that of PDMS–CL 20 wt% due to the presence of a large number of ethoxy groups. Nevertheless, it is postulated that the thermal properties of PDMS materials might be more influenced by the PDMS chain length than by DC [2,25–28];

therefore, these thermal degradation behaviors of PDMS–CLs are expected to vary with respect to the PDMS chain length. A similar trend was noticed under aerobic conditions, and the corresponding T_{d5} values are systematically presented in Table 2.

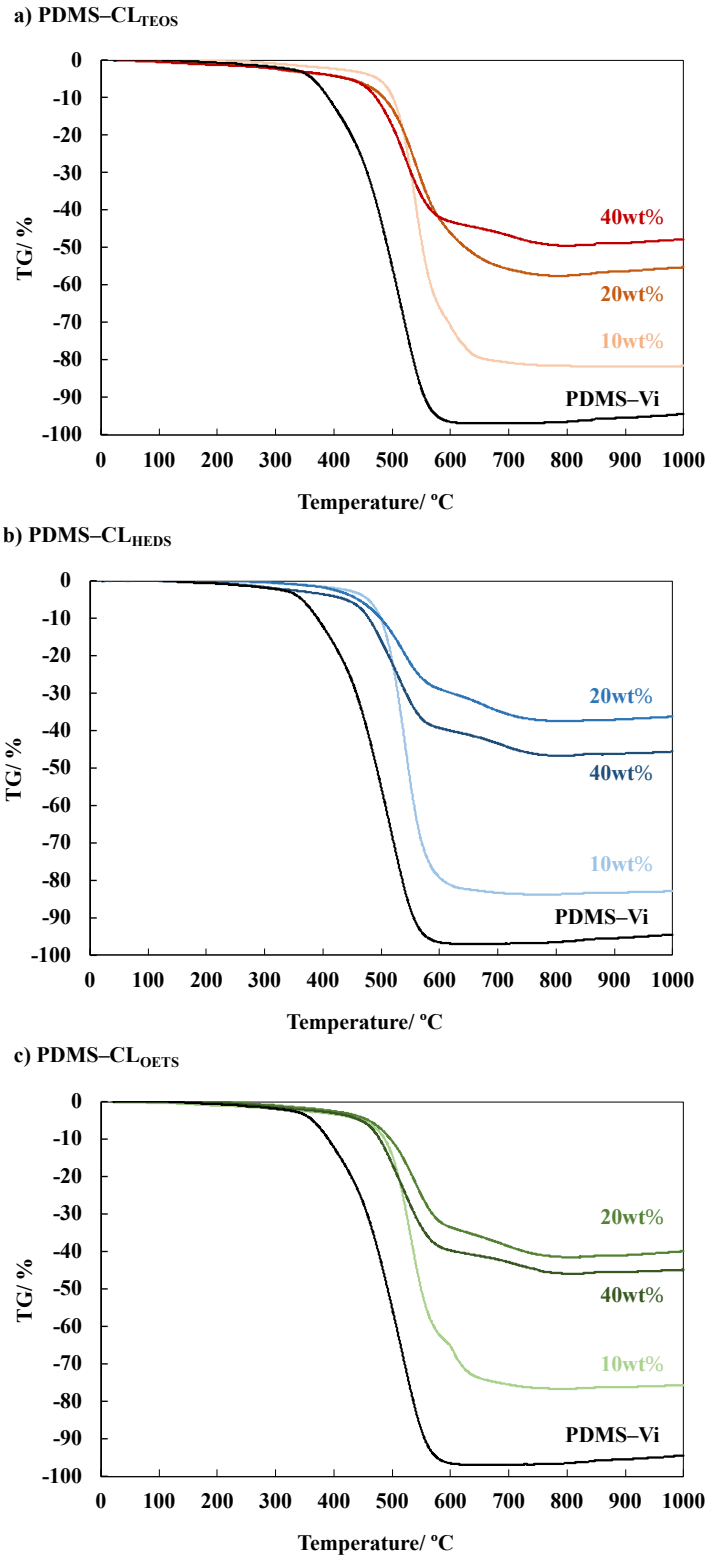

Figure 10. TGA traces of PDMS–Vi and a) PDMS–CL$_{TEOS}$, b) PDMS–CL$_{HEDS}$, and c) PDMS–CL$_{OETS}$ under N_2 flow.

Table 2. Summary of the T_{d5} values of PDMS–CLs under air flow

CL	Content of CL (wt%)	T_{d5}[a] (°C)
none	0	234
CL_{TEOS}	10	365
	20	343
	40	326
CL_{HEDS}	10	336
	20	347
	40	339
CL_{OETS}	10	336
	20	341
	40	309

[b]Measured by TG-DTA under air flow; T_{d5}: temperatures of 5% weight loss

To explore the mechanical reinforcement effects of CL incorporation into PDMS, the tensile properties of PDMS–CLs were evaluated. Outcomes of the tensile strength tests are provided in Figure 11.

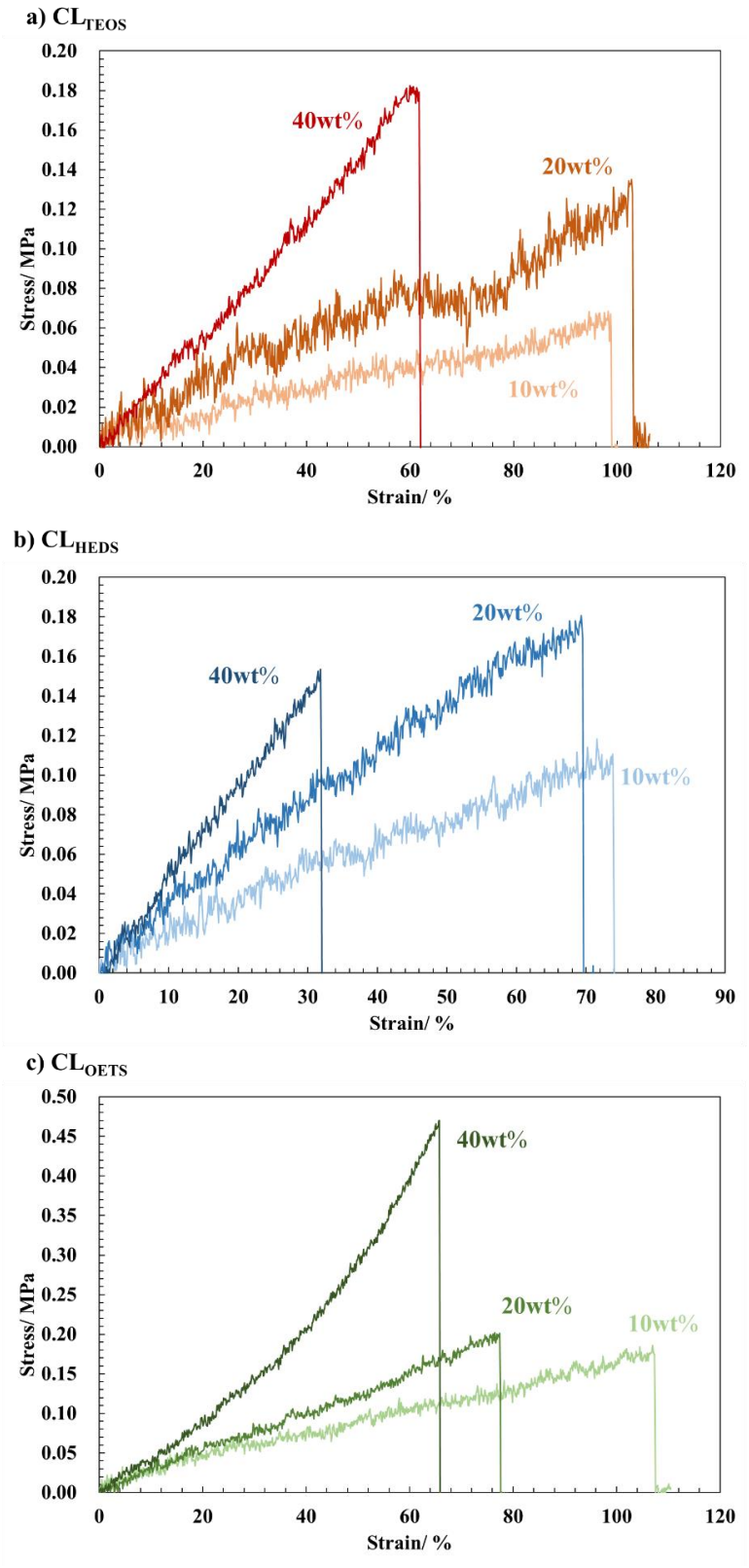

Figure 11. Stress–strain curves for a) PDMS–CL$_{TEOS}$, b) PDMS–CL$_{HEDS}$, and c) PDMS–CL$_{OETS}$.

Secant modulus was determined from the tensile strength and strain values at the breaking point. PDMS–CLs demonstrated low secant moduli and tensile strengths, ranging from 0.67 MPa (for PDMS with 10 wt% CL_{TEOS}) to 1.4 MPa (for PDMS with 40 wt% CL_{OETS}) and from 0.06 MPa (for PDMS with 10 wt% CL_{TEOS}) to 0.96 MPa (for PDMS with 40 wt% CL_{OETS}), respectively. Behaviors of the secant moduli of PDMS–CLs with respect to the CL content are shown in Figure 12. With an increase in the CL content, the secant moduli of PDMS–CLs also increased. Mackenzie *et al.* highlighted that the mechanical properties of PDMS–SiO_2 were influenced by the composition ratio of PDMS and silicates [29]. Furthermore, the secant moduli and tensile strengths of PDMS materials depend on the crosslinked network [25,30]. Consequently, CL_{HEDS} and CL_{OETS} are inferred to exhibit superior crosslinking efficiencies as compared to that of CL_{TEOS}, consistent with earlier findings.

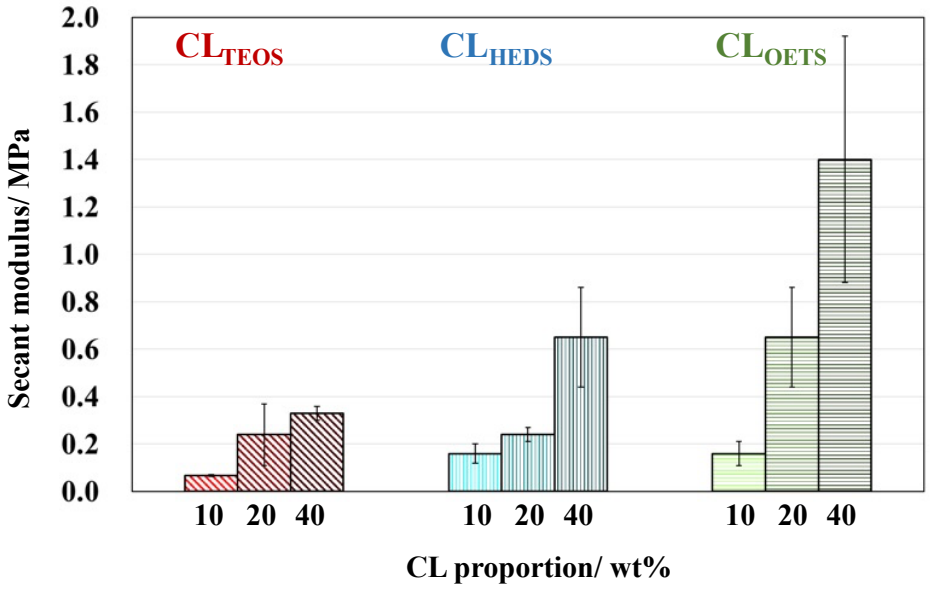

Figure 12. Behaviors of the secant moduli of elastomers.

Swelling tests of PDMS–CLs were conducted by measuring the solvent uptakes of PDMS–CLs stored in toluene at approximately 23 °C for 3 days. Results of these tests are depicted in Figure 13. No soluble fraction was detected in the swelling test, which validated that all PDMS–CLs underwent reaction and crosslinking. Degree of swelling is inversely proportional to DC; with an increase in DC, the swelling degree diminishes [2,31–33]. With an increase in the CL content, the swelling degree correspondingly decreased. This trend implies an increase in DC with an increase in the CL content. Solvent uptakes of CLs decreased in the following sequence: $CL_{TEOS} < CL_{HEDS} \leq CL_{OETS}$. Both CL_{HEDS} and CL_{OETS} are speculated to demonstrate superior crosslinking efficiencies to that of CL_{TEOS}. This hypothesis stems from the supposed relationship of crosslinking efficiency with the contents of four-membered cyclic siloxane derivatives and silylation on Q^3 silicon atom [1,33]. However, when the CL content reached 40 wt%, the swelling degree did not exhibit a significant difference. As aggregates were observed in the SEM image of PDMS–CLs 40 wt% and the interface between PDMS chain and CLs was bigger, structural characteristics of CLs were speculated to be weak.

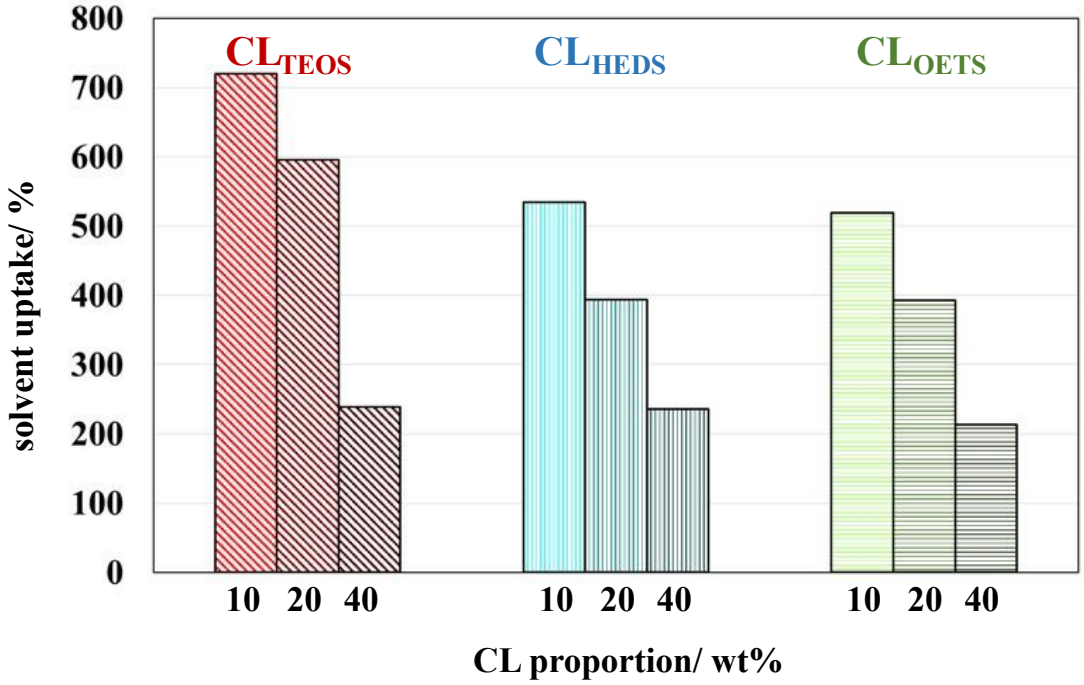

Figure 13. Swelling behaviors of elastomers after storage in toluene for 3 days.

4 Conclusion

Herein, CLs were employed as cross-linkers for PDMS based silicone elastomers. All CLs demonstrated similar M_w values (approximately 1400 Da), M_w/M_n values (1.1), and OEt/Si–H ratios (4). Nevertheless, their structures were different: CL_{TEOS} was primarily composed of cyclic siloxane derivatives silylated on Q^4 silicon atom; CL_{HEDS} mainly consisted of four-membered cyclic siloxane derivatives silylated on Q^4 silicon atom; and CL_{OETS} predominantly comprised cyclic siloxane derivatives silylated on both Q^3 and Q^4 silicon atom. Properties of PDMS–CLs are provided in Table

3. Influences of these distinct cross-linker structures on the transmittance, thermal stability, tensile strength, and swelling behavior in toluene were assessed. These evaluations indicated superior crosslinking efficiencies of CL_{HEDS} and CL_{OETS} to that of CL_{TEOS}. These differences are believed to arise from the presence of four-membered cyclic siloxane derivatives and silylation on Q^3 silicon atom. Thus, the properties of the elastomers are concluded to be considerably affected by the cross-linker structures.

Table 3. Summary of physical properties of the elastomers prepared from PDMS−Vi and PDMS−CLs

CL	Content of CL (wt%)	Thickness (μm)	Transmittance[a]	T_{d5}[b] (°C)	Residual mass[b] (%)	Swelling to toluene[c] (%)	Secant modulus (MPa)	Tensile strength (MPa)
none	0	-	-	364	5.5	-	-	-
CL_{TEOS}	10	199	80	478	19.8	720	0.067±0.003	0.06±0.0008
	20	110	87	427	44.8	595	0.24±0.13	0.18±0.04
	40	271	84	425	52.3	239	0.33±0.03	0.24±0.02
CL_{HEDS}	10	162	81	478	17.1	534	0.16±0.04	0.07±0.003
	20	156	87	460	63.7	394	0.24±0.03	0.12±0.04
	40	204	89	439	54.4	236	0.65±0.21	0.32±0.27
CL_{OETS}	10	148	86	447	24.3	519	0.16±0.05	0.086±0.06
	20	181	89	460	60.1	393	0.65±0.21	0.17±0.02
	40	183	85	446	55.2	213	1.4±0.52	0.96±0.45

[c]Measurement by UV-Vis spectra; the values are calculated at 500 nm

[b]Measurement by TG-DTA: T_{d5}; temperatures of 5% weight loss

[c]Solvent uptake calculated as 100 × solvent (g)/film (g)

References

1. I. B. Meshkov, A. A. Kalinina, V. V. Gorodov, A. V. Bakirov, S. V. Krasheninnikov, S. N. Chvalun, A. M. Muzafarov, *Polymers*, **13**, 2848 (2021). https://doi.org/10.3390/polym13172848

2. R. Hayami, I. Nishikawa, T. Hisa, H. Nakashima, Y. Sato, Y. Ideno, T. Sagawa, S. Tsukada, K. Yamamoto, T. Gunji, *J. Sol-Gel Sci. Technol.*, **88**, 660–670 (2018). https://doi.org/10.1007/s10971-

018-4839-z

3. Y. Sato, R. Hayami, T. Gunji, *J. Sol-Gel Sci. Technol.*, **104**, 36–52 (2022). https://doi.org/10.1007/s10971-022-05920-y

4. L. W. Kelts, N. J. Armstrong, *J. Mater. Res.*, **4**, 423–433 (1989). https://doi.org/10.1557/JMR.1989.0423

5. R. J. Hook, *J. Non-Cryst. Solids*, **195**, 1–15 (1996). https://doi.org/10.1016/0022-3093(95)00508-0

6. B. Unger, H. Jancke, M. Hähnert, H. Stade, *J. Sol-Gel Sci. Technol.*, **2**, 51–56 (1994). https://doi.org/10.1007/BF00486212

7. Y. Satoh, K. Fuchise, T. Nozawa, K. Sato, M. Igarashi, *Chem. Commun.*, **56**, 8218–8221 (2020). https://doi.org/10.1039/D0CC03379K

8. T. Gunji, T. Igarashi, S. Tsukada, Y. Abe, *J. Sol-Gel Sci. Technol.*, **81**, 21–26 (2017). https://doi.org/10.1007/s10971-016-3998-z

9. H. Barthel, E. Nikitina, *Silicon Chem.*, **1**, 239–247 (2002). https://doi.org/10.1023/B:SILC.0000018351.78847.f7

10. H. Barthel, E. Nikitina, *Silicon Chem.*, **1**, 261–279 (2002). https://doi.org/10.1023/B:SILC.0000018353.32350.c9

11. M. R. Ramli, M. B. H. Othman, A. Arifin, Z. Ahmad, *Polym. Degrad. Stab.*, **96**, 2064–2070 (2011). https://doi.org/10.1016/j.polymdegradstab.2011.10.001

12. Q-F. Si, X. Wang, X-D. Fan, S-J. Wang, *J. Polym. Sci., Part A: Polym. Chem.*, **43**, 1883–1894 (2005). https://doi.org/10.1002/pola.20675

13. R. E. Richards, H. W. Thompson, *J. Chem. Soc.*, 124–132 (1949). https://doi.org/10.1039/JR9490000124

14. F. Rubio, J. Rubio, J. L. Oteo, *Spectrosc. Lett.*, **31**, 199–219 (1998). https://doi.org/10.1080/00387019808006772

15. J. Ji, X. Ge, X. Pang, R. Liu, S. Wen, J. Sun, W. Liang, J. Ge, X. Chen, *Polymers*, **11**, 1142 (2019). https://doi.org/10.3390/polym11071142

16. R. Y. Lukin, A. V. Sukhov, A. D. Kachmarzhik, A. B. Dobrynin, K. R. Khayarov, O. G. Sinyashin, D. G. Yakhvarov, *Organometallics*, **42**, 2447–2452 (2023). https://doi.org/10.1021/acs.organomet.2c00671

17. G. Camino, S. M. Lomakin, M. Lazzari, *Polymer*, **42**, 2395–2402 (2001). https://doi.org/10.1016/S0032-3861(00)00652-2

18. D. Chen, S. Yi, W. Wu, Y. Zhong, J. Liao, C. Huang, W. Shi, *Polymer*, **51**, 3867–3878 (2010). https://doi.org/10.1016/j.polymer.2010.06.028

19. G. Camino, S. M. Lomakin, M. Lageard, *Polymer*, **43**, 2011–2015 (2002). https://doi.org/10.1016/S0032-3861(01)00785-6

20. K. Tanaka, S. Adachi, Y. Chujo, *J. Polym. Sci., Part A: Polym. Chem.*, **47**, 5690–5697 (2009).

https://doi.org/10.1002/pola.23612

21. Y. Sato, R. Hayami, Y. Miyase, Y. Ideno, K. Yamamoto, T. Gunji, *J. Sol-Gel Sci. Technol.*, **95**, 474–481 (2020). https://doi.org/10.1007/s10971-020-05291-2

22. N. Takamura, K. Taguchi, T. Gunji, Y. Abe, *J. Sol-Gel Sci. Technol.*, **16**, 227–234 (1999). https://doi.org/10.1023/A:1008765103113

23. Y. Abe, K. Kagayama, N. Takamura, T. Gunji, T. Yoshihara, N. Takahashi, *J. Non-Cryst. Solids*, **261**, 39–51 (2000). https://doi.org/10.1016/S0022-3093(99)00614-6

24. S. Sabhani, S. Bastani, U. W. Gedde, M. G. Sari, B. Ramezanzadeh, *Prog. Org. Coat.*, **113**, 117–125 (2017). https://doi.org/10.1016/j.porgcoat.2017.08.012

25. K. Yamamoto, T. Shimoda, Y. Sato, T. Nakaya, J. Ohshita, T. Gunji, *J. Sol-Gel Sci. Technol.*, **104**, 724–734 (2022). https://doi.org/10.1007/s10971-022-05806-z

26. N. Grassie, I. G. Macfarlane, *Eur. Polym. J.*, **14**, 875–884 (1978). https://doi.org/10.1016/0014-3057(78)90084-8

27. N. Grassie, I. G. Macfarlane, K. F. Francey, *Eur. Polym. J.*, **15**, 415–422 (1979). https://doi.org/10.1016/0014-3057(79)90053-3

28. Y. Han, J. Zhang, L. Shi, S. Qi, J. Cheng, R. Jin, *Polym. Degrad. Stab.*, **93**, 242–251 (2008). https://doi.org/10.1016/j.polymdegradstab.2007.09.010

29. J. D. Mackenzie, Q. Huang, T. Iwamoto, *J. Sol-Gel Sci. Technol.*, **7**, 151–161 (1996).

https://doi.org/10.1007/BF00401034

30. R. Seghir, S. Arscott, *Sens. Actuators A: Phys.*, **230**, 33–39 (2015). https://doi.org/10.1016/j.sna.2015.04.011

31. A. M. Sawvel, S. C. Chinn, M. Gee, C. K. Loeb, A. Maiti, H. E. Mason, R. S. Maxwell, J. P. Lewicki, *Macromolecules*, **52**, 410–419 (2019). https://doi.org/10.1021/acs.macromol.8b01939

32. A. M. Sawvel, J. C. Crowhurst, H. E. Mason, J. S. Oakdale, S. Ruelas, H. V. Eshelman, R. S. Maxwell, *Macromolecules*, **54**, 4300–4312 (2021). https://doi.org/10.1021/acs.macromol.1c00086

33. X. Fan, X. Cao, X. Shang, X. Zhang, C. Huang, J. Zhang, K. Zheng, Y. Ma, *Polym. Chem.*, **12**, 5149–5158 (2021). https://doi.org/10.1039/D1PY00688F

Chapter 4

Syntheses of coordination polymers using acetylacetonato-terminated polyhedral oligomeric silsesquioxanes and their properties

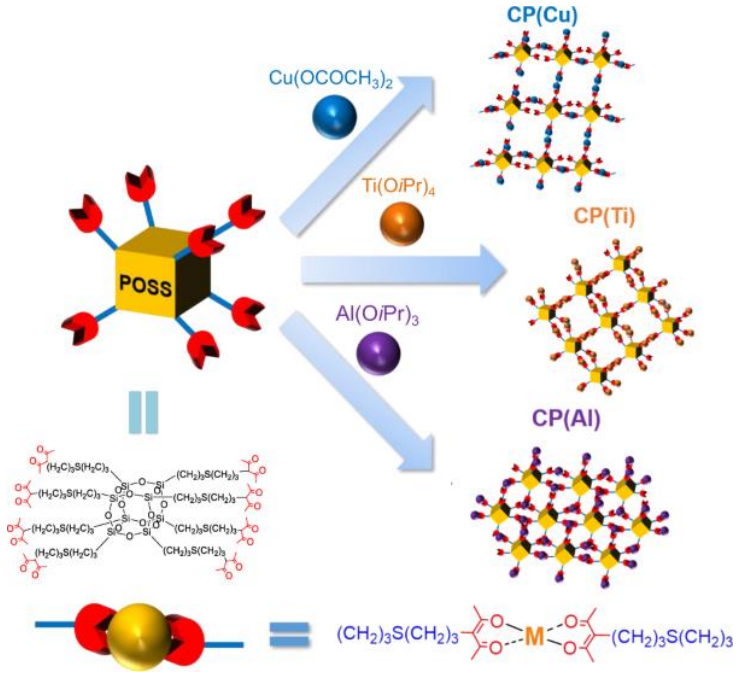

1 Introduction

Polyhedral oligomeric silsesquioxanes (POSSs) have been used as nanosized building blocks in the preparation of organic–inorganic hybrid polymers because of their advantages such as high thermal, mechanical, and chemical stabilities, uniform shapes, and the possibility of introducing various functional groups into them [1–3]. Abbenhuis reported the polymerization of cage silsesquioxanes with hydroxy groups and metal species including aluminum and titanium [4,5]. These polymers demonstrated catalytic activities in the epoxidations of alkenes and Diels–Alder reactions [4–6]. However, metallosiloxane bonding (M–O–Si) is highly sensitive to moisture in the air [7]. Hence, studies on the syntheses of heterometal–POSS polymers comprising metallosiloxane bonding are limited.

Recently, Banerjee [8] and Xu [9] produced a metal coordination polymer (CP) using carboxyl-

terminated POSS, which was formed by covalent and coordination bondings between the terminal carboxyl group and metal ions. Carboxylic ligands are useful for coordination with Cu, Zn, alkali, and alkaline-earth metals because they generate salts with high hydrolytic stabilities. This metal coordination POSS polymer constitutes a breakthrough for the synthesis of heterometal–POSS polymers. Nevertheless, realizing the binding of carboxylic ligands to metals (for example, aluminum and titanium) is difficult because carboxylato–metal bonding (M–OOCR) is unstable against hydrolysis [10]. Fabrication of metal coordination POSS polymers using other functional groups, such as terpyridine-type [11,12] and Schiff base-type functional groups [13], has been investigated; particularly, a terpyridine-type material has been employed with late transition metals to form coordination bonds.

I focused on the acetylacetonato (acac) group because it can bind to several metal species [14,15], and the corresponding complexes exhibit higher stabilities against hydrolysis than those of carboxylato–metal complexes [10]. In this chapter, I report the synthesis and characterization of acac-terminated POSS and its CPs with copper, titanium, aluminum, zinc species (Scheme 1).

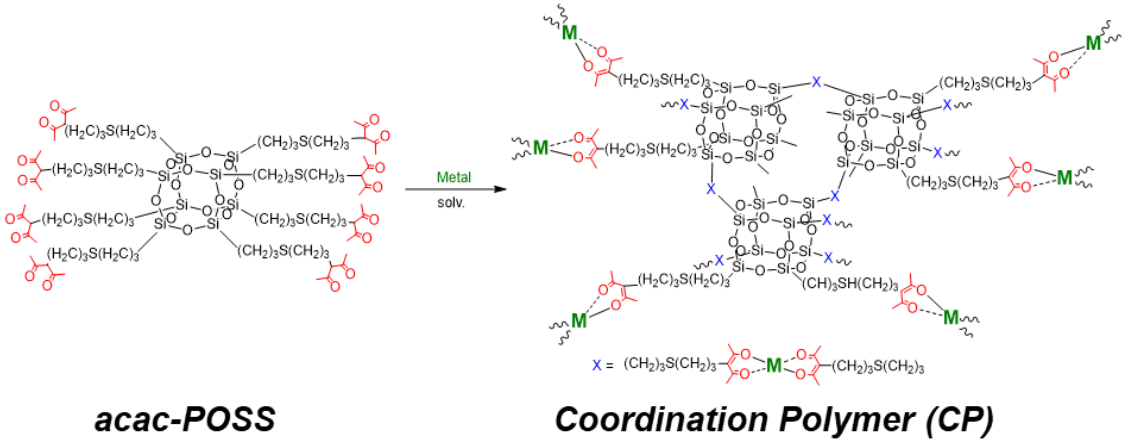

Scheme 1. Schematic of the formation of CP (Metal).

2 Experimental section

2.1 Measurements

Nuclear magnetic resonance (NMR) spectra were recorded using a JEOL Resonance JNM-ECP 300 spectrometer (JEOL, Tokyo, Japan; ^{1}H: 300.53 MHz and ^{29}Si{^{1}H}: 59.70 MHz) and JNM-ECZ 500 spectrometer (^{1}H: 500 MHz and ^{13}C{^{1}H}: 125 MHz). Chemical shifts are reported in ppm relative to chloroform-*d* ($CDCl_3$) (for ^{1}H: 7.26 ppm and ^{13}C{^{1}H}: 77.16 ppm in residual chloroform) and tetramethylsilane (for ^{29}Si{^{1}H}: 0.00 ppm) as internal standards. For ^{29}Si{^{1}H} NMR spectroscopy, $Cr(acac)_3$ was added to the sample as a paramagnetic relaxation agent. Fourier transform infrared (FTIR) spectra were obtained using an FTIR-6100 spectrophotometer (JASCO, Tokyo, Japan) with neat samples sandwiched between two KBr crystal disks or using the attenuated total reflectance method (JASCO ATR PRO 0450-S, ZnSe prism). High-resolution electrospray ionization time-of-

flight mass spectrometry (HR-ESI-TOF MS) was conducted by JEOL JMS-T100CS AccuTOF CS. Elemental analyses were performed using a Perkin Elmer 2400II elemental analyzer (PerkinElmer Japan, Kanagawa, Japan). Thermogravimetric analysis (TGA) was conducted using a TG-DTA analyzer 2000SE (Netzsch Japan, Kanagawa, Japan) heated at a rate of 10 °C min^{-1} up to 1000 °C under air flow. Ultraviolet–visible (UV–Vis) absorption spectra were recorded by a JASCO V-670 UV–VIS/NIR spectrophotometer. X-ray diffraction (XRD) patterns were acquired using IC Vario (PANAlytical, Tokyo, Japan) with monochromatic Cu Kα radiation as the X-ray source. Pore size distributions and surface areas were measured using a BELSORP-max system (MicrotracBEL, Osaka, Japan). Surface morphologies were analyzed using a JSM-7600F Schottky field emission scanning electron microscope (SEM, JEOL, Tokyo, Japan). X-ray photoelectron spectroscopy (XPS) data were obtained using a Shimadzu KRATOS Nova system with monochromatic Al Kα radiation (15 kV, 150 W) as an X-ray source. Spectra were standardized using the C 1s peak at 284.6 eV. Formulas of CP(Cu, Ti, Al)s were calculated using the following equation:

$8[SiO_2] + [MO_x]_n$ / [acac–POSS] + $[M]_n$ = Theoretical ceramic yield

where M denotes CP (Cu):Cu, CP (Ti):Ti, Ti_2O_2, or CP (Al):Al.

2.2 Materials

Solvents were purified by standard processes and stored over activated molecular sieves.

Tetrahydrofuran (THF), toluene, hexane, acetylacetone (Hacac), 2,2'-azobisisobutyronitrile (AIBN), aluminum triisopropoxide ($Al(OiPr)_3$), tetramethylammonium hydroxide (aq.), and tetrabutylammonium fluoride were purchased from Tokyo Chemical Industry (Tokyo, Japan). Ethanol, isopropyl alcohol (*i*PrOH), dichloromethane, hydrochloric acid (6 mol/L), anhydrous copper(II) acetate ($Cu(OAc)_2$), anhydrous zinc(II) acetate ($Zn(OAc)_2$), and lithium hydroxide ($LiOH \cdot H_2O$) were procured from FUJIFILM Wako Pure Chemical Corporation (Osaka, Japan). 3-Mercaptopropyl trimethoxysilane, titanium tetraisopropoxide ($Ti(OiPr)_4$), and triethylamine (TEA) were purchased from Shin-Etsu Chemical (Tokyo, Japan), FUJIFILM Wako Pure Chemical Corporation (Osaka, Japan), and Tokyo Chemical Industry (Tokyo, Japan), respectively, and purified by distillation before use.

2.3 Synthesis of octamercaptopropyl POSS (POSS-SH)

POSS-SH was prepared by acid-catalyzed hydrolytic polycondensation of 3-mercaptopropyl trimethoxysilane [16]. Herein, 36% HCl (2.5 mL) and H_2O (17.5 mL) were added to a MeOH (240 mL) solution of 3-mercaptopropyl trimethoxysilane (10.6 g, 54.0 mmol) in an ice bath. After stirring the resulting solution for 15 min, the attained solution was stirred at 22 ± 3 °C for 15 min followed by reflux for 48 h. The acquired solution was cooled to 22 ± 3 °C and allowed to stand for several days. The precipitated solid was filtered and washed with ice-cooled MeOH. After drying the resulting solid

under reduced pressure, POSS-SH was obtained as a white solid (1.5 g, 22%).

^{1}H NMR (300 MHz, $CDCl_3$): δ (ppm) 2.55 (q, *J* = 10.0 Hz, $CH_2CH_2\mathbf{CH_2}SH$, 16H), 1.71 (quin, *J* = 10.0 Hz, $CH_2\mathbf{CH_2}CH_2SH$, 16H), 1.38 (t, *J* = 10.0 Hz, **SH**, 8H), 0.76 (t, *J* = 10.0 Hz, $\mathbf{CH_2}CH_2CH_2SH$, 16H).

^{29}Si NMR (60 MHz, $CDCl_3$): δ (ppm) −67.1 (T_8 cage).

FTIR (ATR/cm^{-1}): 2928 (νC–H), 2549 (νS–H), 1076 (νSi–O–Si)

2.4 Synthesis of 3-allylacetylacetonato (3-allylacac)

3-Allylacac was prepared via the reaction of Hacac and allyl bromide with *tert*-butoxy potassium [17]. Typically, Hacac (27.0 g, 0.2 mol) was introduced dropwise into KOtBu (22.4 g, 0.2 mol) dispersed in THF (120 mL). Potassium salt was precipitated and then heated at 80 °C for 2 h. Thereafter, allyl bromide was added to the mixture followed by reflux overnight. After the precipitate was filtered, the solvent was evaporated, and 3-allylacac was isolated as a colorless liquid (16.2 g 58%) by distillation under reduced pressure (lit. [22] 69.0–72.3 °C under 5.5 mmHg, 81–82 °C under 16 mmHg).

^{1}H NMR (300 MHz, $CDCl_3$): δ (ppm) 1.85 (s, 4H), 1.97 (s, 2H), 2.37 (t, *J* = 7.0 Hz, 1H), 2.79 (m, 1H), 3.56 (t, *J* = 7.3 Hz, 0.5H), 4.91–4.76 (m, 2H), 5.63–5.55 (m, 0.5H), 5.76–5.69 (m, 0.5H).

GC/MS (EI) m/z: 141.1 [M-H]+ (Calcd. for $C_8H_{13}O_2$: 141.08).

2.5 Synthesis of octakis(8-acetyl-9-oxo-4-thiadecyl) POSS (POSS-acac)

POSS-SH (0.11 g, 0.1 mmol) and AIBN (1.6 mg) were added to 3-allylacac (1.16 g, 8.2 mmol). After bubbling with N_2 gas (50 mL min^{-1}) for 30 min, the mixture was heated at 80 °C for 24 h. Subsequently, AIBN (1.6 mg) was added into the abovementioned mixture followed by heating at 80 °C for 24 h. The resulting mixture was washed thrice with hexane and twice with hexane/dichloromethane (100/3 v/v), and the achieved residue was dried under reduced pressure. POSS-acac was obtained as a light-yellow viscous liquid (0.20 g, 93%).

^{1}H NMR (300 MHz, $CDCl_3$): δ (ppm) 0.76–1.00 (br, 8H), 1.40–1.53 (m, 4H), 1.56–1.81 (m, 16H), 1.81–2.01 (m, 16H), 2.15 (s, 7.7H), 2.16 (s, 8.3H), 2.18 (s, 14.8H), 2.20 (s, 17.2H), 2.21–2.44 (m, 8H), 2.44–2.60 (m, 16H), 2.60–2.72 (m, 8H), 2.72–2.94 (br, 16H), 2.94–3.08 (br, 4H), 3.54–3.84 (br, 4H).

^{29}Si NMR (60 MHz, $CDCl_3$): δ (ppm) −67.0, −67.8.

HRMS (HR-ESI-TOF) *m/z*: Calcd. for $C_{88}H_{152}O_{28}S_8Si_8Na$: 2159.6288 $[M+Na]^+$; Found: 2159.6314.

Anal. calculated for $C_{88}H_{152}O_{28}S_8Si_8$: C, 49.44; H, 6.96; Found: C, 49.41; H, 7.16.

2.6 Synthesis of 8-acetyl-9-oxo-4-thiadecyl(trimethoxy)silane (TMS-acac)

3-Mercaptopropyl trimethoxysilane (3.9 g, 20 mmol), AIBN (10 mg), and 3-allylacac (2.8 g, 20 mmol) were mixed and degassed by bubbling N_2 gas (50 mL min^{-1}) for 30 min. The mixture was

heated at 80 °C for 24 h followed by evaporation and drying under reduced pressure. TMS-acac was acquired as a residual light-yellow liquid (6.2 g, 92%).

^{1}H NMR (500 MHz, $CDCl_3$): δ (ppm) 0.67–0.78 (m, 2H), 1.42–1.52 (m, 1H), 1.58–1.71 (m, 2.6H), 1.86–1.94 (m, 1.4H), 2.10 (s, 2H), 2.14 (s, 4H), 2.23–2.35 (m, 1H), 2.44–2.52 (m, 4H), 3.43–3.61 (m, 9.5H).

^{13}C NMR (125 MHz, $CDCl_3$): δ (ppm) 8.34, 8.38, 22.69, 22.74, 22.84, 26.41, 26.93, 27.13, 27.24, 27.33, 28.86, 30.11, 31.24, 31.43, 34.76, 35.04, 50.32, 68.11, 109.57, 190.89, 203.89.

^{29}Si NMR (60 MHz, $CDCl_3$): δ (ppm) −42.3.

HRMS (HR-ESI-TOF) m/z: Calcd. for $C_{14}H_{28}O_5SSiNa$: 359.1324 $[M+Na]^+$; Found: 359.1330.

2.7 Synthesis of heptaisobutylsilsesquioxane trisilanol

Heptaisobutylsilsesquioxane trisilanol was prepared via lithium hydroxide ($LiOH·H_2O$)-catalyzed hydrolytic polycondensation of triethoxy(isobutyl)silane [18]. $LiOH·H_2O$ (2.00 g, 48 mmol) and H_2O (1.60 mL, 69 mmol) were added to a 100 mL acetone/methanol solution (88:12). Then, triethoxy(isobutyl)silane (27.6 mL, 105 mmol) was introduced dropwise into the reaction mixture, and the resulting solution was refluxed at 70 °C for 24 h. The resulting solution was cooled to 22 ± 3 °C and neutralized with 1 M HCl (100 mL). The solution was stirred for 2 h, and the resulting white precipitate was decanted and washed three times with acetonitrile. Recrystallization from

dichloromethane and acetonitrile (v/v = 1/1) afforded colorless crystals.

^{1}H NMR (500 MHz, $CDCl_3$): δ (ppm) 0.56–0.60 (m, 14H), 0.94–0.97 (m, 42H), 1.80–1.90 (m, 3H)

^{29}Si NMR (100 MHz, $CDCl_3$): δ (ppm) −59.1,−67.4, −68.8 (T_8 cage).

2.8 Reaction of heptaisobutylsilsesquioxane trisilanol with 3-mercaptopropyl trimethoxysilane

Heptaisobutylsilsesquioxane trisilanol**,** 3-mercaptopropyl trimethoxysilane, catalyst, and solvent were mixed followed by stirring at 85 °C, 60 °C, or r. t. for o. n. or 3 days. White solid was recovered by recrystallization from acetone and sublimation under reduced pressure.

2.9 Synthesis of Cu-coordinated POSS polymer (CP(Cu))

A mixture of $Cu(OAc)_2$ (90 mg, 0.47 mmol) and POSS-acac (0.25 g, 0.12 mmol) in 20 mL EtOH was heated at 80 °C for 24 h. The insoluble solid was filtered and washed with ethanol. After drying the resulting solid under reduced pressure, a dark blue solid of CP(Cu) was obtained (0.23 g).

2.10 Synthesis of Ti-coordinated POSS polymer (CP(Ti))

A mixture of $Ti(OiPr)_4$ (0.14 g, 0.47 mmol) and POSS-acac (0.25 g, 0.12 mmol) in 20 mL THF was heated at 80 °C for 24 h. Thereafter, the solution was added to iPrOH (such that the iPrOH/THF volume ratio = 5/1), and the resulting residue was washed with THF followed by drying

under reduced pressure. Consequently, CP(Ti) was obtained as an orange solid (0.31 g).

2.11 Synthesis of Al-coordinated POSS polymer (CP(Al))

A mixture of $Al(OiPr)_3$ (64 mg, 0.31 mmol) and POSS-acac (0.25 g, 0.12 mmol) in 20 mL THF was heated at 80 °C for 24 h. The acquired insoluble solid was filtered and washed with THF. After drying this solid under reduced pressure, CP(Al) was achieved as an orange solid (0.20 g).

2.12 Preparation of Zn-coordinated POSS polymer (CP(Zn))

A mixture of $Zn(OAc)_2$ (specified molar amounts) and POSS-acac (0.25 g, 0.12 mmol) in 20 mL EtOH was heated at 80 °C for 24 h. After being heated and cooled down to room temperature, the resulting mixture was evaporated followed by extraction three times with CH_2Cl_2/brine. The organic layer was dried over anhydrous sodium sulfate followed by filtration and evaporation. After drying under reduced pressure, CP(Zn) was obtained as a viscous liquid.

3 Results and discussion

3.1 Synthesis of POSS-acac

POSS-acac was synthesized by a thiol-ene reaction of POSS-SH and 3-allylacac (Scheme 2). When the 3-allylacac/POSS-SH molar ratio was 80 and solvent-free conditions were used, the

mercaptopropyl group was completely consumed; in contrast, the reaction hardly proceeded in the presence of solvent. FTIR spectrum of POSS-SH exhibited υS–H and υSi–O band at 2549 and 1076 cm^{-1}, respectively. FTIR spectrum of POSS-acac did not demonstrate the υS–H band and exhibited the νC=O bands at 1697 and 1723 cm^{-1} and a δCH_3 band related to the acac moiety at 1417 cm^{-1} (Figure 1a). Band corresponding to the asymmetric stretching vibration of the cage siloxane framework was detected at ~1100 cm^{-1} [19], suggesting that the POSS structure was retained in POSS-acac. ^{1}H NMR spectrum of POSS-SH demonstrated a triplet at 1.38 ppm that was assigned to the thiol proton. ^{1}H and ^{13}C NMR spectra of POSS-acac (Figure 2) were complicated by the similarity of the chemical environments such as the existence of keto-enol tautomers.

Relative band intensities of the acetylacetonato and propylsulfane moieties were equal, *i.e.*, POSS-acac possessed eight acac groups. ^{29}Si NMR spectrum of POSS-acac exhibited two singlet signals at −66.6 and −67.5 ppm, which were different from the signal of POSS-SH (−67.1 ppm) (Figure 1b). Generally, the signal of a POSS derivative formed by corner cleavage appears at a magnetic field 10 ppm lower than that of closed POSS [20]. In the cases of POSS derivatives bearing heterofunctional groups, the chemical environments and chemical shifts of the silicon atoms in the POSS corners are different [21]. We hypothesized the presence of keto-enol tautomers; hence, a ^{29}Si NMR spectrum was obtained in the presence of TEA because enolization is enhanced by hydrogen bonding between acetylacetonate and TEA [22]. However, no differences were noticed in the ^{29}Si NMR spectra,

implying that the two singlet signals were not related to keto-enol tautomers. Although the reason for the two signals observed in the ^{29}Si NMR spectrum is unclear, we propose direction-dependent chemical shift, the existence of isomers generated by Markovnikov addition, and aggregation of POSS-acac. Elemental analyses and MS spectrum of POSS-acac suggested the formation of the desired compound. These results indicate that POSS-acac comprises eight acac groups and demonstrates no collapse of the POSS structure.

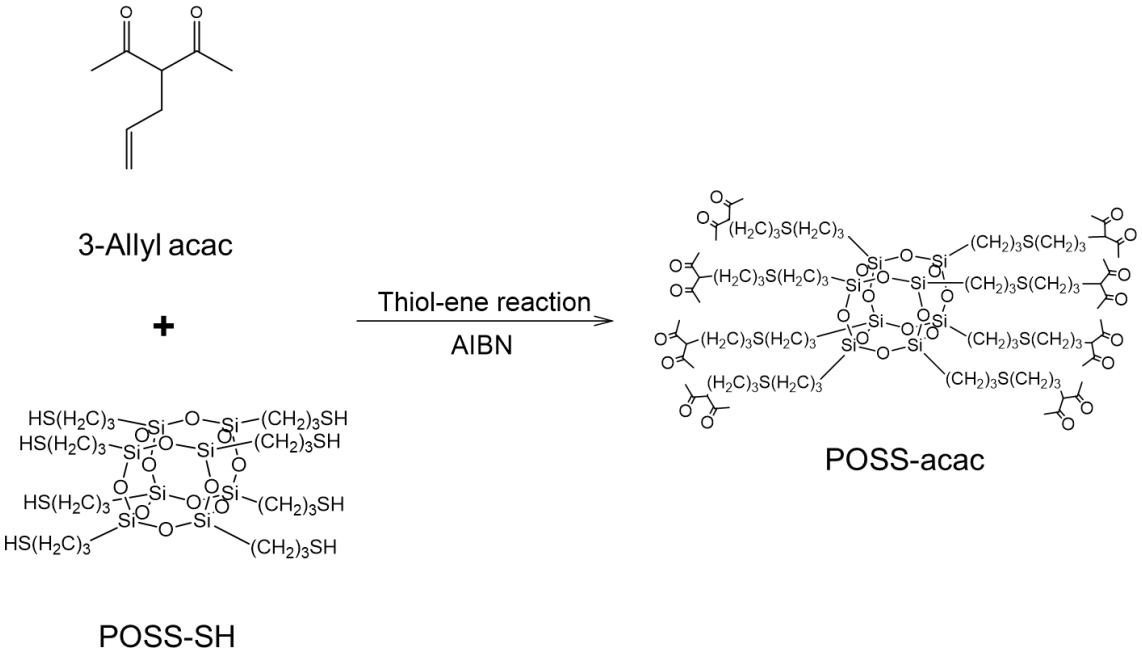

Scheme 2. Schematic of the synthesis of POSS-acac.

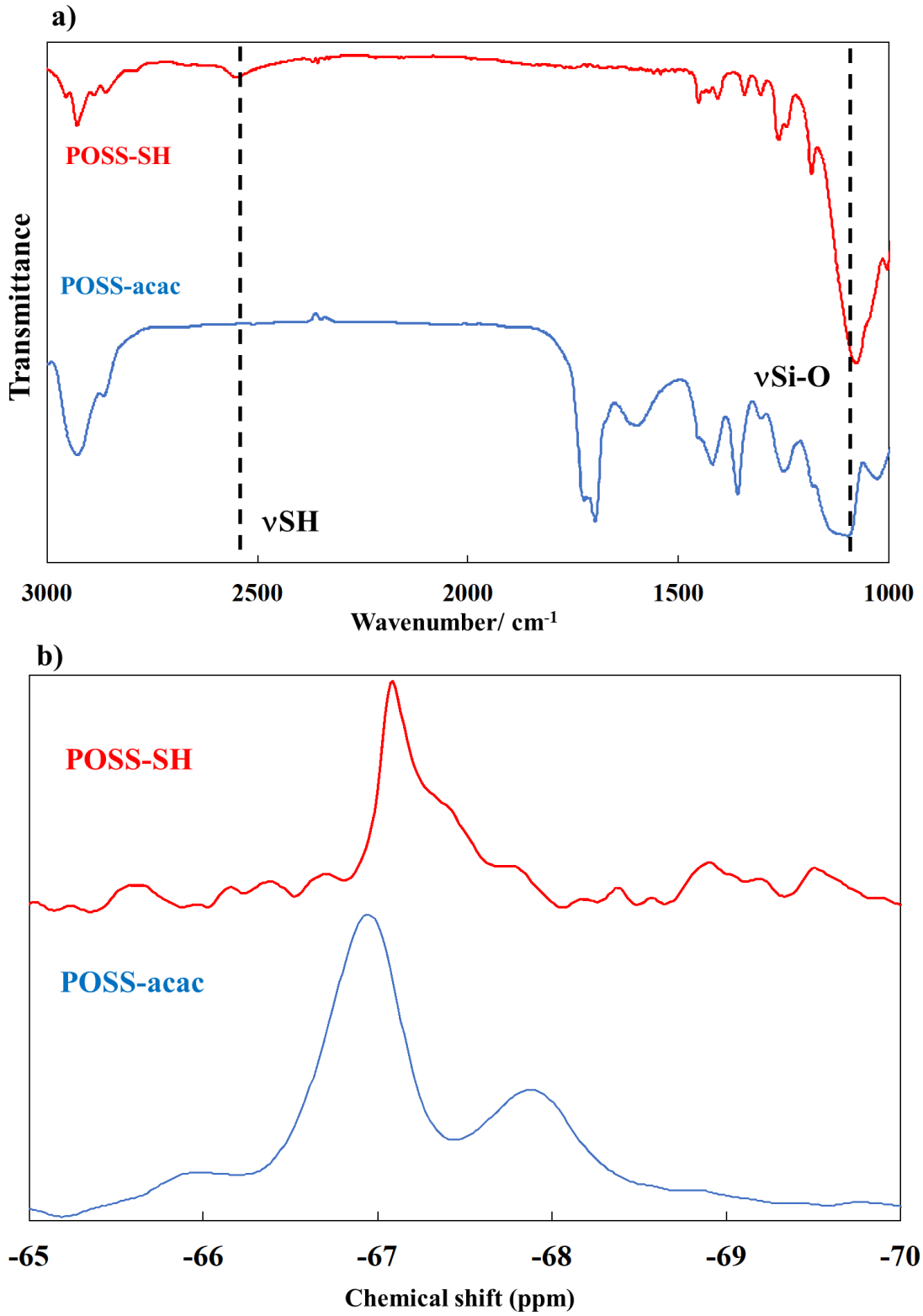

Figure 1. a) FTIR and b) $^{29}Si\{^{1}H\}$ NMR spectra of POSS-SH and POSS-acac.

a)

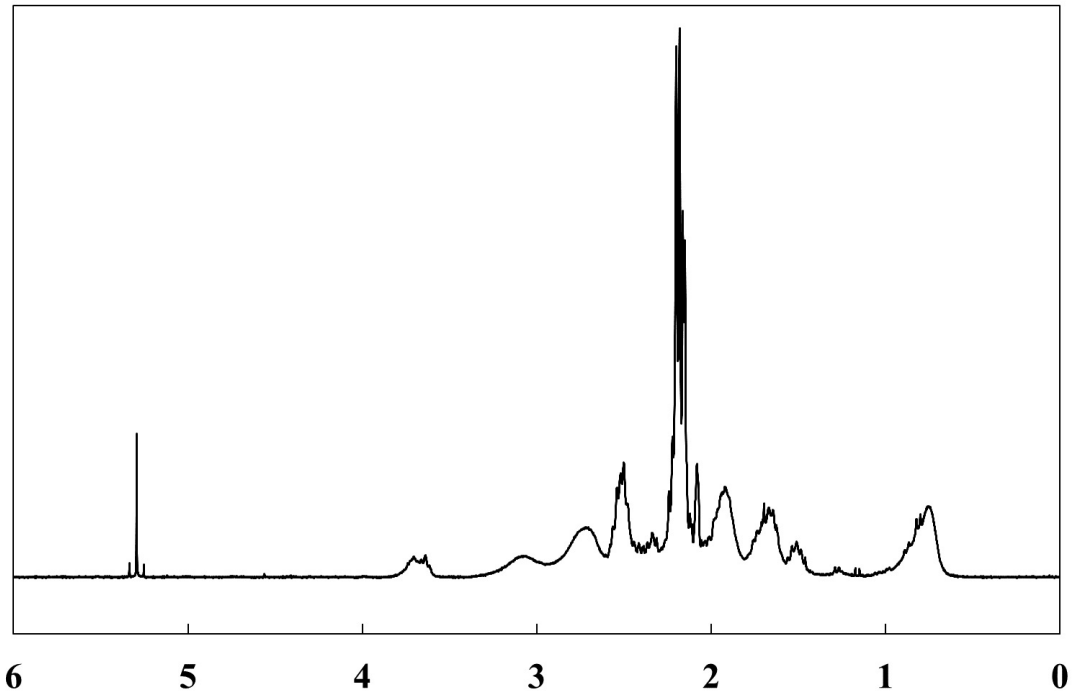
6
5
4
3
2
1
0
Chemical shift/ ppm

b)

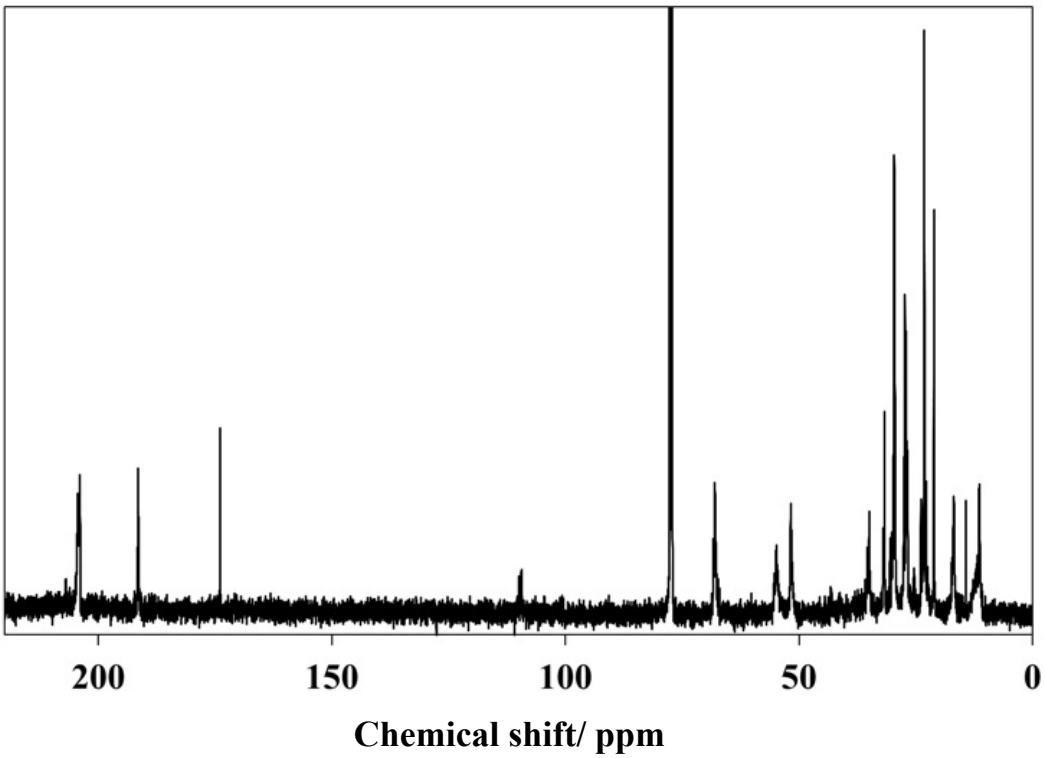
200
150
100
50
0
Chemical shift/ ppm

Figure 2. a) ^{1}H NMR and b) $^{13}C\{^{1}H\}$ NMR spectra of POSS-acac.

3.2 Synthesis of a model molecule for POSS-acac

TMS-acac was synthesized as a model molecule for POSS-acac because mono-mercaptopropyl POSS, which is a precursor of mono-acetylacetonate POSS, cannot be prepared and isolated. Results of the reaction of heptaisobutylsilsesquioxane trisilanol with 3-mercaptopropyl trimethoxysilane are provided in Table 1.

Table 1 Synthesis of mono-3-mercaptopropyl-substituted POSS[a)]

Entry	Catalyst (catalyst/SiOH molar ratio)	Temp. (°C)	Time (h)	solvent
1	triethylamine (catalytic amount)	85	o.n.	THF
2	triethylamine (TEA/SiOH = 1)	85	o.n.	THF/ethanol
3	triethylamine (TEA/SiOH = 3)	85	o.n.	THF/ethanol
4	triethylamine (TEA/SiOH = 3)	85	3 days	THF/ethanol
5	triethylamine (TEA/SiOH = 5)	85	3 days	THF/ethanol
6	tetramethylammonium hydroxide aq. (catalytic amount)	r.t.	o.n.	ethanol
7	tetrabutylammonium fluoride (catalytic amount)	60	3 days	toluene

[a)]TEA: triethylamine, r.t.: room temperature, and o.n.: overnight

Progress of the reaction was monitored by FTIR or ^{1}H NMR spectroscopy. ^{1}H NMR spectrum of the recrystallized product demonstrated an unknown signal at 2.6 ppm. Additionally, when the recrystallized product was sublimed, heptaisobutylsilsesquioxane trisilanol was obtained by hydrolysis.

3.3 Reactions of POSS-acac with metal sources (Cu, Ti, and Al)

UV–Vis spectra acquired after the reactions of metal sources with POSS-acac were analyzed to determine the extent of POSS-acac consumption. POSS-acac was reacted with $Cu(OAc)_2$ and $Ti(OiPr)_4$; nevertheless, TMS-acac was reacted with $Al(OiPr)_3$ because the reaction of POSS-acac with $Al(OiPr)_3$ quickly proceeded to form an insoluble solid.

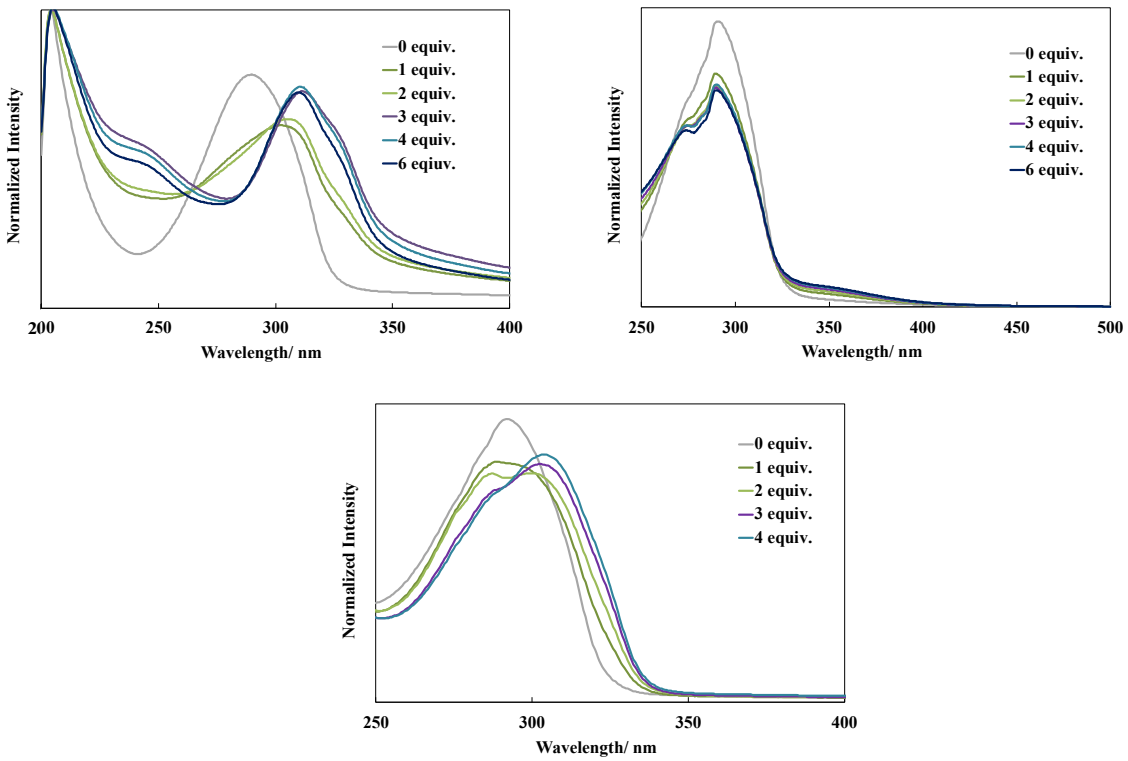

Figure 3. UV–Vis spectra of (a) CP(Cu) obtained from the reaction of POSS-acac and $Cu(OCOCH_3)_2$ in EtOH, (POSS-acac, $Cu(OCOCH_3)_2$: 4.7×10^{-5} mol/L), (b) CP(Ti) acquired from the reaction of POSS-acac and $Ti(OiPr)_4$ in THF (POSS-acac, $Ti(OiPr)_4$: 8.2×10^{-5} mol/L), and (c) CP(Al) produced from the reaction of POSS-acac and $Al(OiPr)_3$ in THF (POSS-acac, $Al(OiPr)_3$: 1.2×10^{-5} mol/L).

In the UV–Vis spectrum obtained after the reaction of POSS-acac with $Cu(OAc)_2$ in ethanol (Figure 3a), the intensity of the peak at 290 nm related to the π–π* transition of the free acac group decreased, whereas the intensities of the peaks at 240 nm corresponding to ligand-to-metal charge transfer and at 311 nm [23] related to the π–π* transition of the coordinated acac group increased with an increase in the molar amount of $Cu(OAc)_2$ used. This result suggested that a complex was formed by the reaction of POSS-acac with $Cu(OAc)_2$. When the $Cu(OAc)_2$/POSS-acac molar ratio of 3 was employed, the absorption peaks for unreacted POSS-acac disappeared; hence, POSS-acac was completely consumed.

In the UV–Vis spectrum acquired after the reaction of POSS-acac with $Ti(OiPr)_4$ in THF (Figure 3b), the intensity of the peak at 291 nm corresponding to the π–π* transition of the free acac group decreased, whereas that of the peak at 350 nm [24] related to the π–π* transition of the coordinated acac group increased with an increase in the molar amount of $Ti(OiPr)_4$ used. Moreover, the broad absorption peak at ~270 nm was attributed to the π–π* transition of the coordinated acac group [25]. However, unreacted POSS-acac was observed even after the addition of 6 equivalents of $Ti(OiPr)_4$; thus, the rate of the reaction between POSS-acac and $Ti(OiPr)_4$ in solution may be low.

In the UV–Vis spectrum obtained after the reaction of TMS-acac with $Al(OiPr)_3$ in THF (Figure 3c), the intensity of the peak at 285 nm corresponding to the π–π* transition of the free acac group decreased, whereas that of the peak at 305 nm [26] related to the π–π* transition of the coordinated

acac group increased with an increase in the molar amount of $Al(OiPr)_3$ used. When the $Al(OiPr)_3$/TMS-acac molar ratio was 3, TMS-acac was completely utilized. Based on this result, POSS-acac might have been completely consumed when the $Al(OiPr)_3$/POSS-acac molar ratio was ~2.67.

3.4 Characterizations of CP(Cu, Ti, Al)s

CP(Cu), CP(Ti), and CP(Al) were synthesized using the metal sources $Cu(OAc)_2$, $Ti(OiPr)_4$, and $Al(OiPr)_3$, respectively (Table 2). CP(Cu) and CP(Al) were precipitated and isolated as dark blue and orange solids, respectively. CP(Ti) was achieved as an orange solid via precipitation with iPrOH.

Table 2 Synthesis of coordination polymers

Materials	Metal source	Solvent	Molar ratio (Metal/POSS)	yield (g)[a)]	state
CP(Cu)	$Cu(CH_3COO)_2$	Ethanol	4.00	0.23	Dark blue solid
CP(Ti)	$Ti(O^iPr)_4$	THF	4.00	0.31	Orange solid
CP(Al)	$Al(OiPr)_3$	THF	2.67	0.20	Orange solid

[a)]Scale in operation: POSS-acac: 0.25 g (0.123 mmol), $Cu(CH_3COO)_2$: 0.090 g (0.467 mmol), $Ti(OiPr)_4$: 0.14 g (0.467 mmol), and $Al(OiPr)_3$: 0.064 g (0.312 mmol).

FTIR spectra of CP(Cu, Ti, Al)s are depicted in Figure 4, and the corresponding data are presented in Table 2. Typically,, metal acetylacetonate complexes are indicated by the absorption bands of the carbonyl groups in the acac moieties because these moieties are converted from the keto form into the enol form by complexation. Hence, complex formation was confirmed by the absorption band of the enol-carbonyl group in the acac moiety. FTIR spectra of CP(Cu, Ti, Al)s exhibited decreases in the intensities of the absorption bands at 1760–1660 cm^{-1} related to the keto-carbonyl group and 1417 cm^{-1} corresponding to the methyl group of the keto form (*i.e.*, free acac moiety) in addition to increases in the intensities of the new band at ~1570 cm^{-1} [27–29] assigned to the enol-carbonyl group and the band at ~1440 cm^{-1} related to the methyl group of the enol form. Furthermore, a new band at 1290 cm^{-1} [30] assigned to C–O was noticed in the FTIR spectra of CP(Cu, Ti, Al)s. These results reveal that CP(Cu, Ti, Al)s are composed of POSS and metal species bound via covalent bonding and chelate formation. Additionally, the sharp absorption bands at 1120–1090 cm^{-1} are attributed to Si–O–Si stretching vibrations of the cage structure [19]. When the cage structure collapses, this band becomes broadened and complicated [31]. Cage structure was maintained in CP(Cu, Ti, Al)s. FTIR spectrum of CP(Cu) demonstrated an absorption band at 608 cm^{-1} [32] assigned to τCH or τCOO

of the acetate group, presumably the remaining acetate group and unreacted acac group. FTIR spectrum of CP(Ti) exhibited a τCH_3 peak at 850 cm^{-1} ascribed to the isopropoxy group [24], suggesting that the isopropoxy group was retained in CP(Ti). FTIR spectrum of CP(Al) demonstrated $\upsilon C–O$ peaks at 1022 and 910 cm^{-1} [33] related to terminal and bridging isopropoxy groups, respectively, implying that CP(Al) retained an isopropoxy group and exhibited an alkoxide-bridged cluster structure [34].

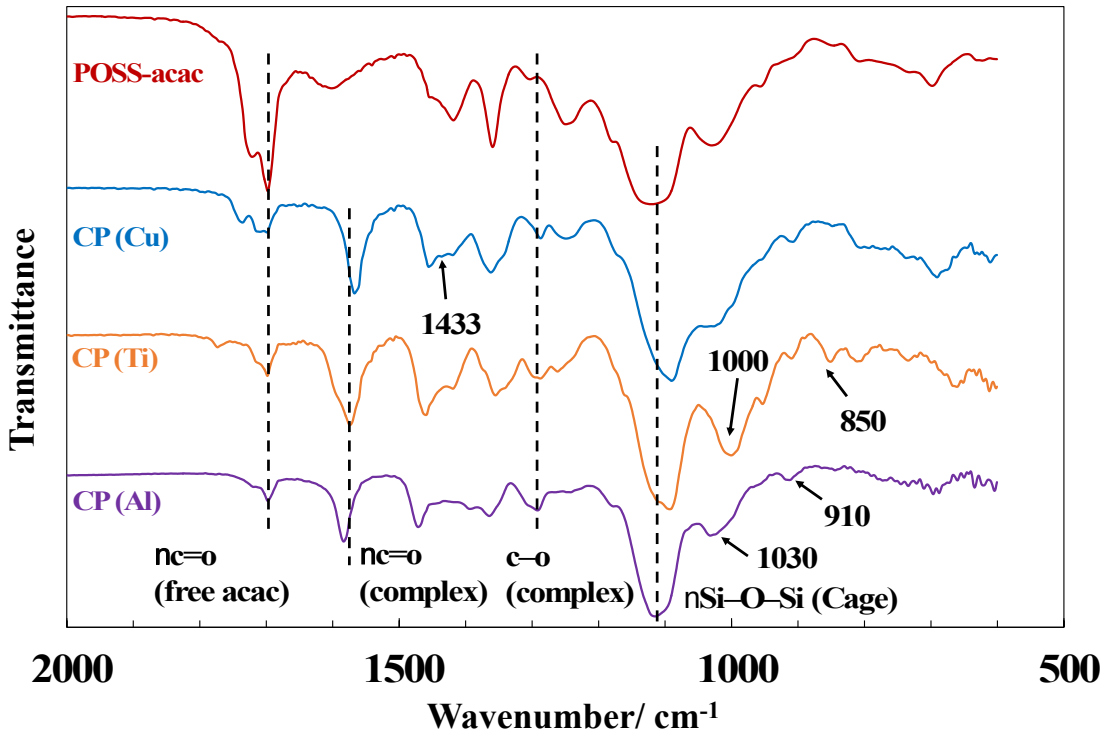

Figure 4. FTIR spectra of POSS-acac obtained by the neat method and CP(Metal) attained by the ATR method.

Table 3 FTIR assignments of CP(Cu, Ti, Al)s

Wavenumber (cm^{-1})				Assignment[a]
POSS-acac	CP(Cu)	CP(Ti)	CP(Al)	
1760–1660	1760–1670	1725–1680	1725–1680	νC=O (free-acac)
	1567	1574	1583	νC=O (coord.)
1417	1419	1458	1444	δCH_3 (free-acac)
	1455	1479	1471	δCH_3 (coord.)
	1286	1286	1291	νC–O (coord. acac)
1120–1090	1090			νSi–O–Si
		1000	1030 (term.)	νC–O (alkoxy)
			910 (bridge)	
		850		τCH or τCOO

[a]ν: stretching, δ: scissoring, and τ: twisting

CP(Cu, Ti, Al)s were exposed to water vapor at 90 °C for 1 day to evaluate their hydrolytic stabilities. Steam-treated CP(Cu, Ti, Al)s were examined by FTIR spectroscopy using the ATR method (Figure 5). After steam treatment of CP(Cu, Ti, Al)s, the peak intensity for the free acac moiety slightly

increased. Therefore, CP(Cu, Ti, Al)s were highly stable against hydrolysis as compared to the cases of the corresponding acac chelates, which hydrolyzed, generating metal oxides or hydroxides, upon being treated with steam under the same conditions.

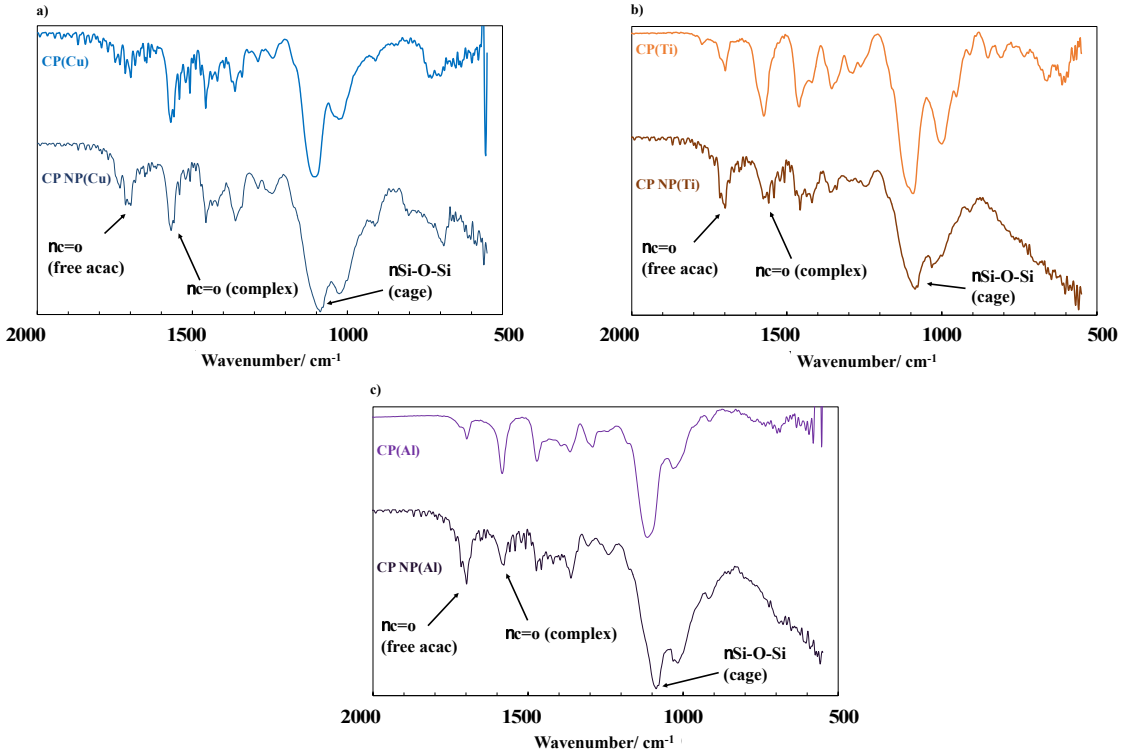

Figure 5. FTIR spectra of CP(Metal) and water-treated CP(Metal) (CP NP (Metal)) acquired by the ATR method.

SEM images of CP(Cu, Ti, Al)s are shown in Figure 6. SEM images of CP(Al) and CP(Ti) demonstrated highly particle-like morphologies. Furthermore, CP(Al) appeared to be more particulate than CP(Ti). In contrast, CP(Cu) was flat and built from nanoparticles. These morphologies are related to the polymer structures. CP(Al) and CP(Ti) are highly particulate because of their highly cross-linked structures [27,28,35]. Contrarily, CP(Cu) exhibits a planar morphology owing to its low cross-linked

structure [35,36]. Moreover, the morphologies of CP(Cu, Ti, Al)s did not substantially change after annealing at 150 °C.

.

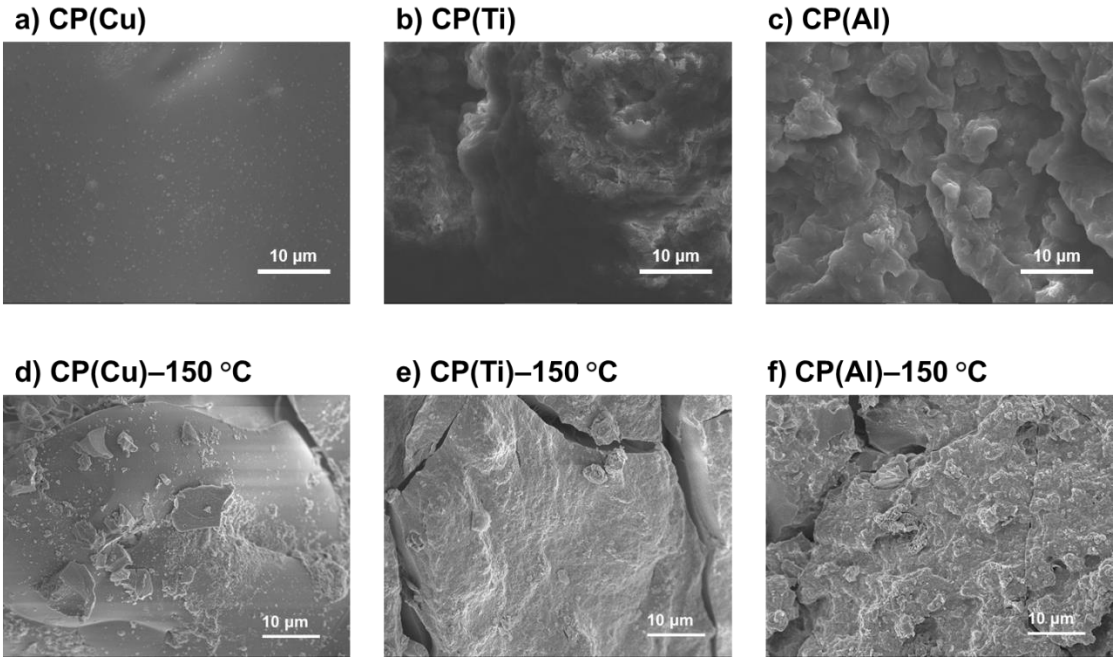

Figure 6. SEM images of a) CP(Cu), b) CP(Ti), c) CP(Al), d) CP(Cu)–150 °C, e) CP(Ti)–150 °C, and f) CP(Al)–150 °C.

Furthermore, CP(Cu, Ti, Al)s were characterized by XRD and specific surface area determinations (Figures 7 and 8). Although typical CPs with organic ligands are often porous structures, CP(Cu, Ti, Al)s adsorb a minimal amount of N_2, indicating that they are nonporous. Moreover, amorphous structures are assigned to CP(Cu, Ti, Al)s. POSS-acac comprises a long flexible thioether chain between POSS and the acac moiety; thus, CP(Cu, Ti, Al)s are nonporous amorphous

materials.

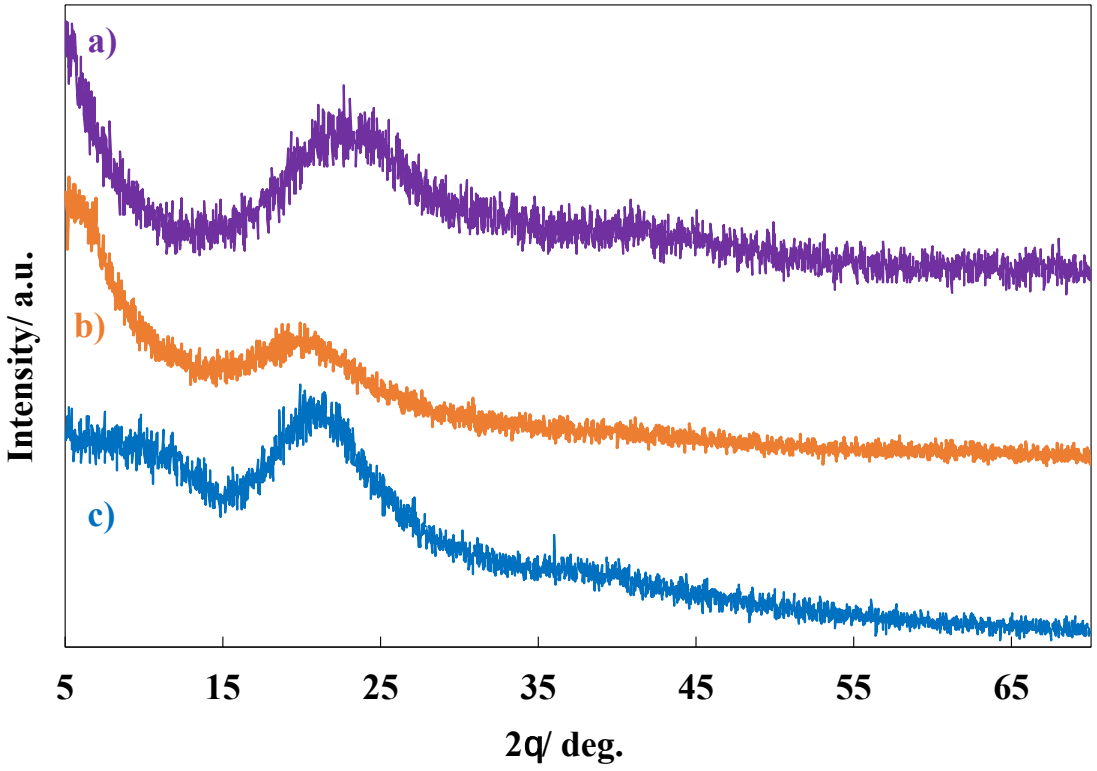

Figure 7. XRD patterns of a) CP(Al), b) CP(Ti), and c) CP(Cu).

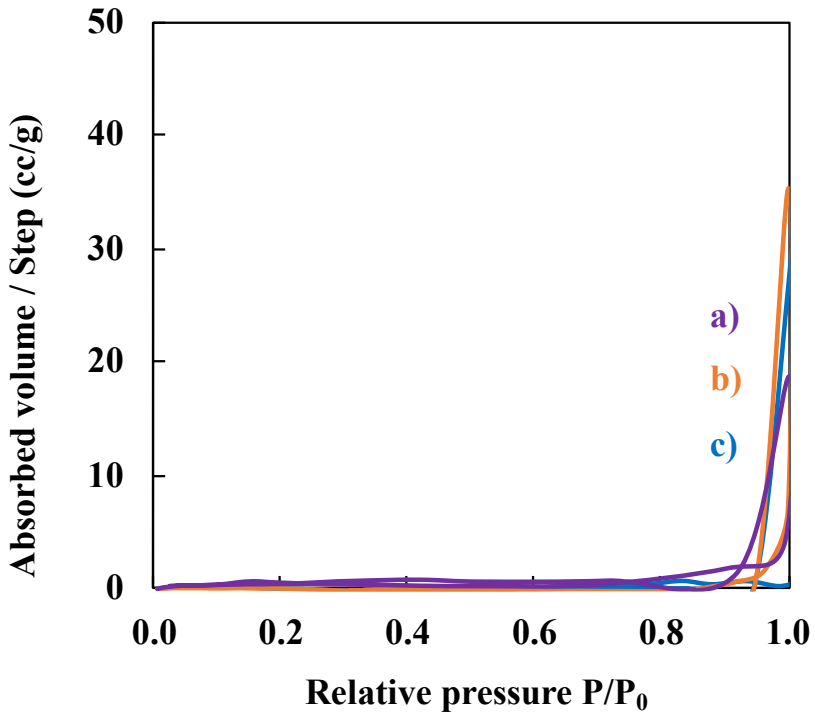

Figure 8. N_2 adsorption–desorption isotherms of a) CP(Al), b) CP(Ti), and c) CP(Cu).

3.5 Chemical formulas of CP(Cu, Ti, Al)s

Formulas of CP(Cu, Ti, Al)s were calculated via TGA under air (Figure 9).

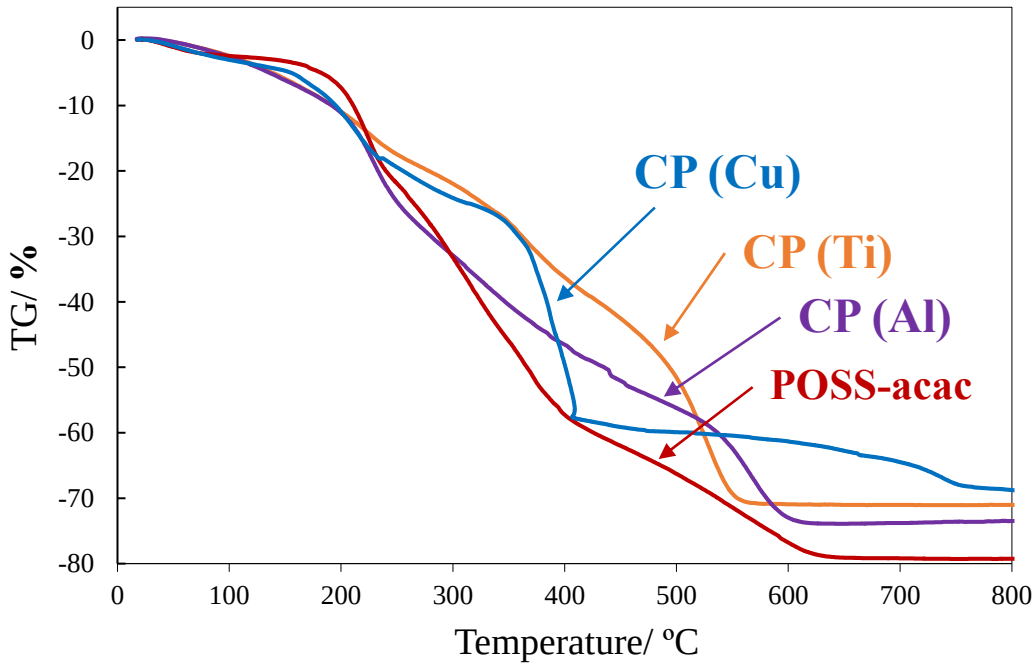

Figure 9. TGA curves of POSS-acac and CP(metal)s analyzed under air.

Residual masses (ceramic yields) for pristine POSS-acac, CP(Cu), CP(Ti), and CP(Al) were 21.5, 29.2, 28.7, and 27.1%, respectively. In the XPS spectra, the burned residues exhibited individual peaks for Si, O, and the metal in CP(Cu, Ti, Al)s; furthermore, no peaks related to S atoms were detected (Figure 10).

a)

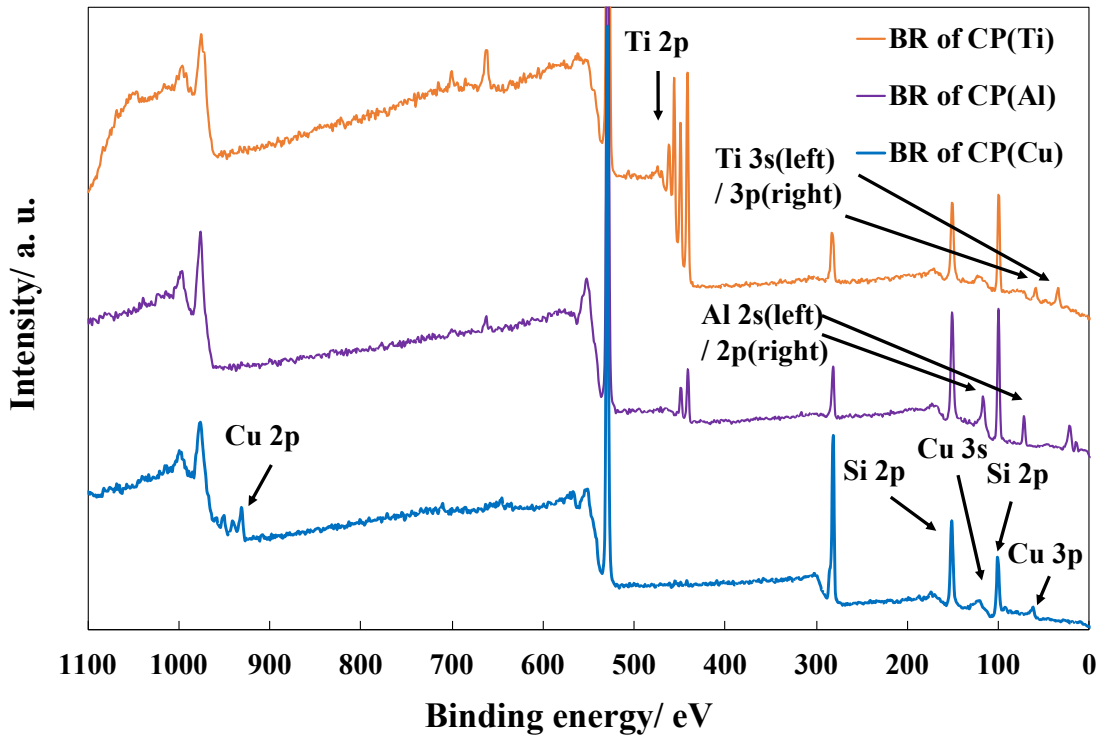
Intensity/ a. u.
Ti 2p
BR of CP(Ti)
BR of CP(Al)
BR of CP(Cu)
Ti 3s(left)
/ 3p(right)
Al 2s(left)
/ 2p(right)
Cu 2p
Si 2p
Cu 3s
Si 2p
Cu 3p
1100 1000 900 800 700 600 500 400 300 200 100 0
Binding energy/ eV

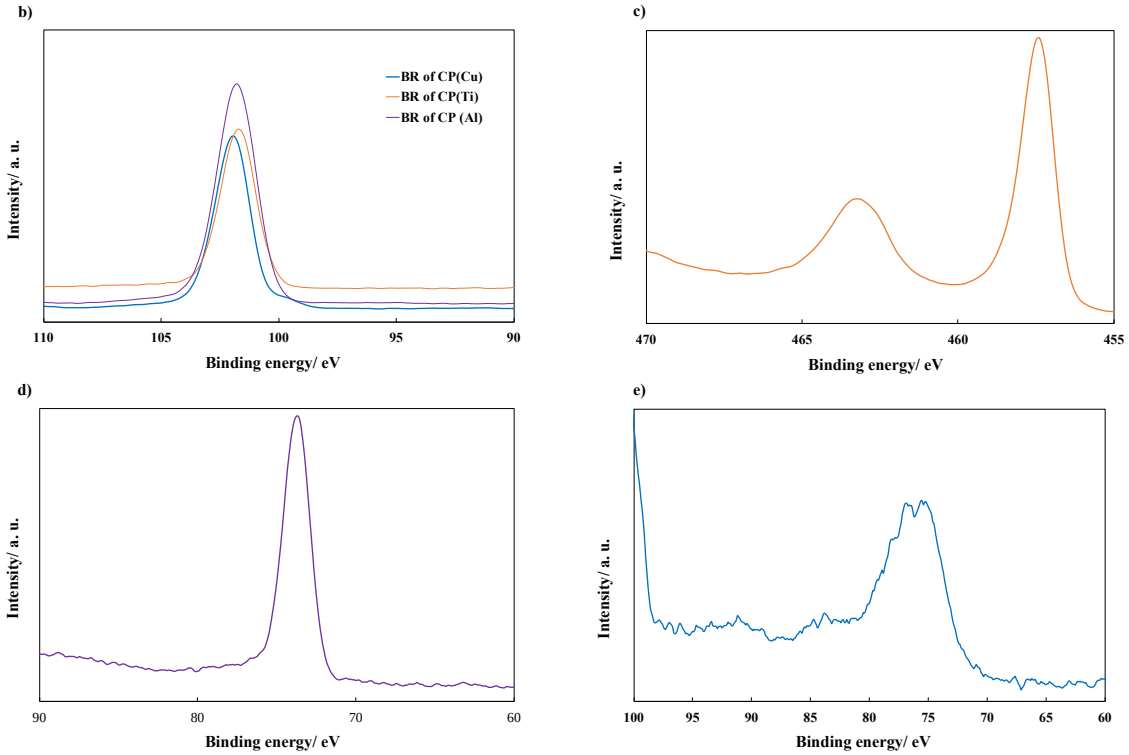
b)
BR of CP(Cu)
BR of CP(Ti)
BR of CP (Al)
Intensity/ a. u.
110 105 100 95 90
Binding energy/ eV
c)
Intensity/ a. u.
470 465 460 455
Binding energy/ eV
d)
Intensity/ a. u.
90 80 70 60
Binding energy/ eV
e)
Intensity/ a. u.
100 95 90 85 80 75 70 65 60
Binding energy/ eV

Figure 10. a) Wide XPS spectra of burned residue (BR), b) Si 2s XPS spectra of CP(Metal), c) Ti 2p XPS spectra of BR of CP(Ti), d) Al 2p XPS spectra of BR of CP(Al), and e) Cu 3p XPS spectra of BR of CP(Cu) (The two peaks at 442 and 440 eV were attributed to In 3d).

Formulas for CP(Cu, Ti, Al)s evaluated using residual masses were as follows: [POSS-acac][Cu]$_{2.3}$ (theoretical ceramic yield: 29.1%) for CP(Cu), [POSS-acac][$Ti(OiPr)_2$]$_{4.1}$ (theoretical ceramic yield: 28.7%) for CP(Ti), and [POSS-acac][Al]$_{2.3}$ (theoretical ceramic yield: 27.2%) for CP(Al). Proportion of titanium in CP(Ti) was larger than that in the composition of the expected structure [POSS-acac][$Ti(OiPr)_2$]$_4$, which consisted of octahedral titanium species such as $Ti(acac)_2(O\textit{i}Pr)_2$. The reason for this is the formation of a doubly catenated titanoxane species (Ti_2O_2 bond) from a nonaqueous reaction of Hacac with titanium alkoxide [27,37]. To discuss this topic, the model reaction of $Ti(OiPr)_4$ with TMS-acac was monitored by FTIR spectroscopy (Figure 11).

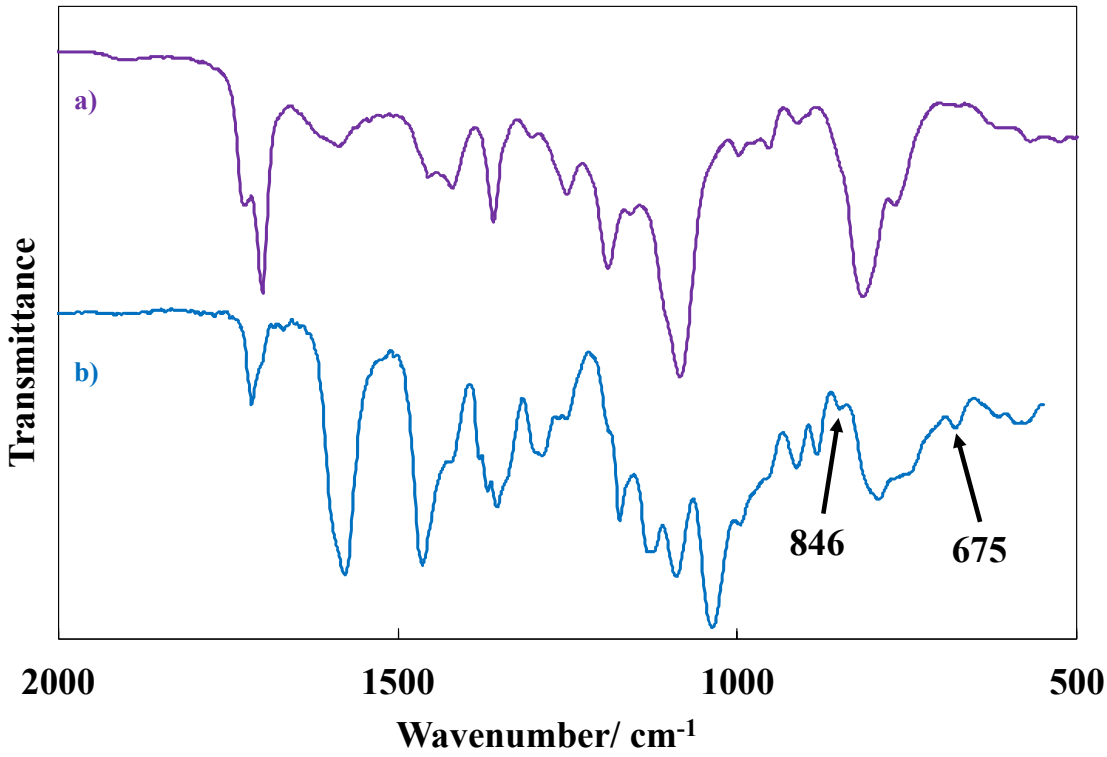

Figure 11. FTIR spectra of a) TMS-acac and b) the product of the reaction of TMS-acac with $Ti(OiPr)_4$.

Absorption bands ascribed to Ti_2O_2 bonds were observed at 846 and 675 cm^{-1} [38]. Therefore, we propose the formation of doubly catenated Ti_2O_2 for CP(Ti), suggesting that the chemical formula for the CP(Ti) residue was [POSS-acac][$Ti(OiPr)_2$]$_{2.5}$[Ti_2O_2]$_{0.5}$ (theoretical ceramic yield: 28.5%).

Based on this result, the number of acac groups used for complexation in POSS-acac, which were estimated from the chemical formulas of CP(Cu), CP(Ti), and CP(Al), were 4.6, 7.0, and 6.9, respectively (Table 4).

Table 4 Compositions of coordination polymers

Polymer	Metal source	Estimated chemical formula[a)]	Number of acac groups used for complexation[b)]
CP(Cu)	$Cu(CH_3COO)_2$	$[POSS\text{-}acac][Cu]_{2.3}$	4.6
CP(Ti)	$Ti(OiPr)_4$	$[POSS\text{-}acac][Ti(OiPr)_2]_{2.5}[Ti_2O_2]_{0.5}$	7.0
CP(Al)	$Al(OiPr)_3$	$[POSS\text{-}acac][Al]_{2.3}$	6.9

[a)]Calculated by TGA; [b)]Estimated from the chemical formula

3.6 Synthesis of CP(Zn) as a soluble CP

CP(Metal)s, which were acquired using $Cu(OAc)_2$, $Ti(OiPr)_4$, and $Al(OiPr)_3$ as metal sources, were insoluble solids, as mentioned earlier. Nevertheless, CP(Zn) obtained using $Zn(OAc)_2$ remained stable after evaporation. Therefore, CP(Zn) was isolated as a viscous liquid by extraction with CH_2Cl_2/H_2O. Results of the preparation of CP(Zn) are provided in Table 5.

Table 5 Synthesis of coordination polymers

run	Metal source	molar ratio (Metal/POSS)	yield (%)[a)]	state
1	$Zn(OCOCH_3)_2$	2	71.5	Dark orange viscous liquid
2	$Zn(OCOCH_3)_2$	4	73.3	Dark orange viscous liquid
3	$Zn(OCOCH_3)_2$	6	70.2	Dark orange viscous liquid

[a)]Scale in operation: POSS-acac: 0.25 g (0.117 mmol); Calculated based on run 1: $[POSS][Zn]_2$ and runs 2 and 3: $[POSS][Zn]_4$

CP(Zn) was obtained as a dark viscous liquid in approximately 70% yield regardless of the metal precursor/POSS molar ratio. Reaction progress was indicated by the presence of the peak of eliminated acetic acid in the ^1H NMR spectrum of the evaporated solvent. FTIR spectra of these products are depicted in Figure 12.

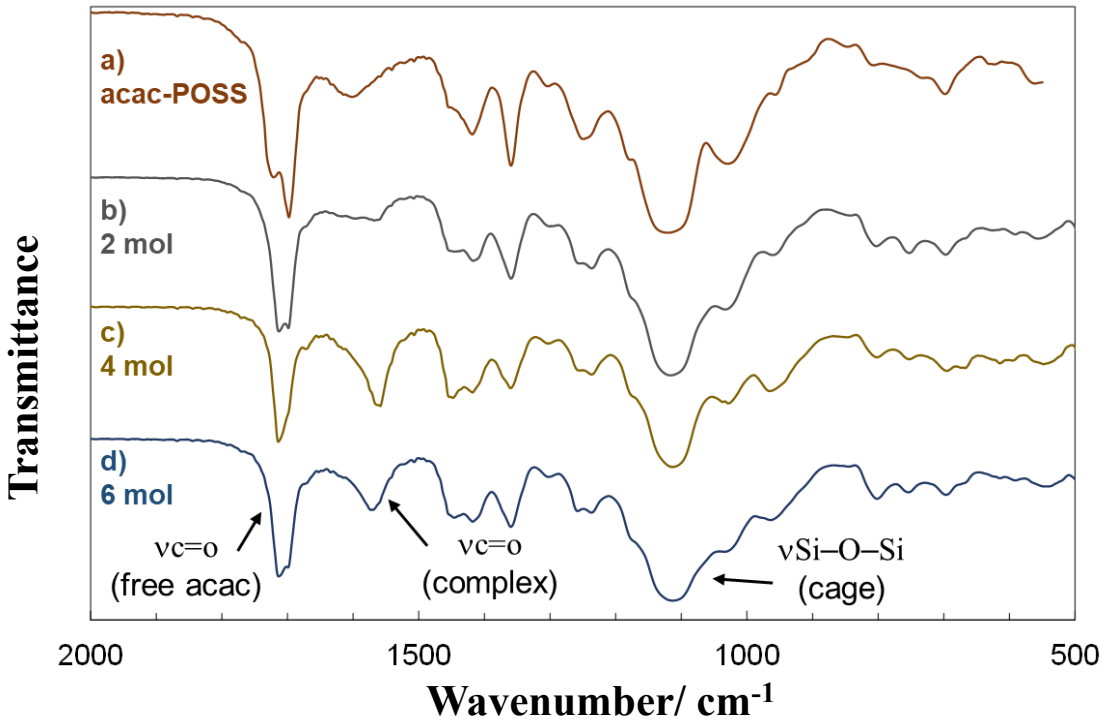

Figure 12. FTIR spectra of a) POSS-acac and b, c, and d) CP(Zn) achieved using 2, 4, and 6 mol of $Zn(OAc)_2$, respectively, by the neat method.

FTIR spectra of CP(Zn) also demonstrated decreases in the intensities of the absorption bands at 1760–1660 cm^{-1} corresponding to the keto-carbonyl group and 1417 cm^{-1} related to the methyl group of the free acac moiety in addition to increases in the intensities of the new band at ~1570 cm^{-1} [27–29] assigned to the enol-carbonyl group and the band at ~1440 cm^{-1} attributed to the methyl group of the enol form. Moreover, the FTIR spectra of CP(Zn) exhibited a new band at 1290 cm^{-1} [30] assigned to C–O. Therefore, CP(Zn) is composed of POSS and metal species bound via covalent bonding and chelate formation similar to the cases of other CP(Metal)s. Additionally, the intensity of the band of the enol-carbonyl group was the strongest for CP(Zn) synthesized using 4 mol $Zn(OAc)_2$. Sharp

absorption bands at 1120–1090 cm^{-1} are attributed to Si–O–Si stretching vibrations of the cage structure [19]; this implied the retention of the cage structure of POSS. ^{13}C NMR spectra of POSS-acac and CP(Zn) are shown in Figure 13. CP(Zn) was also suggested to comprise POSS and metal species bound via covalent bonding and chelate formation because of the disappearance of the peak of α-carbon related to free acetylacetonate moiety and the shift of carbonyl and alcohol C peaks.

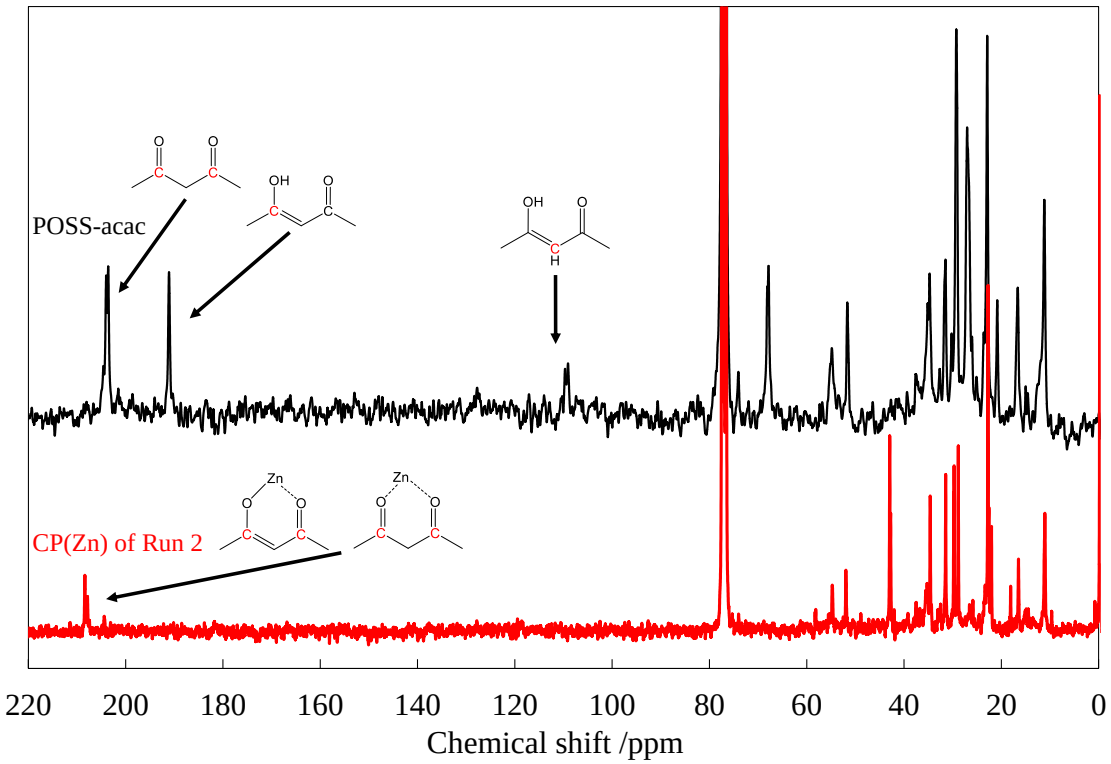

Figure 13. ^{13}C NMR spectra of POSS-acac and CP(Zn) of Run 2.

4 Conclusion

POSS-acac was synthesized via a thiol-ene reaction of POSS-SH and 3-allylacac in the presence of AIBN. Inorganic CPs based on POSS-acac were prepared by separately mixing POSS-acac with the metal sources $Cu(OAc)_2$, $Ti(OiPr)_4$, $Al(OiPr)_3$, and $Zn(OAc)_2$. Formation of the complexes and retentions of the POSS core structures for CP(metal)s were verified by FTIR spectroscopy. Analyses of SEM images revealed that the structures of CP(Cu, Ti, Al)s were controlled by the metal sources. Formulas of CP(Cu, Ti, Al)s were estimated to be [POSS-acac]$[Cu]_{2.3}$, [POSS-acac]$[Ti(OiPr)_2]_{2.5}[Ti_2O_2]_{0.5}$, and [POSS-acac]$[Al]_{2.3}$ according to the TGA ceramic yields, respectively. Degree of crosslinking decreased in the following order: CP(Al) > CP(Ti) > CP(Cu). However, CP(Cu, Ti, Al)s were nonporous amorphous materials because of the existence of a long flexible thioether chain in POSS-acac. In contrast, when $Zn(OAc)_2$ was used, CP(Zn) was obtained as a soluble viscous liquid. Structure of CP(Zn) was suggested to be regulated by the molar ratio of $Zn(OAc)_2$.

References

1. Y. Abe, T. Gunji, *Prog. Polym. Sci.*, **29**, 149–182 (2004). https://doi.org/10.1016/j.progpolymsci.2003.08.003

2. R. M. Laine, *J. Mater. Chem.*, **15**, 3725–3744 (2005). https://doi.org/10.1039/B506815K

3. D. B. Cordes, P. D. Lickiss, F. Rataboul, *Chem. Rev.*, **110**, 2081–2173 (2010). https://doi.org/10.1021/cr900201r

4. H. C. L. Abbenhuis, S. Krijnen, R. A. van Santen, *Chem. Commun.*, 331–332 (1997). https://doi.org/10.1039/A607935K

5. H. C. L. Abbenhuis, H. W. G. van Herwijnen, R. A. van Santen, *Chem. Commun.*, 1941–1942 (1996). https://doi.org/10.1039/CC9960001941

6. M. T. Hay, B. Seurer, D. Holmes, A. Lee, *Macromolecules*, **43**, 2108–2110 (2010). https://doi.org/10.1021/ma9026756

7. S. Marcinko, A. Y. Fadeev, *Langmuir*, **20**, 2270–2273 (2004). https://doi.org/10.1021/la034914l

8. S. Banerjee, S. Kataoka, T. Takahashi, Y. Kamimura, K. Suzuki, K. Sato, A. Endo, *Dalton Trans.*, **45**, 17082–17086 (2016). https://doi.org/10.1039/C6DT02868C

9. Q. Xu, Z. Li, M. Chen, H. Li, *CrystEngComm*, **18**, 177–182 (2016). https://doi.org/10.1039/C5CE01664A

10. C. Sanchez, P. Belleville, M. Popall, L. Nicole, *Chem. Soc. Rev.*, **40**, 696–753 (2011). https://doi.org/10.1039/C0CS00136H

11. E. Carbonell, L. A. Bivona, L. Fusaro, C. Aprile, *Inorg. Chem.*, **56**, 6393–6403 (2017). https://doi.org/10.1021/acs.inorgchem.7b00471

12. A. C. Kucuk, J. Matsui, T. Miyashita, *RSC Adv.*, **8**, 2148–2156 (2018).

https://doi.org/10.1039/C7RA12290J

13. M. Hashimoto, S. Fujii, H. Imoto, K. Naka, *J. Polym. Sci., Part A: Polym. Chem.*, **57**, 2260–2266 (2019). https://doi.org/10.1002/pola.29521

14. R. H. Holm, F. A. Cotton, *J. Am. Chem. Soc.*, **80**, 5658–5663 (1958). https://doi.org/10.1021/ja01554a020

15. N. V. Zolotareva, V. V. Semenov, *Russ. Chem. Rev.*, **82**, 964–987 (2013). https://doi.org/10.1070/rc2013v082n10abeh004364

16. X. Ma, F. Tao, Y. Zhang, T. Li, F. M. Raymo, Y. Cui, *J. Mater. Chem. A.*, **5**, 14343–14354 (2017). https://doi.org/10.1039/C7TA04351A

17. R. B. Davis, P. Hurd, *J. Am. Chem. Soc.*, **77**, 3284–3287 (1955). https://doi.org/10.1021/ja01617a039

18. N. Prigyai, S. Chanmungkalakul, V. Ervithayasuporn, N. Yodsin, S. Jungsuttiwong, N. Takeda, M. Unno, J. Boonmak, S. Kiatkamjornwong, *Inorg. Chem.*, **58**, 15110–15117 (2019). https://doi.org/10.1021/acs.inorgchem.9b01836

19. E. S. Park, H. W. Ro, C. V. Nguyen, R. L. Jaffe, D. Y. Yoon, *Chem. Mater.*, **20**, 1548–1554 (2008). https://doi.org/10.1021/cm071575z

20. L. A. Bivona, O. Fichera, L. Fusaro, F. Giacalone, M. Buaki-Sogo, M. Gruttadauria, C. Aprile, *Catal. Sci. Technol.*, **5**, 5000–5007 (2015). https://doi.org/10.1039/C5CY00830A

21. D. Gnanasekaran, K. Madhavan, J. Tsibouklis, B. S. R. Reddy, *Aust. J. Chem.*, **64**, 309–315 (2011). https://doi.org/10.1071/CH10367

22. L. W. Reeves, *Can. J. Chem.*, **35**, 1351–1365 (1957). https://doi.org/10.1139/v57-179

23. S. Giuffrida, G. G. Condorelli, L. L. Costanzo, I. L. Fragalà, G. Ventimiglia, G. Vecchio, *Chem. Mater.*, **16**, 1260–1266 (2004). https://doi.org/10.1021/cm034782h

24. A. Leaustic, F. Babonneau, J. Livage, *Chem. Mater.*, **1**, 248–252 (1989). https://doi.org/10.1021/cm00002a016

25. R. Hayami, T. Sagawa, S. Tsukada, K. Yamamoto, T. Gunji, *Polyhedron*, **147**, 1–8 (2018). https://doi.org/10.1016/j.poly.2018.02.030

26. K. Jinno, H. Mae, C. Fujimoto, *J. High Resol. Chromatogr.*, **13**, 13–17 (1990). https://doi.org/10.1002/jhrc.1240130104

27. A. Yamamoto, S. Kambara, *J. Am. Chem. Soc.*, **79**, 4344–4348 (1957). https://doi.org/10.1021/ja01573a028

28. M. Shirodker, V. Borker, C. Naether, W. Bensch, K. S. Rane, *Indian J. Chem., Sect. A: Inorg., Bio-inorg., Phys., Theor. Anal. Chem.*, **49**, 1607–1611 (2010).

29. C. Pereira, S. Patrício, A. R. Silva, A. L. Magalhães, A. P. Carvalho, J. Pires, C. Freire, *J. Colloid Interface Sci.*, **316**, 570–579 (2007). https://doi.org/10.1016/j.jcis.2007.07.053

30. L. Li, S. Feng, H. Liu, *RSC Adv.*, **4**, 39132–39139 (2014). https://doi.org/10.1039/C4RA05577B

31. L. -H. Lee, W. -C. Chen, W. -C. Liu, *J. Polym. Sci., Part A: Polym. Chem.*, **40**, 1560–1571 (2002). https://doi.org/10.1002/pola.10246

32. K. C. Patil, G. V. Chandrashekhar, M. V. George, C. N. R. Rao, *Can. J. Chem.*, **46**, 257–265 (1968). https://doi.org/10.1139/v68-040

33. Y. P. Singh, S. Saxena, A. K. Rai, *Synth. React. Inorg. Met.-Org. Chem.*, **14**, 237–251 (1984). https://doi.org/10.1080/00945718408066657

34. J. H. Wengrovius, M. F. Garbauskas, E. A. Williams, R. C. Goint, P. E. Donahue, J. F. Smith, *J. Am. Chem. Soc.*, **108**, 982–989 (1986). https://doi.org/10.1021/ja00265a024

35. B. R. Saunders, B. Vincent, *Adv. Colloid Interface Sci.*, **80**, 1–25 (1999). https://doi.org/10.1016/S0001-8686(98)00071-2

36. T. S. Piper, R. L. Belford, *Mol. Phys.*, **5**, 169–181 (1962). https://doi.org/10.1080/00268976200100171

37. G. D. Smith, C. N. Caughlan, J. A. Campbell, *Inorg. Chem.*, **11**, 2989–2993 (1972). https://doi.org/10.1021/ic50118a024

38. A. Yamamoto, S. Kambara, *Nippon Kagaku Zasshi*, **80**, 1239–1243 (1959). https://doi.org/10.1246/nikkashi1948.80.11_1239

Chapter 5

Conclusion

5.1 Conclusion

Herein, I investigated the (i) hydrolysis and condensation behaviors of tetraethoxysilane (TEOS), hexaethoxydisiloxane (HEDS), and octaethoxytrisiloxane (OETS), (ii) preparation of PDMS elastomers cross-linked with hydrolyzates of TEOS, HEDS, and OETS and their properties, and (iii) syntheses of coordination polymers using acac-terminated polyhedral oligomeric silsesquioxanes and their properties.

Chapter 1 described the background of my research and defined the aims and evaluations of my research.

Chapter 2 explained the synthesis of linear ethoxy oligosiloxanes and assessments of their reactivities. HEDS and OETS, which were the initial hydrolysis products of TEOS, were achieved in 3.5 and 8.4% total yields, respectively, from diethoxydiicocyanatosilane by controlling the functionality. Hydrolyzates of TEOS, HEDS, and OETS were trimethylsilylated and analyzed by mass spectrometry, gel permeation chromatography, and nuclear magnetic resonance spectroscopy. Linear and cyclic oligosiloxanes were generated in the initial stage of hydrolysis–condensation. TEOS was estimated to be a network-type polymer containing a cyclic siloxane. HEDS mainly consisted of four-membered cyclic siloxanes. OETS primarily comprised cyclic siloxanes. These precursors finally afforded ladder- or cage-like polymers via an intermediate with a six-membered cyclic structure. Additionally, the electron densities of the ethoxysilane oligomers calculated using density functional

theory were investigated. Optimized HEDS and OETS structures demonstrated high electron densities on the O atoms in the siloxane bond and alkoxy group. These results imply that electron density may affect the reactivities of TEOS, HEDS, and OETS.

Chapter 3 presented the applications of organic–inorganic hybrid materials constructed using the hydrolyzates of linear ethoxy oligosiloxanes. Si–H-terminated ethoxy oligosiloxanes (CLs) were employed as cross-linkers for PDMS elastomers. All CLs exhibited similar M_w values (approximately 1400 Da), M_w/M_n values (1.1), and OEt/Si-H ratios (4). Nevertheless, their structures were different: CL_{TEOS} was primarily composed of cyclic siloxane derivatives silylated on Q^4 silicon atom; CL_{HEDS} mainly consisted of four-membered cyclic siloxane derivatives silylated on Q^4 silicon atom; and CL_{OETS} predominantly comprised cyclic siloxane derivatives silylated on both Q^3 and Q^4 silicon atom. Effects of these distinct cross-linker structures on transmittance, thermal stability, tensile strength, and swelling behavior in toluene were assessed. Results indicated superior crosslinking efficiencies of CL_{HEDS} and CL_{OETS} to that of CL_{TEOS}. These differences are believed to arise from the presence of four-membered cyclic siloxane derivatives and silylation on Q^3 silicon atom. Thus, the properties of the elastomers are inferred to be influenced by the cross-linker structures.

Chapter 4 describes the syntheses of coordination polymers using polyhedral oligomeric silsesquioxanes and their properties. Acetylacetonato-terminated cage silsesquioxane (POSS-acac), which can be a ligand, was synthesized via a thiol-ene reaction of POSS-SH and 3-allylacac in the

presence of AIBN. Inorganic coordination polymers (CPs) based on POSS-acac were fabricated by separately mixing POSS-acac and metal sources such as $Cu(OAc)_2$, $Ti(OiPr)_4$, $Al(OiPr)_3$, and $Zn(OAc)_2$. Formation of the complexes and retention of the POSS-core structures were confirmed for CP(metal)s by Fourier transform infrared spectroscopy. Analyses of the SEM images revealed that the structures of CP(Cu, Ti, Al)s were regulated by the metal sources. Formulas of CP(Cu, Ti, Al)s were estimated to be [POSS-acac][Cu]$_{2.3}$, [POSS-acac][Ti(OiPr)$_2$]$_{2.5}$[Ti$_2$O$_2$]$_{0.5}$, and [POSS-acac][Al]$_{2.3}$ from the TGA ceramic yields. Degree of crosslinking decreased in the following order: CP(Al) > CP(Ti) > CP(Cu). However, CP(Cu, Ti, Al)s were nonporous amorphous materials because of the presence of a long flexible thioether chain in POSS-acac. In contrast, when $Zn(OAc)_2$ was used, CP(Zn) was obtained as a soluble viscous liquid. Structure of CP(Zn) was suggested to be controlled by the molar ratio of $Zn(OAc)_2$.

These results suggest that the properties of organic–inorganic hybrid materials can be regulated by selecting appropriate raw materials.

5.2 Research publications

1) **Y. Sato**, R. Hayami, K. Yamamoto, T. Gunji, Syntheses and properties of Cu(II), Al(III), and Ti(IV) coordination polymers using an acetylacetonato-terminated polyhedral oligomeric silsesquioxane. *Polym. J.,* **54**, 985–993 (2022).

DOI: https://doi.org/10.1038/s41428-022-00651-x

2) **Y. Sato**, A. Sugimoto, T. Iwashina, R. Hayami, K. Yamamoto, T. Gunji, Hydrolysis and condensation behavior of tetraethoxysilane, hexaethoxydisiloxane, and octaethoxytrisiloxane. *J. Sol-Gel Sci. Technol.,* **108**, 377–391 (2023).

DOI: https://doi.org/10.1007/s10971-023-06159-x

3) **Y. Sato**, R. Hayami, K. Yamamoto, T. Gunji, Preparation and properties of PDMS elastomer cross-linked with hydrolyzate of tetraethoxysilane, hexaethoxydisiloxane, and octaethoxytrisiloxane: influence of cross-linker structure. *J. Sol-Gel Sci. Technol.,* **109**, 22–31 (2023).

DOI: https://doi.org/10.1007/s10971-023-06247-y

5.3 Acknowledgement

I would like to thank Dr. Ryohei Hayami, Emeritus professor Yoshimoto Abe, Lecturer Kazuki Yamamoto, and Professor Takahiro Gunji for helpful encouragement to complete my research.

I acknowledge the following people for their significant cooperation to my thesis:

Ms. Asahi Sugimoto (hydrolysis and condensations of TEOS and HEDS in Chapter 2)

Mr. Tatsuya Iwashina (DFT in Chapter 4)

Dr. Takuya Sagawa (DFT in Chapter 2)

Mr. Naoya Tanihata (SEM in Chapter 3)

Mr. Wataru Nakamoto (SEM in Chapter 4)

Special thanks to my family who supported me with a financial aid and Mr. Masaki Ishii who is friend since undergraduate days of doctoral course and provided helpful advice about life and chemistry. Furthermore, I would like to acknowledge the present and past members of Gunji group.

Supporting Information

Table S1. Estimated Structure for ethoxysilane–TMS

M_W	structure	TEOS–TMS	HEDS–TMS	OETS–TMS
365	$Si_2O(OEt)_6$		○	
409	$Si_2O(OEt)_5(OSiMe_3)$		○	
453	$Si_2O(OEt)_4(OSiMe_3)_2$		○	
497	$Si_2O(OEt)_3(OSiMe_3)_3$		○	
499	$Si_3O_2(OEt)_8$		○	○
543	$Si_3O_2(OEt)_7(OSiMe_3)_1$	○	○	○
587	$Si_3O_2(OEt)_6(OSiMe_3)_2$	○	○	○
603	$Si_4O_4(OEt)_7(OSiMe_3)_1$	○		
631	$Si_3O_2(OEt)_5(OSiMe_3)_3$	○	○	○
633	$Si_4O_3(OEt)_{10}$	○	○	○
647	$Si_4O_4(OEt)_6(OSiMe_3)_2$	○	○	
675	$Si_3O_2(OEt)_4(OSiMe_3)_4$	○		○
677	$Si_4O_3(OEt)_9(OSiMe_3)_1$	○	○	○

691	$Si_4O_4(OEt)_5(OSiMe_3)_3$	○	○	
693	$Si_5O_5(OEt)_{10}$		○	
721	$Si_4O_3(OEt)_8(OSiMe_3)_2$	○	○	○
737	$Si_5O_5(OEt)_9(OSiMe_3)_1$	○	○	
765	$Si_4O_3(OEt)_7(OSiMe_3)_3$	○	○	○
767	$Si_5O_4(OEt)_{12}$	○		○
781	$Si_5O_5(OEt)_8(OSiMe_3)_2$	○	○	○
809	$Si_4O_3(OEt)_6(OSiMe_3)_4$	○	○	
811	$Si_5O_4(OEt)_{11}(OSiMe_3)_1$	○		○
825	$Si_5O_5(OEt)_7(OSiMe_3)_3$	○		○
853	$Si_4O_3(OEt)_5(OSiMe_3)_5$	○		
855	$Si_5O_4(OEt)_{10}(OSiMe_3)_2$	○	○	○
869	$Si_5O_5(OEt)_6(OSiMe_3)_4$	○		
871	$Si_6O_6(OEt)_{11}(OSiMe_3)_1$			○
899	$Si_5O_4(OEt)_9(OSiMe_3)_3$	○	○	○
901	$Si_6O_5(OEt)_{14}$	○		○
913	$Si_5O_5(OEt)_5(OSiMe_3)_5$	○		

915	$Si_6O_6(OEt)_{10}(OSiMe_3)_2$	○		○
917	$Si_7O_{10}(OEt)_8(OSiMe_3)_2$			○
931	$Si_7O_8(OEt)_{11}(OSiMe_3)_1$	○		
943	$Si_5O_4(OEt)_8(OSiMe_3)_4$	○		○
945	$Si_6O_5(OEt)_{13}(OSiMe_3)_1$	○		○
959	$Si_6O_6(OEt)_9(OSiMe_3)_3$	○	○	○
961	$Si_7O_7(OEt)_{14}$	○		○
975	$Si_7O_8(OEt)_{10}(OSiMe_3)_2$	○	○	
987	$Si_5O_4(OEt)_7(OSiMe_3)_5$	○		
989	$Si_6O_5(OEt)_{12}(OSiMe_3)_2$	○	○	○
1003	$Si_6O_6(OEt)_8(OSiMe_3)_4$	○		
1005	$Si_7O_7(OEt)_{13}(OSiMe_3)_1$	○		
1031	$Si_5O_4(OEt)_6(OSiMe_3)_6$	○		
1033	$Si_6O_5(OEt)_{11}(OSiMe_3)_3$	○	○	○
1047	$Si_6O_6(OEt)_7(OSiMe_3)_5$	○	○	
1049	$Si_7O_7(OEt)_{12}(OSiMe_3)_2$	○	○	
1077	$Si_6O_5(OEt)_{10}(OSiMe_3)_4$	○	○	○

1079	$Si_7O_6(OEt)_{15}(OSiMe_3)_1$	○	○	○
1093	$Si_7O_7(OEt)_{11}(OSiMe_3)_3$	○	○	
1121	$Si_6O_5(OEt)_9(OSiMe_3)_5$	○	○	
1137	$Si_7O_7(OEt)_{10}(OSiMe_3)_4$	○		
1167	$Si_7O_6(OEt)_{13}(OSiMe_3)_3$	○	○	
1211	$Si_7O_6(OEt)_{12}(OSiMe_3)_4$	○	○	
1255	$Si_7O_6(OEt)_{11}(OSiMe_3)_5$	○		
1257	$Si_8O_7(OEt)_{16}(OSiMe_3)_2$	○	○	
1299	$Si_7O_6(OEt)_{10}(OSiMe_3)_6$	○		
1301	$Si_8O_7(OEt)_{15}(OSiMe_3)_3$	○		
1345	$Si_8O_7(OEt)_{14}(OSiMe_3)_4$	○		

Table S2. Estimated Structure for Cs–LS

M_W	structure	C_{TEOS}–LS	C_{HEDS}–LS	C_{OETS}–LS
559	$Si_4O_4(OEt)_8$		○	
603	$Si_4O_4(OEt)_7(OSiMe_3)_1$		○	○
647	$Si_4O_4(OEt)_7(OSiMe_3)_2$		○	○

677	$Si_4O_3(OEt)_9(OSiMe_3)$	○		
677	$Si_5O_7(OEt)_3(OSiMe_3)_3$	○		
691	$Si_4O_4(OEt)_5(OSiMe_3)_3$		○	
721	$Si_4O_3(OEt)_8(OSiMe_3)_2$	○	○	
721	$Si_5O_7(OEt)_2(OSiMe_3)_4$	○	○	
735	$Si_4O_4(OEt)_4(OSiMe_3)_4$		○	
737	$Si_5O_5(OEt)_9(OSiMe_3)$	○	○	○
753	$Si_6O_7(OEt)_{10}$	○	○	○
781	$Si_5O_5(OEt)_8(OSiMe_3)_2$	○	○	
797	$Si_6O_7(OEt)_9(OSiMe_3)$	○	○	○
825	$Si_5O_5(OEt)_7(OSiMe_3)_3$	○		
827	$Si_6O_6(OEt)_{12}$	○		
829	$Si_7O_{10}(OEt)_{10}$			○
841	$Si_6O_7(OEt)_8(OSiMe_3)_2$	○	○	○
844	$Si_7O_{11}(OEt)_8(OSiMe_3)$		○	
858	$Si_7O_9(OEt)_{11}$	○	○	
871	$Si_6O_6(OEt)_{11}(OSiMe_3)$	○	○	

885	$Si_6O_7(OEt)_7(OSiMe_3)_3$	○	○	○
887	$Si_7O_8(OEt)_{12}$	○	○	
901	$Si_6O_5(OEt)_{14}$	○	○	○
902	$Si_7O_9(OEt)_{10}(OSiMe_3)$	○	○	○
915	$Si_6O_6(OEt)_{10}(OSiMe_3)_2$	○	○	
929	$Si_6O_7(OEt)_6(OSiMe_3)_4$	○	○	○
931	$Si_7O_8(OEt)_{11}(OSiMe_3)$			○
945	$Si_6O_5(OEt)_{13}(OSiMe_3)$	○	○	○
945	$Si_7O_9(OEt)_7(OSiMe_3)_3$	○	○	○
959	$Si_6O_6(OEt)_9(OSiMe_3)_3$			○
961	$Si_7O_7(OEt)_{14}$		○	
961	$Si_7O_{10}(OEt)_7(OSiMe_3)_3$		○	
973	$Si_6O_7(OEt)_5(OSiMe_3)_5$	○		○
975	$Si_7O_8(OEt)_{10}(OSiMe_3)_2$	○	○	○
989	$Si_6O_5(OEt)_{12}(OSiMe_3)_2$	○		○
991	$Si_8O_{10}(OEt)_{11}(OSiMe_3)$		○	○
1019	$Si_7O_8(OEt)_9(OSiMe_3)_3$	○	○	○

1035	$Si_7O_6(OEt)_{16}$	○	○	○
1035	$Si_8O_{10}(OEt)_{10}(OSiMe_3)_2$	○		○
1063	$Si_7O_8(OEt)_8(OSiMe_3)_4$			○
1079	$Si_7O_6(OEt)_{15}(OSiMe_3)$	○		○
1079	$Si_8O_{10}(OEt)_9(OSiMe_3)_3$	○		○
1137	$Si_7O_{10}(OEt)_7(OSiMe_3)_3$	○		
1169	$Si_8O_7(OEt)_{18}$	○		